Investigating Mechanisms of Immune Function and New Therapeutic Targets in Rare Autoimmune Diseases

Inaugural-Dissertation

to obtain the academic degree

Doctor rerum naturalium (Dr. rer. nat.)

submitted to the Department of Biology, Chemistry, Pharmacy

of Freie Universität Berlin

by

Julia Hecker

Berlin, 2024

This work was conducted at the Department of Gastroenterology, Rheumatology and Infectious Diseases at Charité - Universitätsmedizin Berlin, Campus Benjamin Franklin under the supervision of Prof. Dr. Britta Siegmund between April 2020 and May 2024.

1st reviewer: Prof. Dr. Britta Siegmund

2nd reviewer: Prof. Dr. Petra Knaus

Date of defense: 11.11.24

Acknowledgement

First and foremost, I would like to thank my first supervisor Prof. Britta Siegmund for giving me the opportunity to work on such an interesting project and for her support and mentorship throughout my whole time in her lab and while writing this thesis. In addition, I would especially like to thank Prof. Carl Weidinger for supervising my thesis, for always being positive, motivating me and for giving me the freedom to develop my own ideas and skills.

Furthermore, I would like to thank Prof. Petra Knaus for being my second supervisor and for reviewing this thesis.

I'm glad that I had the opportunity to be part of the Center of Infection Biology and Immunity (ZIBI) and the integrated Research Training Group (iRTG) of the Transregio Collaborative Research Center (TRR)241, where I could connect with other researchers, attend courses to develop scientific skills and soft skills and participate in great retreats. I would also like to thank Prof. Ahmed Hegazy and Prof. Raja Atreya for their valuable ideas and suggestions at my thesis advisory committee meetings.

Many thanks to all present and past members of the AG Siegmund for helpful discussions about projects, for always being supportive and for fun times outside the lab. Special thanks to Inka Freise, not only for her technical support during experiments, but also for the helpful discussions about protocols and experimental setups. Many thanks also to Toka Omar for her help while writing this thesis. Furthermore, I would like to thank Judith Saurenbach for her contribution to this work as part of her master's thesis.

In addition, I would like to thank all collaboration partners, especially Prof. Peter Kühnen, Dr. Lisa Ruck, Dr. Désirée Kunkel, Prof. Andre Franke, Dr. Britt-Sabina Löscher, Dr. Anja Schütz and the TRR241 IBDome Consortium for their contribution to this work and their helpful ideas and suggestions.

Finally, I would like to thank my family and friends for always supporting me, for listening to my worries and for positive distraction after stressful days.

Declaration of authorship

I hereby declare that I alone am responsible for the content of my doctoral dissertation and that I have only used the sources or references cited in the dissertation.

Berlin, 16.05.24

Julia Hecker

Table of contents

Summary

Autoimmune diseases affect approximately 5-8% of the population worldwide and are characterized by defective or misdirected immune responses. Studies have shown that most autoimmune diseases result from a complex interplay of several factors, including genetic susceptibility, environmental stimuli and defects in immune regulation. However, in some cases, autoimmune diseases can also be caused by mutations in a single gene. The underlying mechanisms of those rare autoimmune diseases are often poorly understood, leading to inadequate management of disease symptoms and to a reduced life expectancy and quality of life for patients. Research on rare diseases provides the unique opportunity to study the function of the affected genes in humans, which not only contributes to a better understanding of the human immune system, but is also relevant for identifying new therapeutic targets for autoimmune diseases.

In this thesis, we investigated mechanisms of immune regulation and function by studying three rare diseases.

First, we studied the function of the alpha kinase ALPK1 in immune regulation by analyzing the immune cell composition and function of a patient with ROSAH syndrome, which is caused by a mutation in *ALPK1*. We found that the gain-of-function mutation in *ALPK1* leads to an increased expression of TNFα and IL-6 by myeloid cells which triggers the auto-inflammatory symptoms observed in ROSAH patients. Consequently, blockade of TNFα resulted in a reduction of auto-inflammatory symptoms in our ROSAH patient.

Furthermore, we investigated the role of mutations in the IL-36 receptor antagonist (*IL36RN*) in the pathogenesis of inflammatory bowel disease to better understand the function of IL-36 signaling in intestinal homeostasis and inflammation. We demonstrated that pathogenic *IL36RN* mutations are present in patients with Crohn's disease (CD) and that anti-IL-36R therapy resulted in a reduced intestinal inflammation in one *IL36RN*-mutated patient. Thus, our data suggest that defects in IL-36 signaling might be involved in the pathogenesis of CD in a subgroup of patients and that blocking IL-36 signaling might represent a personalized treatment for these patients.

Finally, we studied the role of the leptin-melanocortin signaling pathway in immune regulation by performing an in-depth immune cell profiling of patients with monogenic obesity. We observed a decreased frequency of pro-inflammatory myeloid cells in patients with mutations in the leptin receptor (*LEPR*), an increased frequency of effector T cells in patients with mutations in proopiomelanocortin (*POMC*) and an increased frequency of B cells in patients with mutation in the melanocortin 4 receptor (*MC4R*). These data indicate that LEPR, POMC and MC4R are not only important for appetite regulation but also have specific functions in the immune system.

In summary, the data presented here highlight the importance of rare diseases in investigating the mechanisms of immune regulation and function and to identify new therapeutic targets for the treatment of autoimmune diseases. Based on our research performed here, we also developed a pipeline for characterizing rare autoimmune diseases, thus enabling a more precise diagnosis and identification of targeted treatment options for patients.

Zusammenfassung

Autoimmunerkrankungen betreffen weltweit etwa 5-8% der Bevölkerung und sind durch fehlerhafte oder fehlgeleitete Immunreaktionen gekennzeichnet. Studien haben gezeigt, dass die meisten Autoimmunerkrankungen auf ein komplexes Zusammenspiel mehrerer Faktoren zurückzuführen sind, darunter genetische Prädisposition, Umweltfaktoren und Störungen der Immunregulation. In einigen Fällen können Autoimmunerkrankungen jedoch auch durch Mutationen in einem einzigen Gen verursacht werden. Die zugrundeliegenden Mechanismen dieser seltenen Autoimmunerkrankungen sind oft nur unzureichend bekannt, was zu einer inadäquaten Behandlung der Krankheitssymptome und zu einer verminderten Lebenserwartung und Lebensqualität der Patientinnen und Patienten führt. Die Erforschung seltener Erkrankungen bietet die einzigartige Möglichkeit, die Funktion der betroffenen Gene im Menschen zu untersuchen, was nicht nur zu einem besseren Verständnis des menschlichen Immunsystems beiträgt, sondern auch für die Suche nach neuen therapeutischen Ansatzpunkten für Autoimmunerkrankungen relevant ist.

In dieser Arbeit haben wir Mechanismen der Immunregulation und -funktion anhand von drei seltenen Erkrankungen untersucht.

Zunächst haben wir die Funktion der Alpha-Kinase ALPK1 in der Immunregulation untersucht, indem wir die Zusammensetzung und Funktion von Immunzellen einer Patientin mit ROSAH-Syndrom, das durch eine Mutation in *ALPK1* ausgelöst wird, analysiert haben. Wir konnten zeigen, dass die *gain-of-function*-Mutation in *ALPK1* zu einer erhöhten Expression von TNFα und IL-6 in myeloischen Zellen führt, was wiederum die Ursache für die autoinflammatorischen Symptome in ROSAH-Patientinnen und -Patienten sein könnte. Folglich führte die Blockade von TNFα bei unserer ROSAH-Patientin zu einer Verringerung der autoinflammatorischen Symptome.

Darüber hinaus haben wir die Rolle von Mutationen im IL-36 Rezeptorantagonisten (*IL36RN*) in der Pathogenese von chronisch entzündlichen Darmerkrankungen untersucht, um die Bedeutung des IL-36-Signalwegs für die intestinale Homöostase und die Entstehung von Entzündungen besser zu verstehen. Wir konnte zeigen, dass pathogene *IL36RN*-Mutationen bei Morbus Crohn (MC)-Patientinnen und -Patienten vorkommen. Bei einer Patientin mit *IL36RN*-Mutation konnte außerdem eine verringerte intestinale Entzündungsaktivität durch eine Anti-IL-36R-Therapie nachgewiesen werden. Unsere Daten deuten also darauf hin, dass Defekte im IL-36-Signalweg bei einer Untergruppe von Patientinnen und Patienten an der Pathogenese von MC beteiligt sein könnten und dass die Blockierung des IL-36- Signalwegs einen personalisierten Therapieansatz für diese Patientinnen und Patienten darstellen könnte.

Schließlich haben wir die Rolle des Leptin-Melanocortin-Signalwegs bei der Immunregulation untersucht, indem wir eine detaillierte Immunzellcharakterisierung von Patientinnen und Patienten

mit monogenetischer Adipositas durchgeführt haben. Wir konnten beobachten, dass Patientinnen und Patienten mit Mutationen im Leptinrezeptor (*LEPR*) eine verringerte Frequenz von pro-inflammatorischen myeloischen Zellen aufweisen, während Patientinnen und Patienten mit Mutationen in Proopiomelanocortin (*POMC*) eine erhöhte Frequenz von Effektor-T-Zellen und Patientinnen und Patienten mit Mutationen im Melanocortin-4-Rezeptor (*MC4R*) eine erhöhte Frequenz von B-Zellen haben. Diese Daten weisen darauf hin, dass LEPR, POMC und MC4R nicht nur für die Appetitregulierung von Bedeutung sind, sondern auch spezifische Funktionen im Immunsystem ausüben.

Zusammenfassend verdeutlichen die hier vorgestellten Daten die Bedeutung seltener Erkrankungen für die Erforschung von Mechanismen der Immunregulation und -funktion sowie für die Identifizierung neuer therapeutischer Ansatzpunkte zur Behandlung von Autoimmunerkrankungen. Auf der Grundlage unserer hier durchgeführten Forschung haben wir außerdem eine Pipeline zur Charakterisierung seltener Autoimmunerkrankungen entwickelt, die eine präzisere Diagnose und die Identifizierung gezielter Behandlungsmöglichkeiten für Patientinnen und Patienten ermöglicht.

1. Introduction

1.1 Rare mutations can cause autoimmune diseases

The immune system plays a crucial role in the body's defense against infections and malignant cells. However, defective or misdirected immune responses can result in autoimmune diseases, which affect around 5-8% of the world's population [1]. Autoimmune diseases can affect different parts of the body, such as the skin, joints, the central nervous system or the gastrointestinal tract. For instance, inflammatory bowel disease (IBD) is characterized by chronic inflammation of the gastrointestinal tract and causes symptoms such as abdominal pain, diarrhea and bleeding. Arthritis, on the other hand, primarily affects the joints, causing pain, swelling and stiffness [1]. Although the etiology of most autoimmune diseases remains unknown, studies revealed that several factors such as genetic susceptibility, environmental stimuli and defects in immune regulation are involved in the pathogenesis of autoimmune diseases [2].

However, in some cases, autoimmune diseases can also be caused by germline mutations in a single gene. These conditions are typically rare diseases, meaning that they affect less than 1 in 2000 individuals [3]. Currently, approximately 7000 different rare diseases have been identified, making them a relevant health issue [4]. Thus, research on rare diseases provides both challenges and opportunities. Rare diseases provide the unique opportunity to study gene function in humans and to understand molecular pathomechanisms [3]. This is highlighted by research on the immune dysregulation, polyendocrinopathy, enteropathy, X-linked (IPEX) syndrome, a rare monogenic autoimmune disease caused by a mutation in forkhead box P3 (FOXP3). The study of this disease has led to the identification of FOXP3 as the key modulator of regulatory T cell (Treg) function and significantly improved our understanding of the role of Tregs in immune regulation [5]. Furthermore, research on rare diseases has also helped to understand the function of the common gamma chain (γc) as a subunit of several cytokine receptors [6] and the involvement of the recombination-activating gene (RAG) 1 and RAG2 in antibody and T cell receptor V(D)J recombination [7].

However, the diagnosis and treatment of rare diseases remains challenging. Patients often spend several years or even decades without a diagnosis, resulting in a considerable burden for patients and their families [8]. Although patients more frequently undergo genome sequencing, this often does not lead to a molecular diagnosis and effective treatment for the individual patient [9]. One reason for this is the high number of variants of unknown significance in clinical databases such as ClinVar [10]. These variants are often difficult to interpret, as the exact effect of the mutation on the protein function remains unclear [11]. Thus, linking identified mutations to the clinical phenotype of a patient remains a major challenge in the field of rare diseases. Therefore, a standardized pipeline for the diagnosis of rare diseases that combines clinical and genomic data with functional assays could facilitate the

understanding of molecular mechanisms of rare diseases and the identification of targets for personalized treatment.

1.2 Identification and function of distinct immune cell subsets

Autoimmune diseases are associated with changes in immune regulation and function. Identifying the key cell types and cell states involved in the development and progression of these diseases remains challenging. Newly developed single cell techniques such as single-cell RNA sequencing and mass cytometry, provide the opportunity to study the cellular complexity of the human immune system at the single-cell level, enabling an in-depth immune cell profiling of individual patients [12]. Within these techniques, immune cell subsets are identified by the expression of a distinct pattern of proteins, which reflects their cellular ontogeny and function.

Traditionally, immune cells are categorized as either part of the innate or the adaptive immune system. Immune cells of the innate immune system such as monocytes, macrophages, dendritic cells (DCs), granulocytes and natural killer (NK) cells express receptors that can only recognize a limited number of antigens, which are evolutionary conserved and shared by many infectious agents. In contrast, immune cells of the adaptive immune system, such as B and T cells, have somatically recombined receptors that specifically recognize a wide range of antigens including self and foreign antigens [13].

Immune cells of the innate immune system

Monocytes, macrophages and DCs belong to the group of mononuclear phagocytes that share the property of phagocytosis, a mechanism for the ingestion and elimination of pathogens and debris. Monocytes are circulating mononuclear phagocytes that can be identified by the expression of cluster of differentiation (CD) 11b, CD14 and CD16. Besides phagocytosis, monocytes can produce pro- and anti-inflammatory cytokines and present antigens. Additionally, monocytes can migrate into tissues and differentiate into macrophages, which are tissue-resident cells with similar functions to monocytes. Monocytes can also give rise to DCs, which express markers such as CD11c and major histocompatibility complex (MHC) II and whose main function is to process and present antigens. Of note, DCs and macrophages can also arise independently from monocytes from precursor cells of the bone marrow [14, 15].

Innate lymphoid cells (ILCs) represent a family of cells that derive from common lymphoid progenitors like T and B cells, but do not express specific antigen receptors. The most frequent cell type of ILCs are NK cells, which are found in the blood and in various tissues and can be identified by the expression of CD56. NK cells recognize defective or infected cells based on phenotypic changes such as downregulation of MHC molecules and as a result produce interferon γ (IFNγ) and tumor necrosis factor α (TNFα) or directly lyse cells by using granzymes and perforin [16, 17].

Immune cells of the adaptive immune system

T cells play a central role in the adaptive immune response and have a variety of functions. T cells recognize antigens with their T cell receptor (TCR) only when the antigen is presented by MHC molecules of antigen presenting cells (APCs). In the majority of T cells, the TCR consists of the α and β chain (αβ T cells), while a small subset of T cells express the γ and δ chain (γδ T cells). αβ T cells can be further divided into $CD4^+$ and $CD8^+$ T cells based on the expression of the CD4 or CD8 co-receptor [18]. T cells that have not encountered their antigen yet are called naïve T cells and can be identified by the expression of CD45RA, C-C chemokine receptor type 7 (CCR7) and CD27 [19]. These cells circulate through the body until they recognize their cognate antigen, become activated and undergo clonal expansion and differentiation. Depending on the cytokine environment, $CD4^+$ T cells can differentiate into different subsets including T helper (Th) 1 cells, Th2 cells, Th17 cells, T follicular helper (TfH) cells or Tregs. Th1, Th2 and Th17 cells secrete different cytokines to recruit other immune cells to fight infections, TfH cells provide help to B cells and Tregs are important for maintaining immune tolerance. Activated $CD8^+$ T cells can produce cytokines such as IFNγ and TNFα and have the ability to directly kill target cells. T cells can also develop into memory T cells, which can be quickly activated upon re-encountering their antigen [18, 20].

B cells express a B cell receptor (BCR) that is similar to the TCR of T cells. However, unlike T cells, B cells can recognize antigens without the need for APCs. Once activated, B cells can differentiate into memory B cells and antibody-producing plasma cells, which play a crucial role in neutralizing pathogens. Furthermore, B cells can produce cytokines and serve as APCs by ingesting and presenting recognized antigens. In general, B cells can be identified by the expression of CD19, while memory B cells additionally express CD27 and plasma cells CD27 and CD38 (**Figure 1**) [15, 21].

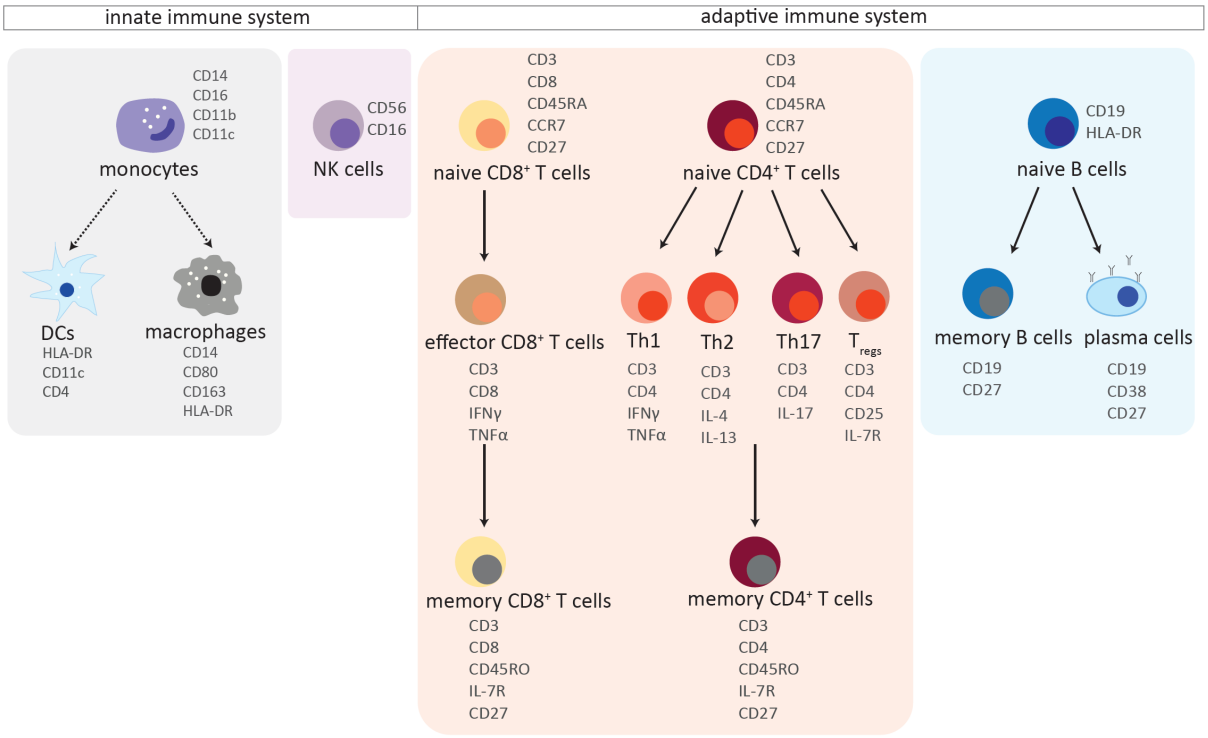

Figure 1: Overview of human immune cells.
Monocytes, dendritic cells (DCs), macrophages and natural killer (NK) cells belong to the innate immune system, while B and T cells belong to the adaptive immune system. T cells can be further divided into $CD4^+$ and $CD8^+$ T cells as well as into naive, effector and memory T cells. B cells can be further divided into naive B cells, memory B cells and antibody-producing plasma cells. The markers used in this thesis to identify the different immune cell subsets are shown below or next to the cell symbol.

1.3 Mutations in *ALPK1* can lead to the rare ROSAH syndrome

1.3.1 Function of ALPK1

Protein phosphorylation is one of the most important mechanisms for controlling protein activity and function and plays an important role in signal transduction. During phosphorylation, a phosphate group is covalently attached to a protein. This process is mediated by protein kinases and leads to changes in the structural confirmation of the protein and thus to a change in protein function. Phosphate groups can be removed again from the protein by phosphatases, which returns the protein back to its original state [22]. Protein kinases can be divided into different groups based on the structure of the catalytic domain. Around 90% of the protein kinases belong to the family of conventional kinases, while 10% of the protein kinases have a different structure of the catalytic domain and are therefore called atypical kinases [23].

One group of kinases that belongs to the family of atypical kinases are the alpha protein kinases. Unlike other kinases, most alpha protein kinases phosphorylate residues located within alpha helices [24]. Until now, six human alpha kinases have been identified including eukaryotic elongation factor 2 kinase

(eEF2K), alpha-kinase (ALPK) 1, ALPK2, ALPK3, transient receptor potential melastatin (TRPM) type 6 and TRPM type 7 [23].

ALPK1 is expressed in multiple tissues and by a wide range of cells and has been shown to regulate apical transport in epithelial cells by phosphorylating myosin 1 [25]. More recently, ALPK1 has also been identified to act as a pattern recognition receptor (PPR) [26]. PPRs play a crucial role in innate immunity by recognizing conserved microbial-derived molecules known as pathogen-associated molecular patterns (PAMPs) and initiating pro-inflammatory and anti-microbial responses. One such PAMP is lipopolysaccharide (LPS), a major component of the cell wall of Gram-negative bacteria, which is recognized by the Toll-like receptor 4 (TLR4). However, it has recently been shown that also metabolites of the LPS biosynthesis pathway, such as D-glycero-β-D-manno-heptose 1,7-bisphosphate (HBP) and ADP-L-glycero-β-D-manno-heptose (ADP-heptose) can induce pro-inflammatory and anti-microbial responses in host cells [27]. HBP and ADP-heptose are secreted into the host cells in a type III or type IV secretion system-dependent manner [28]. Furthermore, ADP-heptose can freely penetrate the host cell wall. Inside the host cell, HBP is converted to ADP-heptose 7-P by host-derived adenylyltransferases. Both ADP-heptose and ADP-heptose 7-P can bind to ALPK1 which activates ALPK1, leading to the phosphorylation and activation of TRAF-interacting protein with forkhead-associated domain (TIFA). This results in the recruitment and activation of tumor necrosis factor receptor-associated factor 6 (TRAF6), which initiates nuclear factor kappa-light-chain-enhancer of activated B cells (NFκB) activation and the production of pro-inflammatory cytokines and chemokines (**Figure 2**) [26].

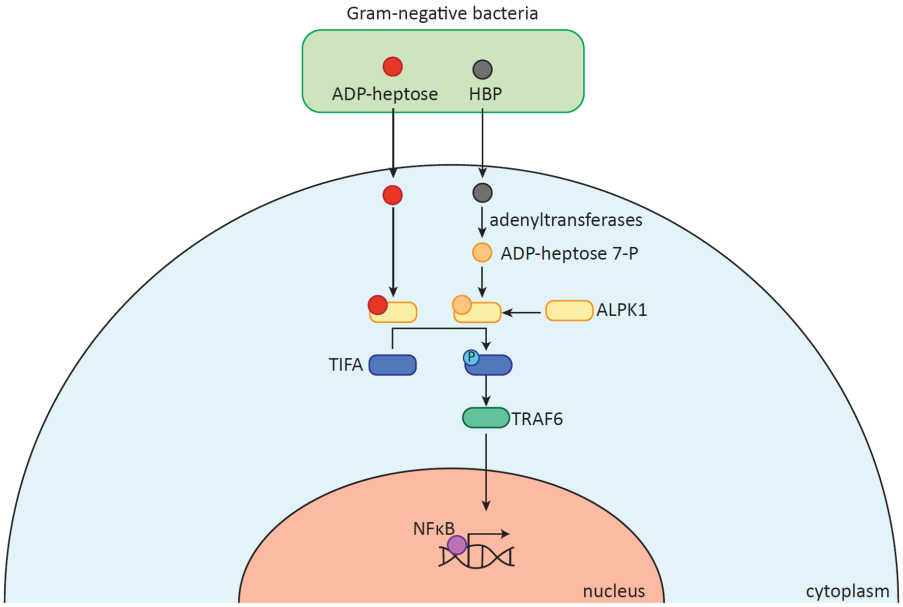

Figure 2: The ADP-heptose-ALPK1 signaling pathway.
D-glycero-β-D-manno-heptose 1,7-bisphosphate (HBP) and ADP-L-glycero-β-D-manno-heptose (ADP-heptose) are secreted by Gram-negative bacteria into host cells in a type III or type IV secretion system-dependent manner. Furthermore, ADP-heptose can freely penetrate the host cell wall. Inside the host cell, HBP is converted to ADP-heptose 7-P by host-derived adenylyltransferases. Both ADP-heptose and ADP-heptose 7-P can bind to alpha-kinase 1 (ALPK1) which activates ALPK1, leading to the phosphorylation and activation of TRAF-interacting protein with forkhead-associated domain (TIFA). This results in the recruitment and activation of tumor necrosis factor receptor-associated factor 6 (TRAF6), which initiates nuclear factor kappa-light-chain-enhancer of activated B cells (NFκB) activation and the production of pro-inflammatory cytokines and chemokines. Adapted from Xue et al., 2018 [29].

1.3.2 The role of ALPK1 in inflammatory diseases

Single nucleotide polymorphisms (SNPs) in the *ALPK1* gene have been associated with several inflammatory diseases such as gout, chronic kidney disease and type 2 diabetes [30-32]. Furthermore, ALPK1 expression has been found to be elevated in peripheral blood mononuclear cells (PBMCs) of gout patients and in mucosal biopsies of patients suffering from IBD [33, 34]. Studies on gout patients have demonstrated that upregulated ALPK1 expression leads to increased phosphorylation of myosin IIA, causing an increased Golgi-derived TNFα trafficking, thereby driving inflammation [33].

In contrast, studies in mice found that ALPK1 expression is beneficial in the context of *Helicobacter hepaticus* (*H. hepaticus*) induced colitis, as ALPK1-deficient mice showed increased intestinal inflammation caused by an expansion of Th1 cells [34].

A novel heterozygous missense mutation in *ALPK1* (p.T237M) has been recently identified as the cause of the rare ROSAH syndrome, which has only been described in a small number of patients worldwide. This syndrome is named after the main clinical symptoms, which are **r**etinal dystrophy, **o**ptic nerve edema, **s**plenomegaly, **a**nhidrosis, and migraine **h**eadache [35]. Due to the fact that ROSAH patients also present a wide range of auto-inflammatory symptoms, including episodic fevers, uveitis and

arthritis, the ROSAH syndrome has been considered an auto-inflammatory disease [36, 37]. ROSAH patients typically experience a decrease in vision in childhood, associated with the presence of optic nerve edema and shortly thereafter develop other ROSAH-associated symptoms. Over time, vision loss worsens, often resulting in nearly complete blindness by the patient's third decade of life.
Until now, the mechanism by which the p.T237M mutation in *ALPK1* causes these various symptoms linked to the ROSAH syndrome is unclear. Therefore, further research is needed to better understand the disease pathogenesis of the ROSAH syndrome in order to develop targeted treatment options for ROSAH patients.

1.4 The role of IL-36 signaling in inflammatory bowel disease

1.4.1 Inflammatory bowel disease

IBD is a group of inflammatory diseases characterized by chronic and relapsing inflammation of the intestine with symptoms such as abdominal pain, diarrhea and bleeding. In Europe, approximately 1.3 million people are affected by IBD and the incidence is increasing in industrialized countries [38]. IBD is typically classified into two subtypes: Crohn's disease (CD) and ulcerative colitis (UC). CD is characterized by patchy and transmural inflammation that can affect any part of the gastrointestinal tract, but most commonly occurs in the terminal ileum and colon. In contrast, in UC the inflammation is continuous, affects only the colon and is limited to the mucosa and submucosa. Chronic inflammation in IBD can also lead to complications such as stricture formation due to fibrosis and the development of fistulas and colon-associated cancer [39]. Fibrosis and fistulas are especially relevant complications in CD as they occur in about 50% of CD patients and often require surgical intervention (**Figure 3**) [40]. Furthermore, IBD patients may experience extraintestinal symptoms that often involve the skin, joints, biliary tract or the eye [41].
The pathogenesis of IBD is still incompletely understood, but studies have shown that an interplay of environmental, genetic, microbial and immune factors are involved in the development of intestinal inflammation in IBD patients (**Figure 3**). Genetic factors include rare monogenic disease variants and over 200 risk loci identified by genome-wide association studies (GWAS) [42]. Monogenic disease variants, such as mutations in IL-10 and the IL-10 receptor, cause rare and severe cases of very-early-onset IBD. On the other hand, risk loci identified by GWAS are more frequently found in IBD patients, but their effect is usually very small and their functional role is largely unknown [43].
Research on the genetic factors of IBD, as well as studies in mouse models of IBD and in patient samples, have greatly improved our understanding of IBD, by identifying several factors in immune regulation and immune-epithelial crosstalk as critical for maintaining intestinal homeostasis. This data has led to the development of several new therapies in recent years, targeting specific molecules, such

as TNFα and IL-23 or blocking the migration of immune cells [39]. However, the therapeutic success rate of those treatments is around 30-40 % and markers to predict which therapy will be efficient in which patients are still lacking [44]. This indicates that IBD is more heterogeneous than the traditional UC and CD classification suggests, and different patient groups may have distinct disease pathogenesis [45]. Therefore, additional research is required to identify further pathways involved in IBD and predictors of clinical response to enable targeted, personalized and effective treatment of IBD patients.

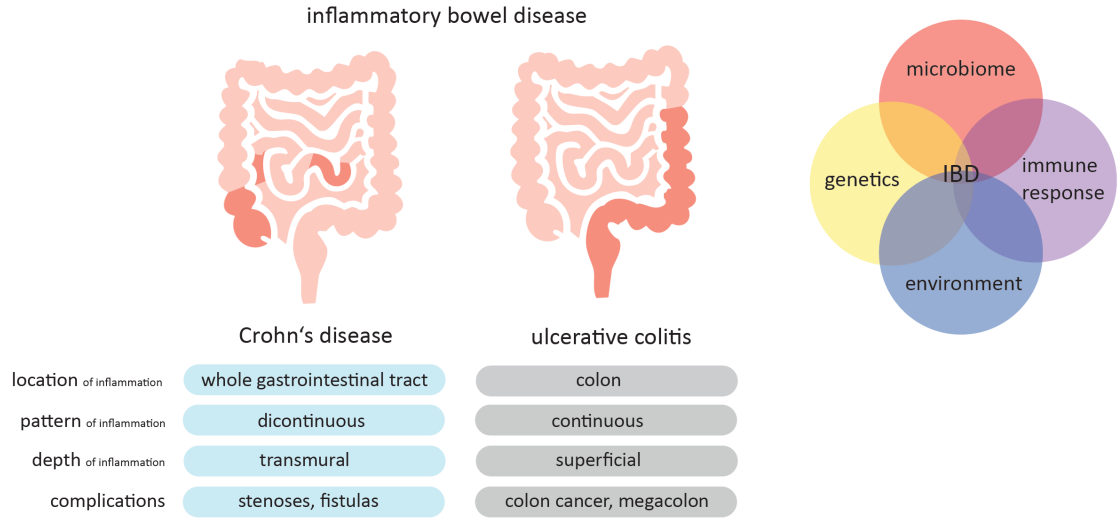

Figure 3: Characteristics and pathogenesis of inflammatory bowel disease.
Left panel: Inflammatory bowel disease (IBD) can be divided into its main subtypes Crohn's disease (CD) and ulcerative colitis (UC). CD is characterized by discontinuous and transmural inflammation that can affect any part of the gastrointestinal tract and can lead to the development of intestinal stenoses and fistulas. UC is characterized by a continuous, superficial inflammation, which is restricted to the colon. Complications include the development of colon cancer and a megacolon. Right panel: The pathogenesis of IBD involves the interplay of several factors including genetics, the microbiome, the environment and defects in the immune response.

1.4.2 The IL-36 cytokine family

The Interleukin (IL) -36 family belongs to the IL-1 family and consists of three agonists called IL-36α, IL-36β and IL-36γ and the natural antagonist IL-36RA. The IL-36 receptor (IL-36R) is a heterodimer composed of the receptor subunit IL-1 receptor-like 2 (IL-1RL2) and the co-receptor IL-1 receptor accessory protein (IL-1RAcP) [46]. Binding of IL-36α, IL-36β and IL-36γ to the extracellular domain of IL-1RL2 leads to the recruitment of IL-1RAcP and subsequently to the interaction of the intracellular Toll/IL-1 receptor (TIR) domains of both receptor subunits. This causes the recruitment of several adaptor molecules, such as myeloid differentiation primary response 88 (MyD88) and IL-1R-associated kinases (IRAK) 1 and 4, which then interact with TRAF6. This ultimately leads to the activation of NFκB and mitogen-activated protein kinases (MAPK), including c-Jun N-terminal kinases

(JNKs), extracellular signal-regulated kinases (ERKs) and p38, resulting in the activation of multiple transcription factors such as NFκB and activator protein 1 (AP-1) and the production of various cytokines such as TNFα and IL-6 [46, 47]. In contrast, binding of IL-36RA to IL-1RL2 does not cause the recruitment of IL-1RAcP and therefore does not initiate a signaling response (**Figure 4**) [48].

Furthermore, it has been shown that IL-38, another member of the IL-1 family, can also act as an IL-36R antagonist similar to IL-36RA [49].

IL-36 isoforms as well as the IL-36R are expressed in a variety of tissues, including synovial, cardiac, neural and lymphatic tissues and by a wide range of cells, most notably myeloid cells, epithelial cells and fibroblasts [50]. Expression of IL-36 isoforms can be induced by IL-36 itself, but also by other cytokines such as IL-17 and TNFα and by bacterial components such as LPS [51, 52]. Unlike other cytokines of the IL-1 family, cytokines of the IL-36 family lack a caspase-1 cleavage site necessary for activation and secretion of IL-1 cytokines. Therefore, the mechanism by which IL-36 cytokines are secreted remains unclear [50]. *In vitro* studies have shown that IL-36α, IL-36β, IL-36γ and IL-36RA require N-terminal truncation for their full activity. However, it is currently unknown, which proteases are involved in the N-terminal truncation and whether this process is associated with the secretion of the respective cytokines [53].

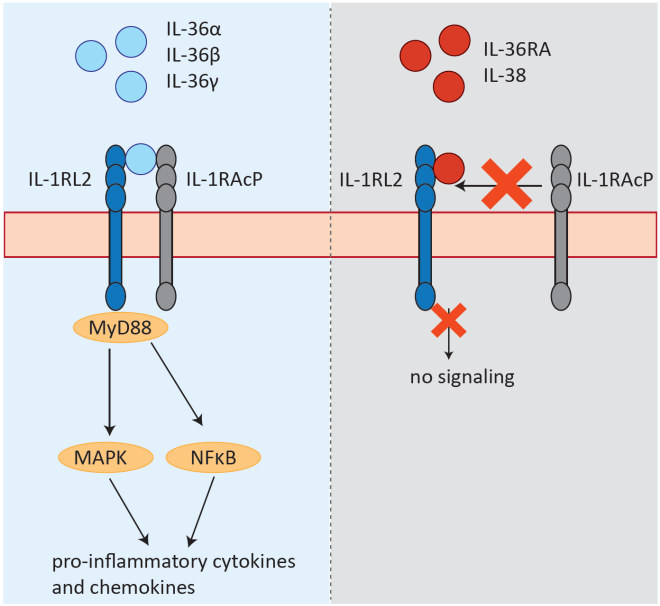

Figure 4: IL-36 signaling.
Binding of IL-36α, IL-36β and IL-36γ to the extracellular domain of IL-1 receptor-like 2 (IL-1RL2) leads to the recruitment of IL-1 receptor accessory protein (IL-1RAcP) and subsequently to the interaction of the Toll/IL-1 receptor (TIR) domains of both receptor subunits. This causes the recruitment of adaptor molecules, such as myeloid differentiation primary response 88 (MyD88), leading to the activation of nuclear factor kappa-light-chain-enhancer of activated B cells (NFκB) and mitogen-activated protein kinase (MAPK) signaling cascades. In contrast, binding of the IL-36 receptor antagonist (IL-36RA) and IL-38 to IL-1RL2 does not cause the recruitment of IL-1RAcP and therefore does not initiate a signaling response. Adapted from Elias et al., 2021 [50].

1.4.3 The role of IL-36 signaling in immune regulation and function

IL-36 cytokines are highly expressed at sites exposed to various pathogens and antigens, such as the lung, the skin and the gut, suggesting that IL-36 signaling is involved in barrier regulation [50].

Several studies have shown that IL-36α, IL-36β and IL-36γ upregulate the expression of matrix metalloproteinases (MMPs), antimicrobial peptides, chemokines and pro-inflammatory cytokines in keratinocytes [54]. Similar effects have also been observed in intestinal epithelial cells, where stimulation with IL-36 agonists induces the proliferation and pro-inflammatory cytokine production of these cells [55]. Additionally, in fibroblasts, IL-36 stimulation leads to the expression of MMPs and collagens involved in tissue remodeling [56]. IL-36γ-stimulated endothelial cells upregulate the expression of cell adhesion molecules like vascular cell adhesion molecule 1 (VCAM-1) and intercellular adhesion molecule 1 (ICAM-1) and secrete pro-inflammatory chemokines such as IL-8, CC chemokine ligand (CCL) 2 and CCL20, resulting in T cell migration to the site [57].

Furthermore, IL-36 agonists have also been shown to directly or indirectly affect the gene expression and function of various immune cells.

In monocytes and macrophages, stimulation with IL-36α, IL-36β and IL-36γ induces the secretion of pro-inflammatory cytokines such as IL-1 and IL-6 [58, 59]. In T cells, IL-36 stimulation leads to increased proliferation and IL-2 production of naïve $CD4^+$ T cells. Furthermore, IL-36 together with IL-12 polarizes naïve T cells into Th1 cells and induces the production of IFNγ and IL-17 in $CD4^+$ T cells [60-62]. In B cells, IL-36 appears to play a role in plasma cell differentiation and survival [63].

Collectively, recent literature suggests that IL-36R signaling plays an important role in immune regulation, particularly in barrier regulation and tissue remodeling. IL-36RA inhibits all effects of IL-36R signaling described here, making it an important player in regulating IL-36 signaling.

1.4.4 IL-36 signaling: role in inflammatory diseases and implications for therapy

Increasing evidence suggests that IL-36 signaling is involved in pathogenesis of several inflammatory diseases including psoriasis, arthritis and IBD.

In psoriasis, the expression of IL-36α, IL-36β, IL-36γ and IL-36RA is significantly increased in skin lesions of patients and in mouse models of psoriasis [64]. Mechanistically, immune cells in psoriatic lesions produce IL-22, IL-17 and TNFα, which in turn stimulates keratinocytes to express IL-36. IL-36 expression induces the production of pro-inflammatory cytokines such as TNFα, IL-6 and IL-8 as well as the expression of Th17 cytokines by immune cells, creating a self-perpetuating cycle that fuels inflammation in the skin [51]. Therefore, IL-$36R^{-/-}$ mice are protected from imiquimod-induced psoriasis, while IL-$36RA^{-/-}$ mice showed an exacerbated pathology upon challenge with imiquimod [65].

Furthermore, homozygous and compound heterozygous mutations in the gene encoding IL-36RA (*IL36RN)* have been identified as a cause of generalized pustular psoriasis, a rare and life-threatening inflammatory skin disease characterized by multiple pustules and systemic inflammation. The specific form of the disease caused by *IL36RN* mutations is called **d**eficiency of **i**nterleukin **t**hirty-six–**r**eceptor **a**ntagonist (DITRA) [66].

In IBD, recent literature demonstrates that the expression of IL-36α and IL-36γ is significantly upregulated in the mucosa of patients with CD and UC and that IL-36α expression is particularly increased in stenotic areas [56, 67, 68]. Animal models suggest that IL-36 signaling plays a dual role in intestinal inflammation. In acute inflammation, IL-36R signaling appears to be important for wound healing, as IL-36R$^{-/-}$ mice fail to recover from acute dextran sulfate sodium (DSS)-induced colitis due to a reduced expression of IL-22 [55, 69]. However, in chronic inflammation, IL-36R signaling contributes to the development of inflammation and fibrosis as shown by the fact that IL-36R$^{-/-}$ mice and mice treated with an IL-36R blocking antibody develop less inflammation and fibrosis in chronic DSS and 2,4,6-trinitrobenzenesulfonic acid (TNBS)-induced colitis. Mechanistically, IL-36 stimulation activates intestinal fibroblasts, leading to their proliferation and to the production of extracellular matrix components that contribute to the development of fibrosis [56]. The role of IL-36 signaling in chronic intestinal inflammation is further supported by the fact that also in T cell transfer colitis, another model of chronic colitis, IL-36R$^{-/-}$ mice develop less intestinal inflammation due to a reduction in Th1 cells [62]. Overall, recent literature indicates that IL-36R signaling is important for barrier regulation and tissue repair, but may also contribute to the development of chronic inflammation. Tight regulation of the IL-36R signaling pathway is therefore crucial and represents an important therapeutic target for patients with inflammatory diseases. Therefore, a monoclonal IL-36R blocking antibody called spesolimab was developed and recently approved in the European Union for the treatment of generalized pustular psoriasis. However, more research is required to understand how IL-36 signaling is involved in the pathogenesis of IBD and whether inhibition of the IL-36R signaling pathway represents a therapeutic approach for IBD patients.

1.5 Rare mutations in the leptin-melanocortin signaling pathway lead to monogenic obesity

1.5.1 The leptin-melanocortin signaling pathway

Controlling food intake and energy balance are crucial for providing the body with enough energy while also preventing obesity and associated diseases, which are prevalent health problems in developed countries [70]. The leptin-melanocortin signaling pathway plays an important role in this process. Leptin is produced in the adipose tissue by adipocytes and the amount of circulating leptin closely

correlates with fat mass [71]. Leptin binds to the leptin receptor, which is encoded by the *LEPR* gene. The *LEPR* gene has several splice variants, but only the LepRb isoform contains the full intracellular domain important for inducing the Janus kinase (JAK)/ signal transducer and activator of transcription protein (STAT) signaling pathway [72]. The LepRb isoform is highly expressed in several regions of the hypothalamus including the arcuate nucleus (ARC). In the ARC, leptin, produced by the adipose tissue, specifically binds to proopiomelanocortin (POMC) and Agouti-related peptide (AgRP)/ neuropeptide Y (NPY) neurons, which have been shown to express the LepRb isoform [73]. In POMC neurons, this induces the cleavage of the precursor peptide POMC into different products by peptidases such as proprotein-convertase 1/3 (PC1/3). In the neurons of the ARC, POMC is cleaved into α-melanocyte-stimulating hormone (α-MSH) and β-MSH [74]. In AgRP/NPY neurons, leptin binding inhibits the secretion of AgRP and NPY. α-MSH and β-MSH bind to melanocortin receptors, including the melanocortin 4 receptor (MC4R) in the paraventricular nucleus, which leads to reduced appetite and increased energy expenditure. In the fasted state, low levels of leptin and high levels of ghrelin lead to the activation of AgRP/NPY neurons. AgRP binds to MC4R and antagonizes all effects of α-MSH and β-MSH resulting in increased appetite and decreased energy expenditure (**Figure 5**) [75].

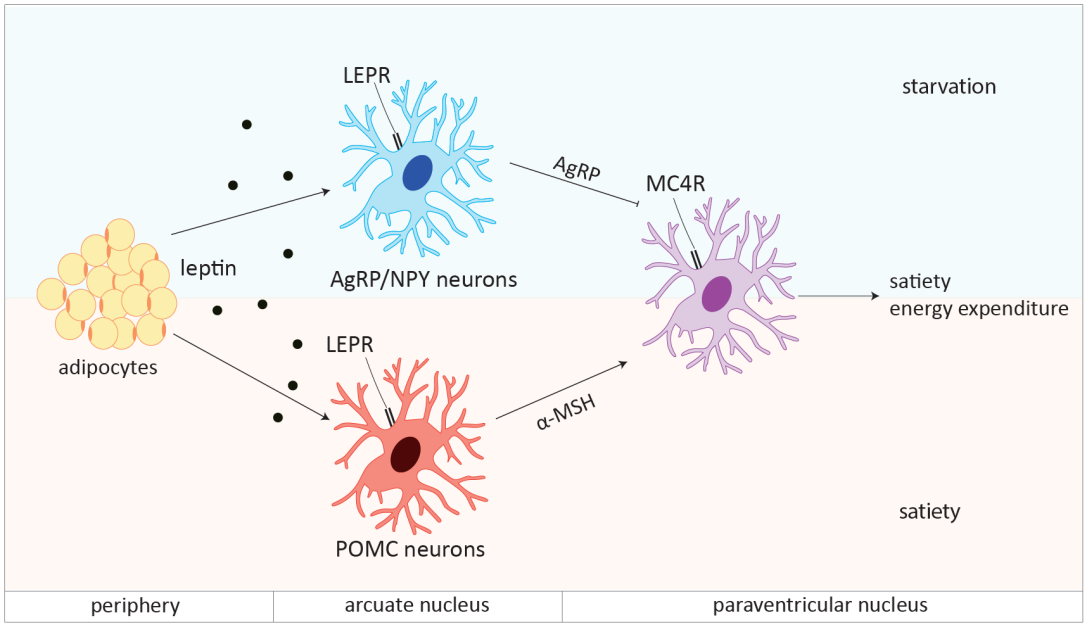

Figure 5: The leptin-melanocortin signaling pathway.
In the arcuate nucleus, leptin, produced by the adipose tissue, binds to proopiomelanocortin (POMC) and Agouti-related peptide (AgRP)/ neuropeptide Y (NPY) neurons. In POMC neurons, this induces the cleavage of the precursor peptide POMC into different products such as α-melanocyte-stimulating hormone (α-MSH) and β-MSH. In AgRP/NPY neurons, leptin binding inhibits the secretion of AgRP and NPY. α-MSH and β-MSH bind to melanocortin receptors, including the melanocortin 4 receptor (MC4R) in the paraventricular nucleus, which leads to reduced appetite and increased energy expenditure. In the fasted state, low levels of leptin and high levels of ghrelin lead to the activation of AgRP/NPY neurons. AgRP binds to MC4R and antagonizes all effects of α-MSH and β-MSH resulting in increased appetite and decreased energy expenditure. Adapted from Lavoie et al., 2023 [73].

1.5.2 Monogenic obesity

For adults, obesity is defined as a body mass index (BMI) greater than or equal to 30, while for children, a BMI greater than or equal to the 95th age and sex specific percentile is considered obese [76]. In 2022, approximately 16% of adults and 8% of children worldwide were considered obese [77, 78]. While reduced physical activity and increased caloric intake are the primary causes of obesity for most people, it has been shown that genetic factors also play a role in its development [79]. More recently, studies have revealed that single mutations in genes of the leptin-melanocortin signaling pathway can cause obesity [80]. This rare, monogenic form of obesity is characterized by severe hyperphagia and early-onset obesity. Until now, several mutations in leptin (*LEP*), the leptin receptor (*LEPR*), *POMC*, *PCSK1* (encoding PC1/3) and *MC4R* have been identified to cause monogenic obesity [81].

Patients with homozygous or compound heterozygous mutations in *LEP* and *LEPR* show early-onset obesity and hypogonadotropic hypogonadism [82].

Patients with homozygous or compound heterozygous mutations in *POMC* exhibit adrenal insufficiency and red hair pigmentation in addition to severe obesity. Red hair pigmentation is caused by the deficiency of α-MSH, which also binds to the melanocortin 1 receptor (MC1R) receptor playing an important role in regulating pigmentation. The lack of adrenocorticotropic hormone (ACTH), which is another cleavage product of POMC, leads to adrenal insufficiency [83].

Individuals with homozygous or compound heterozygous mutations in *PCSK1* suffer from severe obesity, hyperphagia, adrenal insufficiency and malabsorptive diarrhea as PC1/3 is a serine endoprotease involved in the processing of several pro-neuropeptides and pro-hormones [84].

The most common mutations causing monogenic obesity are mutations in *MC4R*, which are present in approximately 5% of obese patients. However, the majority of patients carry heterozygous variants that lead to a less pronounced phenotype in terms of hyperphagia and obesity compared to those carrying homozygous variants [85].

Due to the extreme hyperphagia observed in patients with leptin-melanocortin pathway mutations, conservative treatment strategies such as diet or physical activity are usually unsuccessful in reducing weight. Therefore, extensive research has been conducted to develop specific drugs that directly target the central leptin-melanocortin pathway. The substitution of leptin has been considered as a therapeutic option, but it has been shown to be only successful in *LEP*-mutated patients. Recently, a MC4R agonist called setmelanotide has been developed and is currently undergoing phase III clinical studies for patients with leptin-melanocortin pathway mutations. First data suggest that setmelanotide is highly effective in *POMC*-mutated patients but has only moderate effects in *MC4R*- and *LEPR*-mutated patients [85].

1.5.3 Monogenic obesity and the immune system

Obesity is associated with chronic, low-grade systemic inflammation, which can lead to comorbidities such as non-alcoholic fatty liver disease, cardiovascular disease and insulin resistance. The adipose tissue contains a wide range of different immune cells whose composition and phenotype are altered in obesity. For instance, the frequency of pro-inflammatory macrophages in the adipose tissue of obese patients is strongly increased, resulting in an increased secretion of pro-inflammatory cytokines such as IL-6 and TNFα contributing to the systemic inflammatory state observed in these patients [86, 87]. However, how the members of the leptin-melanocortin signaling pathway are involved in immune regulation and function is still under investigation. The following paragraphs will summarize the current knowledge about the members of the leptin-melanocortin pathway and their function in the immune system.

Leptin and leptin receptor

The initial description of patients with *LEP* mutations revealed that leptin deficiency is associated with a reduced frequency of $CD4^+$ T cells, as well as reduced T cell proliferation and cytokine production, which can be reversed by recombinant leptin administration [88]. Similarly, *LEPR*-mutated patients also exhibited a reduced proliferation and cytokine production of T cells, although the effects were less pronounced compared to *LEP*-mutated patients [80]. Additionally, untreated *LEP*- and *LEPR*-mutated patients experienced early deaths due to infections [89].

That leptin signaling plays an important role in immune regulation is also supported by several studies in leptin-deficient (*ob/ob*) and leptin receptor-deficient (*db/db*) mice. These mice show defects in T cell maturation and function, impaired cell-mediated immunity and a reduced susceptibility to inflammatory diseases [90-92].

Furthermore, *in vitro* and *in vivo* studies have shown that leptin receptor signaling is important for T cell proliferation and Th1 and Th17 differentiation [93-95]. In macrophages, leptin receptor signaling induces the production of pro-inflammatory cytokines and is important for phagocytosis and bacterial killing [96, 97]. In addition, the leptin receptor is also expressed on other immune cell subsets, such as B and NK cells, where leptin signaling appears to be important for cell development and cytokine production [98].

Proopiomelanocortin

POMC is a precursor peptide, which can be cleaved into eight different peptides: α-MSH, β-MSH, γ-MSH, ACTH, β-lipotropin, γ-lipotropin, corticotropin-like intermediate [lobe] peptide (CLIP) and β-endorphin.

ACTH induces the production and secretion of glucocorticoid hormones in the adrenal glands, which are important for regulating immune, cardiovascular and metabolic function. In the immune system, glucocorticoids such as cortisol have anti-inflammatory properties. For instance, studies have shown that glucocorticoids inhibit the NFκB pathway and reduce the expression of IFNγ in NK and T cells. As a result, glucocorticoids are widely used for the treatment of inflammatory diseases [99]. Patients with *POMC* mutations, however, do not have functional ACTH and therefore experience adrenal and cortisol insufficiency, which can be treated with hydrocortisone [83].

Studies have shown that also α-MSH has anti-inflammatory functions and can downregulate pro-inflammatory cytokines *in vitro* [100]. Furthermore, mice treated with α-MSH exhibit less weight loss during DSS colitis, possibly due to the interaction of α-MSH with the MC1R [101, 102].

Proprotein-convertase 1/3

In immune cells, PC1/3 is mainly expressed in macrophages. PC1/3-deficient mice show innate immune defects and increased inflammatory cytokine production after challenge with LPS. However, no similar phenotype has been observed in *PCSK1*-mutated patients [103].

Melanocortin 4 receptor

MC4R is primarily expressed in the brain, but low levels of MC4R expression have been observed in plasma cells in the spleen and thymus [104]. Despite this, no immunological symptoms have been described in *MC4R* knockout mice and *MC4R*-mutated patients so far [105, 106]. Therefore, it is unlikely that the MC4R plays a significant role in immune regulation.

In summary, the available literature suggests that members of the leptin-melanocortin signaling pathway are involved in immune regulation and function. However, as most of the data comes from experiments in mice, further research in humans is needed to fully understand their function in the human immune system.

2 Aims of this thesis

Autoimmune diseases can be caused by mutations in single genes. These rare diseases often remain undetected or poorly understood, leading to a reduced life expectancy and quality of life for patients. Studying rare diseases not only improves therapy options for patients but also provides a unique opportunity to investigate gene function in humans.

In this thesis, we investigated mechanisms of immune regulation and function by studying three rare diseases, which are discussed in detail below. Furthermore, our aim was to develop a pipeline for the diagnosis of rare diseases that combines clinical data and genetic data with functional assays to identify more specific therapies for patients with rare diseases.

Aim 1: Understand pathomechanisms of auto-inflammatory symptoms in ROSAH patients

Patients with the rare ROSAH syndrome, caused by mutations in *ALPK1*, present with symptoms of vision loss, splenomegaly, anhidrosis and migraine headaches, as well as a range of auto-inflammatory symptoms, including episodic fevers, uveitis and arthritis. However, the underlying causes of these auto-inflammatory symptoms remain unclear and effective treatments are still lacking. We here aimed to investigate the pathomechanisms of auto-inflammatory symptoms in ROSAH patients and identify potential targets for therapy.

Aim 2: Investigate the role of *IL36RN* mutations in Crohn's disease

Studies in animal models have shown that IL-36 signaling is involved in the pathogenesis of inflammatory bowel disease and increased IL-36 signaling promotes the development of intestinal inflammation and fibrosis. The IL-36 receptor antagonist, IL-36RA, plays a crucial role in regulating IL-36 signaling. While mutations in the gene encoding IL-36RA (*IL36RN*) have been associated with severe skin inflammation, their role in Crohn's disease (CD) is currently unknown. Therefore, we here investigated if *IL36RN* mutations contribute to inflammation in CD and whether the IL-36 signaling pathway might represent a potential drug target for personalized therapy of a subset of CD patients.

Aim 3: Analyze the function of the leptin-melanocortin signaling pathway in immune regulation

The leptin-melanocortin signaling pathway plays an important role in body weight regulation, and defects in this pathway can lead to rare monogenic forms of obesity. The most common defects include missense or nonsense mutations in the leptin receptor (*LEPR*), proopiomelanocortin (*POMC*) and the melanocortin-4 receptor (*MC4R*). While the effects of these mutations on the metabolism have been extensively studied, their impact on the immune system has not been analyzed in detail. We here aimed to investigate the function of LEPR, POMC and MC4R in the human immune system by characterizing the immune cell composition and function of patients with monogenic obesity.

3 Materials and methods

3.1 Materials

3.1.1 Instruments

Table 1: Instruments

Product	Company
Agarose gel electrophoresis chambers	Peqlab, Erlangen, Germany
Orbital shaker KS15 A	Edmund Bühler, Bodelshausen, Germany
Centrifuge 5810 R	Eppendorf, Hamburg, Germany
CO_2 cell culture incubators	ThermoFisher Scientific, Waltham, USA
CyTOF2 – Helios Upgrade	Standard BioTools, South San Francisco, USA
FACSCanto II	BD biosciences, Franklin Lakes, USA
Heraeus FRESCO 21 Centrifuge	ThermoFisher Scientific
HERAsafe Biological Safety Cabinet	ThermoFisher Scientific
HiSeq 3000 sequencing system	Illumina, San Diego, USA
HLC Heating Thermomixer	Ditabis, Pforzheim, Germany
Infinite F50 plate reader	Tecan, Männedorf, Switzerland
LAS-4000 Mini Fluorescence Image Analyzer	Fujifilm, Tokyo, Japan
Mini Protean System for Western blot	Biorad, Feldkirchen, Germany
NanoDrop™ 2000/2000c spectrophotometer	ThermoFisher Scientific
Primovert light microscope	Zeiss, Oberkochen, Germany
T3000 Thermocycler	Biometra, Göttingen, Germany
Laminar Wash Mini system	Curiox, Woburn, USA

3.1.2 Reagents

Table 2: Reagents

Product	Company	Catalog number
100 bp DNA ladder	Carl Roth, Karlsruhe, Germany	T835.2
Amersham ECL Western Blotting Detection Reagent	GE Healthcare Life Sciences, Chicago, USA	RPN2209
BD TMB Substrate Reagent Set	ThermoFisher Scientific	BDB555214
Benzonase® Nuclease	Sigma-Aldrich, St. Louis, USA	E1014-25KU
β-mercaptoethanol (cell culture)	Gibco, Billings, USA	31350010
Brefeldin A	Sigma-Aldrich	B7651
$CaCl_2$	Merck, Darmstadt, Germany	2382
CD14 MicroBeads, human	Miltenyi Biotec, Bergisch-Gladbach, Germany	130-050-201
Cell-ID™ Intercalator-Ir—125 µM	Standard BioTools	201192A
Chloroquine –diphosphate (salt)	Sigma-Aldrich	C6628

Dimethyl sulfoxide (DMSO)	Corning, Corning, USA	25950CQC
Ficoll® Paque Plus	Merck	17-1440-03
Formaldehyd 4%	VWR, Radnor, USA	FN-5000-10-1
HEPES buffered saline (2x)	Sigma-Aldrich	51558-50ML
Ionomycin (Iono)	Sigma-Aldrich	I0634
Lipopolysaccharide (LPS)	Sigma-Aldrich	L2630
Maxpar® Cell Staining Buffer	StandardBio	201068
OneComp eBeads™ Compensation Beads	ThermoFisher Scientific	01-1111-42
PageRuler prestained Protein Ladder	ThermoFisher Scientific	26617
Phorbol 12-myristate 13-acetate (PMA)	Sigma-Aldrich	P8139
Pierce™ methanol free formaldehyde	ThermoFisher Scientific	28906
Proteomic Stabilizer PROT1	SMART TUBE Inc., Las Vegas, USA	501351691
Q5® High-Fidelity DNA Polymerase	New England BioLabs, Ipswich, USA	M0491L
QUANTI-Blue™ solution	Invivogen, San Diego, USA	rep-qbs2
RNAlater™ solution	Sigma-Aldrich	R0901-500ML
Trypan Blue Solution 0.4% (w/v) in PBS	Corning	25-900-Ci
Trypsin-EDTA (1x) (0.05%/0.02%)	Carl Roth	9127.1
Bio-Rad Protein Assay	Bio-Rad, Hercules, USA	5000001

3.1.3 Kits

Table 3: Kits

Kit	**Company**	**Catalog number**
Cell-ID™ 20-Plex Pd Barcoding Kit	Standard BioTools	201060
DNeasy® Blood & Tissue kit	Qiagen, Hilden, Germany	69504
eBioscience™ Foxp3/Transcription Factor Staining Buffer Set	ThermoFisher Scientific	00-5523-00
EndoFree® Plasmid Purification kit	Qiagen	12362
Human Inflammatory Cytokine Cytometric Bead Array (CBA) - I Kit	BD biosciences	551811
Invisorb® Spin Plasmid Mini Two kit	Stratek, Birkenfeld, Germany	
LEGENDplex™ Human Inflammation Panel 1 (13-plex)	BioLegend, San Diego, USA	740809
NucleoSpin® Gel and PCR Clean-up kit	Macherey-Nagel, Düren, Germany	740609.50
Q5 site-directed Mutagenesis Kit	New England BioLabs	E0554

3.1.4 Software

Table 4: Software

Program	Company
Cytobank	Beckman Coulter, Brea, USA
R version 4.0.5	www.R-project.org
SnapGene Viewer 7.0	SnapGene
FlowJo V 10.06.1	FlowJo, LLC, Ashland, USA
GraphPad Prism 9	GraphPad Software,La Jolla, USA
FCAP Array™ software V3.0	BD biosciences
LEGENDplex™ Data Analysis Software	BioLegend

3.1.5 Buffers

Magnetic-activated cell sorting (MACS) buffer (10X, 100 mL)

5 g bovine serum albumin (BSA) (Fraction V) (Sigma Aldrich, 9048-46-8)

100 ml phosphate-buffered saline (PBS) (1X) (Gibco, 10010023)

Sodium dodecyl sulfate (SDS) running gel (15%, 10 mL)

3.75 mL 40% acrylamide mix (Biorad, 1610140)

2.5 mL 1.5 mM Tris base pH 8.8 (Carl Roth, 4855.2)

0.1 mL 10% SDS (Carl Roth, 2326.2)

0.1 mL 10% ammonium persulfate (APS) (Sigma-Aldrich, 7727-54-0)

0.01 mL tetramethylethylenediamine (TEMED) (Biorad, 161-0800)

3.54 mL distilled water

Stacking gel (5%) (3 mL)

0.38 mL 40% acrylamide mix (Biorad, 1610140)

0.28 mL 1.0 mM Tris base pH 6.8 (Carl Roth, 4855.2)

0.03 mL 10% SDS (Carl Roth, 2326.2)

0.03 mL 10% APS (Sigma-Aldrich, 7727-54-0)

0.003 mL TEMED (Biorad, 161-0800)

4.277 mL distilled water

Lysis buffer (1 mL)

945 µL radioimmunoprecipitation assay (Ripa) buffer (Sigma, R0278)

50 µL 20x Complete, EDTA free protease inhibitor cocktail (Roche/Merck, 11 836 170 001)

5 µL 200 mM Na_3VO_4 (activated) (Merck, S6508)

6x Lämmli loading buffer (20 mL)

1.8 g SDS (Carl Roth, 2326.2)

4.5 ml 1 M Tris-HCl pH 6.8 (Carl Roth, 9090.3)

0.015 g bromophenol blue (Merck, 8122)

7.5 ml glycerol (Carl Roth, 3783.1)

7.5 ml distilled water

+ 12.5% β-mercaptoethanol (freshly added) (Sigma-Aldrich, 60-24-2)

Electrophoresis buffer (10X, 1 L)

144 g glycine (Carl Roth, 3908.3)

30 g Tris base (Carl Roth, 4855.5)

10 g SDS (Carl Roth, 2326.2)

1 L distilled water

Transfer buffer (10x, 1 L)

144 g glycine (Carl Roth, 3908.3)

30.3 g Tris base (Carl Roth, 4855.5)

1 L distilled water

Transfer buffer (1x, 1 L)

100 mL transfer buffer (10X)

200 mL 100% methanol (Merck, 32213)

700 mL distilled water

Tris-buffered saline (TBS) pH 7.6 (10X, 1 L)

24 g Tris base (Carl Roth, 4855.2)

88 g NaCl (Carl Roth, 9265.2)

1 L distilled water

Tris-buffered saline-Tween20 (TBS-T) (1X, 1 L)

100 mL TBS pH 7.6 (10X)

1 mL Tween 20 (Carl Roth, 9127.1)

900 mL distilled water

5% Blocking buffer (50 mL)

2.5 g non-fat dry milk (Carl Roth, T145.3)

50 mL TBS-T (1X)

3.1.6 Media

Complete Roswell Park Memorial Institute Medium (complete RPMI) (for primary human cells and U937 cells)

RPMI medium 1640 (1X) (Gibco, 11875093)

10% fetal calf serum (FCS) (Sigma-Aldrich)

1% penicillin-streptomycin (ThermoFisher Scientific, 15140122)

Complete Dulbecco's Modified Eagle's Medium (complete DMEM) (for HEK 293T cells)

DMEM medium high glucose (Gibco, 41965062)

10% FCS (Sigma-Aldrich)

1% penicillin-streptomycin (ThermoFisher Scientific, 15140122)

Selection media for HEK-Blue™ IL-36 cells

DMEM medium high glucose (Gibco, 41965062)

10% FCS (Sigma-Aldrich)

1% penicillin-streptomycin (ThermoFisher Scientific, 15140122)

100 µg/mL normocin (Invivogen, ant-nr-1)

100 µg/mL zeocin (Invivogen, ant-zn-05)

10 µg/mL blasticidin (Invivogen, ant-bl-05)

Selection media for HEK-Blue™ Null1 Cells

DMEM medium high glucose (Gibco, 41965062)

10% FCS (Sigma-Aldrich)

1% penicillin-streptomycin (ThermoFisher Scientific, 15140122)

100 µg/mL normocin (Invivogen, ant-nr-1)

100 µg/mL zeocin (Invivogen, ant-zn-05)

Lysogeny broth (LB) agar (1 L)

35 g LB agar (Lennox) (Carl Roth, X965.1)

1 L distilled water

+ 100 µg/mL ampicillin (pET-*IL36RN*) (Sigma-Aldrich, 59349)

Or + 50 µg/mL kanamycin (pCMV-*IL36RN*) (ThermoFisher Scientific, 11815024)

LB broth (1 L)

20 g LB-medium (Lennox) (Carl Roth, X964.2)

1 L distilled water

+ 100 µg/mL ampicillin (pET-*IL36RN*) (Sigma-Aldrich, 59349)

Or + 50 µg/mL kanamycin (pCMV-*IL36RN*) (ThermoFisher Scientific, 11815024)

3.1.7 Antibodies

Antibodies for mass cytometry

Table 5: Antibodies for mass cytometry

Target	Metal	Clone	Company	Catalog number	Dilution
CD45	89Y	HI30	Standard BioTools	3089003B	1:100
CD19	142Nd	HIB19	Standard BioTools	3142001B	1:100
CD45RA	143Nd	HI100	Standard BioTools	3143006B	1:100
IL-4	144Nd	MP4-25D2	Standard BioTools	3142002B	1:100
CD4	145Nd	RPA-T4	Standard BioTools	3145001B	1:100
TNFα	146Nd	Mab11	Standard BioTools	3146010B	1:100
CD11c	147Sm	Bu15	Standard BioTools	3147008B	1:200
CD16	148Nd	3G8	Standard BioTools	3148004B	1:100
IL-17A	148Nd	BL168	Standard BioTools	3148008B	1:100

CD25	149Sm	2A3	Standard BioTools	3149010B	1:100
CD138	150Nd	DL-101	Standard BioTools	3150012B	1:50
CD103	151Eu	Ber-ACT8	Standard BioTools	3151011B	1:50
IL-8	151Eu	E8N1	BioLegend	511402	1:200
Fas	152Sm	DX2	Standard BioTools	3152017B	1:50
IgM	153Eu	NHM-88	BioLegend	314527	1:200
CD3	154Sm	UCHT1	Standard BioTools	3154003B	1:100
CD56	155Gd	Bd159	Standard BioTools	3155008B	1:50
IL-6	156Gd	MQ2-13AS	Standard BioTools	3156011B	1:50
IFNγ	158Gd	B27	Standard BioTools	3158017B	1:200
CCR7	159Tb	G043H7	Standard BioTools	3159003A	1:200
CD27	160Gd	0323	BioLegend	302839	1:200
IL-23	161Dy	23dcdp	Standard BioTools	3161010B	1:100
CD8α	162Dy	RPA-T8	Standard BioTools	3162015B	1:100
CD33	163Dy	WM53	Standard BioTools	3163023B	1:100
CD45RO	164Dy	UCHL1	Standard BioTools	3164007B	1:100
CD40	165Ho	5C3	Standard BioTools	3165005B	1:50
IL-2	166Er	MQ117H12	Standard BioTools	3166002B	1:100
CD38	167Er	HIT2	Standard BioTools	3167001B	1:100
CD40L	168Er	24-31	Standard BioTools	3168006B	1:100
IL-13	169Tm	JES105A2	Standard BioTools	3169016B	1:50
IL-12	170Er	REA123	Miltenyi	511005	1:50
CX3CR1	172Yb	2A9-1	Standard BioTools	3172017B	1:25
IL-17	172Yb	BL168	Standard BioTools	3172020B	1:100
HLA-DR	173Yb	L243	Standard BioTools	3173005B	1:200
PD-1	174Yb	EH12.2H7	Standard BioTools	3174020B	1:200
CD14	175Lu	M5E2	Standard BioTools	3175015B	1:200
IL-7R	176Yb	A019D5	Standard BioTools	3176004B	1:50
CD11b	209Bi	ICRF44	Standard BioTools	3209003B	1:100

Antibodies for flow cytometry

Table 6: Antibodies for flow cytometry

Target	Fluorochrome	Clone	Company	Catalog number	Dilution
CD11b	APC-Cy7	ICRF44	BioLegend	301341	1:100
CD14	APC	63D3	BioLegend	367118	1:40
CD14	FITC	61D3	eBioscience, Waltham, USA	11-0149-42	1:50
CD163	PE	GHI/63	BD biosciences	12-1639-42	1:40
CD3	PE	HIT3a	BioLegend	300308	1:100
CD4	BV510	RPA-T4	BioLegend	300546	1:40
CD45RA	PE-Cy7	HI100	BioLegend	304126	1:50
CD8	FITC	RPA-T8	BioLegend	301006	1:100
CD80	FITC	2D10.4	eBioscience	15526456	1:40
HLA-DR	PerCp-Cy5	LN3	eBioscience	45-9956-42	1:100
IFNγ	APC	4S.B3	BioLegend	502512	1:40

IL-2	APC-Cy7	MQ1-17H127	BioLegend	500342	1:50
IL-6	PE-Cy7	MQ2-13A5	BioLegend	501120	1:50
TNFα	PerCP	MAb11	BioLegend	502926	1:50
Viability dye	Zombie aqua	-	BioLegend	423102	1:1000
Viability dye	Zombie violet	-	BioLegend	423114	1:1000
Viability dye	4',6-Diamidino-2-Phenylindole, Dilactate (DAPI)	-	ThermoFisher Scientific	D1306	1:100

Antibodies for Western blot

Table 7: Antibodies for Western blot

Target	Clone	Company	Catalog number	Dilution
DYKDDDDK Tag	D6W5B	Cell Signaling, Danvers, USA	14793	1:1000
β-actin	AC-15	Sigma-Aldrich	A5441	1:2000
Goat anti-rabbit	polyclonal	Agilent, Santa Clara, USA	P0448	1:2000
Rabbit anti-mouse	polyclonal	Agilent	P0161	1:2000

3.1.8 Primers

Primers for Sanger sequencing

Table 8: Primers for Sanger sequencing

Target	Forward Primer	Reverse Primer	Annealing temperature
ALPK1	GGCAAATAGTTCATATGGAGGAA	CCTCCCAATCTCCTGAGAAA	63°C
IL36RN (S113L and L133I)	AGATGCTGAGCCTACTGAAG	TCTGACATCAGCACCTCCTC	67°C
IL36RN-2 (P76L)	TCATGACAGCTGCTGAGAAG	AGCTGCCATCAACAGAATCC	65°C

Primers for site-directed mutagenesis

Table 9: Primers for site-directed mutagenesis

Vector	Forward Primer	Reverse Primer	Annealing temperature
pCMV-*IL36RN*-L133I	GCCTGTCAGAATCACCCAGCT	TGATCGGCTTCAGGCACC	69°C
pCMV-*IL36RN*-P76L	GGGCAGGAGCTGACTCTAACA	CACCCCACATGACAGGCA	68°C
pET-*IL36RN*-L133I	GCCGGTTCGTATTACCCAGCTGC	TGATCTGCTTCCGGAACG	65°C
pET-*IL36RN*-P76L	GGTCAAGAACTGACACTGACC	AACACCACAGCTCAGACA	63°C
pET-*IL36RN*-S113L	CAGCTTTGAACTGGCAGCATATCCTGGTTG	CTGGTCAGACCCATATCAC	59°C

Primers for plasmid sequencing

Table 10: Primers for plasmid sequencing

Vector	Primer name	Sequence
pCMV-*IL36RN*	XL39	ATTAGGACAAGGCTGGTGGG
pET-*IL36RN*	T7	TAATACGACTCACTATAGGG

3.1.9 Cytokines

Table 11: Cytokines

Product	Company	Catalog number
Recombinant human IL-36α/IL-1F6 protein (with carrier)	R&D Systems, Minneapolis, USA	1078-IL-025
Human M-CSF	Peprotech, Cranbury, USA	300-25-50
Human GM-CSF	Peprotech	300-03
Recombinant human leptin	Peprotech	300-27

3.1.10 Enzyme-linked immunosorbent assay (ELISA) kits

Table 12: ELISA kits

ELISA	Company	Catalog number
Human IL-36α/IL-1F6 DuoSet ELISA	R&D Systems	DY1078-05
Human IL-36β/IL-1F8 DuoSet ELISA	R&D Systems	DY1099-05
Human IL-36γ/IL-1F9 DuoSet ELISA	R&D Systems	DY2320-05
Human IL-36RA/IL-1F5 DuoSet ELISA	R&D Systems	DY1275-05
Human interleukin 1 family, member 5 (delta) ELISA Kit	MyBioSource, San Diego, USA	MBS914111

3.1.11 Cell lines and bacterial strains

Table 13: Cell lines and bacterial strains

Cell line/bacteria strain	Company	Catalog number
HEK 293T cells	ATCC, Manassas, USA	-
HEK-Blue™ IL-36 cells	Invivogen	hkb-hil36r
HEK-Blue™ Null1 cells	Invivogen	hkb-null1
NEB 10-β competent *Escherichia coli*	New England BioLabs	C3019H
U937 cells	ATCC	-

Helicobacter hepaticus	Leibniz Institute DSMZ - German Collection of Microorganisms and Cell Cultures GmbH	22909

3.1.12 Plasmids

Table 14: Plasmids

Plasmid	Company	Catalog number
IL36RN (NM_173170) Human Tagged ORF Clone pCMV entry	Origene, Rockville, USA	RC211691
pCMV6-Entry *IL36RN* S113L Plasmid	Addgene, Watertown, USA	58321
pET-(IL36RA)	VectorBuilder, Chicago, USA	VB220506-1124dka (Vector ID)

Plasmid maps

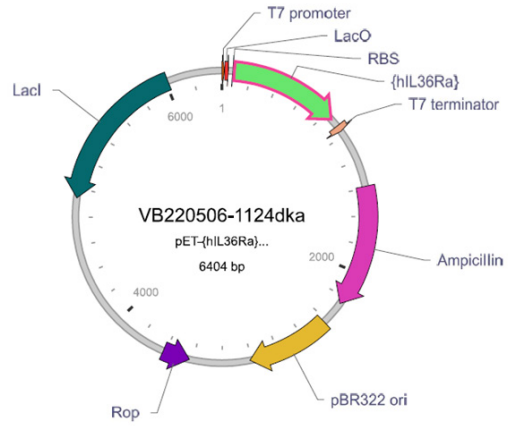

Figure 6: Plasmid map for pET-(IL36RA).

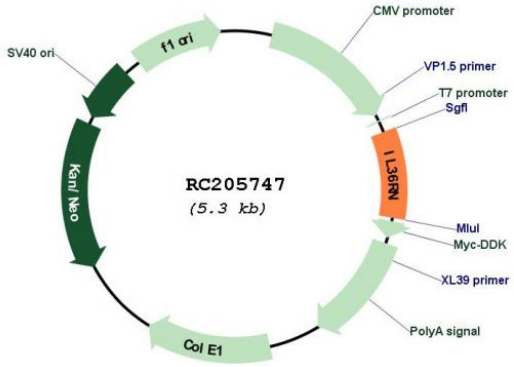

Figure 7: Plasmid map for *IL36RN* human tagged ORF Clone pCMV entry.

3.2 Methods

3.2.1 Ethical regulations

Written informed consent was obtained from all healthy volunteers and patients as approved by the institutional review board of Charité - Universitätsmedizin Berlin (EA1/200/17). All experiments involving human material were conducted in accordance to the principles set out in the WMA Declaration of Helsinki and the Department of Health and Human Services Belmont Report.

3.2.2 Cell culture

U937 cells were cultured in complete RPMI (RPMI +10% FCS +1% penicillin-streptomycin) and were split every 2-3 days. For experiments, U937 cells were differentiated with 80 nM PMA for 2 days, washed once in complete RPMI and rested two days in complete RPMI without PMA. HEK 293T cells were cultured in complete DMEM (DMEM +10% FCS +1% penicillin-streptomycin), medium was changed every 2-3 days and cells were split when 80% confluency was reached. HEK-Blue™ IL-36 cells and HEK-Blue™ Null1 cells were cultured in the respective selection media (section 3.1.6), medium was changed every 2-3 days and cells were split when 80% confluency was reached.

3.2.3 Sample collection

Approximately 36 mL whole blood was collected in heparin-lithium tubes for PBMC isolation and approximately 9 mL whole blood was collected in ethylenediaminetetraacetic acid (EDTA) tubes for genetic analysis. EDTA blood was directly frozen at -20 °C. For serum collection, blood was collected in serum tubes, allowed to clot for 1-2 h at room temperature (RT) and then centrifuged for 7 min at 1500 g at RT. Biopsies were collected in 0.9% NaCl solution. For histology, biopsies were fixed in 4% formaldehyde, subsequently embedded in paraffin and stored until further analysis. For RNA sequencing, biopsies were fixed in RNAlater (Sigma-Aldrich) and afterwards stored at -80 °C.

3.2.4 Isolation of peripheral blood mononuclear cells

PBMCs of patients were isolated by density-gradient centrifugation using SepMate™ PBMC Isolation tubes (Stemcell) and Ficoll-Paque™ PLUS (Merck) following the manufacturer's instructions. PBMCs were either used freshly or were frozen in FCS supplemented with 10% DMSO.

3.2.5 Whole exome sequencing

Deoxyribonucleic acid (DNA) was isolated either from EDTA blood or from PBMCs of patients using the DNeasy Blood & Tissue Kit (Qiagen) following the manufacturer's instructions. Whole exome sequencing and variant annotation were carried out in collaboration with the Institute of Clinical Molecular Biology, Christian-Albrechts-University Kiel. First, exome enrichment was performed using the IDT xGen Exome Research Panel v 1.0 and 2x75bp paired-end sequencing was carried out on an Illumina HiSeq 3000 sequencer. The reads were subsequently mapped against the human reference genome, converted to bam format and indexed with Samtools. PCR duplicates were removed, local realignment around InDels and base quality score recalibration were performed. Subsequently, variant calling and variant quality score recalibration was performed. Variant annotation and filtering were performed using the Alissa Interpret software (Agilent).

3.2.6 Sanger sequencing

All mutations detected by whole exome sequencing were subsequently confirmed by Sanger sequencing. For this, primer pairs were designed for each mutation and polymerase chain reaction (PCR) was performed on a T3000 Thermocycler (Biometra) using a Q5® High-Fidelity DNA Polymerase (New England BioLabs) and Q5® Reaction Buffer (New England BioLabs). The resulting PCR products were loaded onto a 1.5% agarose gel and electrophoresis was performed at 90 V for 80 min. Bands of the expected size were cut out from the agarose gel and purified with the NucleoSpin Gel and PCR Clean-up Kit (Macherey-Nagel). Isolated DNA was sent to LGC genomics for Sanger sequencing. For analysis and visualization SnapGene Viewer was used.

3.2.7 *In vitro* stimulation of PBMCs

In a 24-well plate, $1x10^6$ freshly isolated PBMCs per well were plated in 1 mL complete RPMI supplemented with 1 µL/mL β-mercaptoethanol (Gibco). Cells were either left unstimulated or subsequently treated for 4 h with either 20 ng/ml PMA (Sigma-Aldrich) and 1 µg/ml Iono (Sigma-Aldrich) or with 100 ng/ml LPS (Sigma-Aldrich). In some experiments, cells were stimulated with 1 µg/mL IL36α (R&D Systems) for 7 h. To all conditions, 5 µg/ml Brefeldin A (Sigma-Aldrich) was added for the last 4 h of the incubation period. After incubation, cells were either analyzed by flow cytometry or fixed for mass cytometry. For mass cytometry experiments, cells were supplemented with 25 units/ml benzonase (Sigma-Aldrich) during the last 15 min of stimulation. Cells were then fixed and frozen in Smart Tube buffer (SMART TUBE inc.) and stored at -80 °C until further analysis. If cytokines in the supernatant of PBMCs were analyzed, Brefeldin was not added to the cells.

3.2.8 Mass cytometry staining and analysis

Barcoding and staining for mass cytometry

Fixed PBMCs were thawed at 37°C, washed with Maxpar Cell Staining Buffer (Standard BioTools) and incubated with 25 units/mL benzonase for 20 min at 37 °C. Samples were then barcoded with six different palladium isotopes using the Cell-ID 20-Plex Pd Barcoding Kit (Standard BioTools) following the manufacturer's instructions. Additionally, half of the samples were stained with CD45-89Y for 30 min at 4 °C to barcode up to 40 samples for one run. After barcoding, samples were washed twice with Maxpar Cell Staining Buffer (Standard BioTools) and pooled afterwards. Pooled cells were washed again with Maxpar Cell Staining Buffer (Standard BioTools), and subsequently incubated with the antibody mix for cell surface staining for 30 min at 4 °C. After incubation, cells were washed twice with Maxpar Cell Staining Buffer (Standard BioTools) and then incubated with fixation/permeabilization buffer (ThermoFisher Scientific) for 60 min at 4 °C following the manufacturer's instructions. Cells were washed twice with permeabilization buffer (ThermoFisher Scientific) and subsequently incubated with the antibody mix for intracellular staining for 60 min at RT. Cells were then washed twice with permeabilization buffer (ThermoFisher Scientific) and twice with Maxpar Cell Staining Buffer (Standard BioTools). Cells were subsequently incubated overnight in 2% methanol-free formaldehyde solution (ThermoFisher Scientific). After fixation, cells were washed twice with Maxpar Cell Staining Buffer (Standard BioTools) and were incubated in iridium intercalator solution (Standard BioTools) for 60 min at RT. Cells were then washed twice with Maxpar Cell Staining Buffer (Standard BioTools) and washed with ddH_2O using the Laminar Wash Mini (Curiox). Cells were kept at 4 °C until cytometry by time of flight (CyTOF) measurement.

CyTOF measurement and data analysis

Cells were acquired on a CyTOF2 mass cytometer upgraded to Helios specifications (CyTOF2/Helios) (Standard BioTools). The instrument was tuned according to the manufacturer's instructions. EQ four element calibration beads (Standard BioTools) were added to the sample for normalization of signal changes over the time of the measurement. For data analysis, resulting flow cytometry standard (FCS) files were first normalized and then uploaded to Cytobank (www.cytobank.org) for gating of single, live cells and de-barcoding. Individual FCS files were compensated using the R package CATALYST. If several batches were analyzed together, batch normalization was performed in R using the BatchAdjust() function. Compensated files were again uploaded to Cytobank and reduced-dimensional (2D) t-SNE maps were generated. FCS files harboring the t-SNE data were downloaded from Cytobank and further analyzed using the R packages CATALYST and diffcyt. In some experiments, the t-SNE or UMAP maps were directly generated in R using the package CATALYST. For cluster identification, FlowSOM/ConsensusClusterPlus was used.

3.2.9 Flow cytometry

Cultured cells were harvested and washed once with PBS. If intracellular staining was performed, cells were first stained with the fixable live dead dyes Zombie Violet™ or Zombie Aqua™ (BioLegend) for 10 min at 4 °C to discriminate between living and dead cells. Cells were washed once in MACS buffer (0.5% BSA in PBS) and then incubated with the antibody mix for cell surface staining for 15 min at 4 °C. After incubation, cells were washed once with PBS and then fixed in fixation buffer (ThermoFisher Scientific) for 45 min at 4 °C. Cells were washed once in permeabilization buffer (ThermoFisher Scientific) and then incubated with the antibody mix for intracellular staining for 25 min at RT. After incubation, cells were washed once with MACS buffer and samples were measured with a Canto II flow cytometer (BD Bioscience) or a LSR II cell analyzer (BD Bioscience). If no intracellular staining was performed, the non-fixable live dead dye DAPI (ThermoFisher Scientific) was added for the last 2 min of the surface antibody incubation. Data was analyzed with FlowJo software package V10.6 (FlowJo, LLC).

3.2.10 Cultivation of *Helicobacter hepaticus*

H. hepaticus was prepared by Roodline Cineus (AG Hegazy). Glycerol-stocked *H. hepaticus* was grown in tryptone soya broth (TSB) supplemented with 10% FCS and Skirrow Campylobacter supplements (ThermoFisher Scientific) in anaerobic conditions. For stimulation of macrophages, *H. hepaticus* was harvested and washed twice with PBS.

3.2.11 Macrophage differentiation and stimulation

Monocytes were magnetically sorted from freshly isolated PBMCs using CD14 MicroBeads (Miltenyi Biotec) following the manufacturer's instructions. $CD14^+$ monocytes were cultured in complete RPMI for 6-7 days. For M1 polarization 1 ng/mL GM-CSF (Peprotech) was added to the culture, for M2 polarization 10 ng/mL M-CSF (Peprotech). In some experiments, 1 µg/mL recombinant human leptin (Peprotech) was added to the culture. M1 and M2 polarization was confirmed by microscopy and flow cytometry as described in section 3.2.9.

After 6-7 days of differentiation, macrophages were stimulated either with *H. hepaticus* ($20x10^6$ bacteria/mL) or LPS (100 ng/mL, Sigma-Aldrich) for 4 h at 37 °C. After incubation time, supernatant was collected and stored at -20 °C until further analysis.

3.2.12 Vector design

For overexpression experiments the pCMV6-Entry *IL36RN* plasmid (Origene) was used. pCMV6-Entry *IL36RN* S113L was a gift from Francesca Capon (Addgene plasmid #58321). For bacterial protein

expression, the human *IL36RN* sequence was codon optimized for *E. coli* and a pET-*IL36RN* plasmid was synthesized using VectorBuilder.

Mutations were introduced into the plasmids by using the Q5® Site-Directed Mutagenesis Kit (New England BioLabs) following the manufacturer's instructions. Briefly, primer pairs for the required nucleotide changes were designed, sequences were amplified and transformed into NEB 10-β competent *E. coli* (New England BioLabs). On the next day, colonies were picked and cultured overnight in 3 mL LB media with required antibiotics (section 3.1.6) at 37 °C and 170 rpm shaking. DNA was isolated with the Invisorb Spin Plasmid Mini Two Kit (Stratec) following the manufacturer's instructions and sent to LGC genomics to confirm the plasmid sequences by Sanger sequencing. Colonies with the correct sequence were grown overnight in 200 mL LB media with the required antibiotics (section 3.1.6) at 37 °C and 200 rpm shaking and DNA was isolated using the EndoFree Plasmid Maxi Kit (Qiagen).

3.2.13 Transfection

In a 6-well plate, $5x10^5$ HEK 293T cells per well were seeded in 2 mL complete DMEM. Two days after splitting, when cells reached 80% confluency, calcium phosphate transfection was performed. First, the medium was changed to 2 mL complete DMEM + 25 µM chloroquine and then the following transfection mix was prepared for each well. 2 µg of plasmid DNA was mixed with 16 µL $CaCl_2$ (2 M) and volume was adjusted to 125 µL with water. This mix was added dropwise to 125 µL 2x HEPES buffered saline, mixed to create bubbles and incubated for 5 min at RT. Finally, the mix (250 µL) was added dropwise to the cells. After 4-6 h, medium was changed and after 48 h, medium and cells were collected to analyze protein expression.

3.2.14 Western blot

Frozen cell pellets were thawed and resuspended in 100 µL RIPA buffer (Sigma-Aldrich) containing protease and phosphatase inhibitors. Samples were incubated for 30 min on ice and then centrifuged for 20 min at 14 000 g at 4 °C. Supernatant was transferred into a new vial and protein concentration was determined by Bradford assay. For SDS-PAGE, lysates were incubated with Lämmli buffer for 10 min at 95 °C before loading 20 µg protein per lane onto a 15% gel. Gels were run at 16 mA per gel for 60-90 min. After SDS-PAGE, proteins were transferred to a polyvinylidene difluoride (PVDF) membrane at 250 mA for 60-90 min in a wet tank transfer system. Membranes were blocked in TBS-T + 5% milk at RT for 1 h. After blocking, membranes were washed once in TBS-T and then incubated in the primary antibody mix at 4 °C overnight. The anti-DDK antibody (Cell Signaling) was diluted 1:1000 and the anti-β-actin antibody (Sigma-Aldrich) 1:2000 in TBS-T + 5% milk. After incubation, membranes

were washed three times in TBS-T and then incubated in the secondary antibody mix (all secondary antibodies 1:2000 in TBS-T + 5% milk) for 1 h at RT. Membranes were washed three times in TBS-T and subsequently Western blot detection reagent (GE Healthcare) was added. Detection was performed using the image analyzer LAS-4000 mini (Fujifilm).

3.2.15 Recombinant protein production

Protein production was performed in collaboration with Anja Schütz and the team of the Protein Production & Characterization Technology Platform of the Max Delbrück Center for Molecular Medicine in the Helmholtz Association (MDC), Berlin.

The IL-36RA proteins (wild type and variants) were produced using ClearColi BL21(DE3) cells (Lucigen) and Terrific Broth medium, supplemented with 100 µg/mL ampicillin. The cultures were grown at 37 °C until the OD600 reached about 1.5. Gene expression was induced by the addition of 0.5 mM isopropyl β-D-1-thiogalactopyranoside at 17 °C. After induction, cultures were grown overnight at 17 °C. Cells were harvested by centrifugation and the pellets were stored at -70 °C.

For purification, cells were resuspended in lysis buffer (50 mM Tris pH 8.0, 0.5 M NaCl, 5% glycerol), supplemented with 0.5 mM dithiothreitol (DTT), 1 mM phenylmethyl-sulfonyl fluoride and 100 µL 100 mg/mL lysozyme and 0.3 µL 850 U/µL benzonase per 100 mL total volume and lysed by sonication (SONOPULS HD 2200, Bandelin Electronic GmbH & Co. KG). The extract was cleared by centrifugation at 55 000 g and supplemented with 20 mM imidazole pH 8.0. The protein was captured from the supernatant using affinity chromatography on a 5 mL HisTrap™ FF Crude column (Cytiva), equilibrated with 20 mM Tris-HCl pH 8.0, 0.5 M NaCl and 5 mM imidazole pH 8.0. The bound protein was washed with 5 CV (column volumes) 20 mM Tris-HCl pH 8.0, 0.5 M NaCl and 20 mM imidazole pH 8.0, followed by 5 CV 20 mM Tris-HCl pH 8.0, 0.5 M NaCl and 50 mM imidazole pH 8.0 to remove contaminating proteins. The protein was eluted with 20 mM Tris-HCl pH 8.0, 0.5 M NaCl and 0.25 M imidazole pH 8.0) and supplemented with 5 mM DTT. The fusion tag was cleaved off by adding 1:70 (w/w) yeast Ulp1p SUMO protease (produced in-house) while dialyzing into 20 mM Tris pH 8.0, 0.25 M NaCl, 5 % glycerol and 1 mM DTT. The protein was supplemented with 20 mM imidazole pH 8.0 and reapplied onto the 5 mL HisTrap™ FF Crude column (Cytiva) as described above, collecting the flow through. The protein was supplemented with 5 mM DTT and further purified by gel filtration on a 26/600 Superdex 75 prep grade column (Cytiva) equilibrated with PBS buffer pH 7.4. The purified proteins were concentrated to >2 mg/mL, sterile filtered, flash-frozen in small aliquots with liquid nitrogen and stored at -70 °C until further use. The intact molecular mass of all purified constructs was confirmed by LC/MS TOF mass spectrometry.

3.2.16 ELISA

The concentration of IL-36RA in the supernatant of transfected cells was determined by using the IL-36RA ELISA from R&D Systems according to the manufacturer's instructions. The concentration of IL-36RA in the serum of patients was determined by using the IL-36RA ELISA kit from MyBioSource according to the manufacturer's instructions. Serum levels of IL-36α, IL-36β and IL-36γ in patients were measured using ELISA kits from R&D Systems according to the manufacturer's instructions.

3.2.17 Cytometry bead array

Cytokine concentrations in the supernatant of stimulated cells or in the serum of patients were measured by cytometric bead array (CBA). The human Inflammatory Cytokine CBA - I Kit (BD biosciences) or the LEGENDplex™ Human Inflammation Panel 1 (BioLegend) were used according to the manufacturer's instructions. Data was analyzed using the FCAP Array™ software V3.0 (BD biosciences) or the LEGENDplex™ Data Analysis Software (BioLegend).

3.2.18 Functional test of recombinant IL-36RA in PBMCs

In a 96-well flat-bottom plate, $1x10^5$ freshly isolated PBMCs per well were seeded in 100 µL complete RPMI. Cells were pre-incubated with 100 µg/mL recombinant IL-36RA WT or IL-36RA S113L protein for 15 min and subsequently stimulated with 100 ng/mL IL-36α for 7 h. After 3 h, 5 µg/ml Brefeldin A (Sigma-Aldrich) was added to all wells. After the incubation time, the cells were analyzed by flow cytometry.

3.2.19 Functional test of recombinant IL-36RA in HEK-Blue™ IL-36 cells

HEK-Blue™ IL-36 cells were trypsinized, counted and resuspended in selection media to obtain a cell solution of $2.8x10^5$ cells/mL. 180 µL of this cell solution was plated per well in a 96-well flat-bottom plate. For IL-36RA WT, IL-36RA S113L, IL-36RA P76L and IL-36RA L133I proteins, serial dilutions from 100 µg/mL to 10 ng/mL were performed. The cells were then pre-incubated with 20 µL of these dilutions for 15 min and subsequently stimulated with 10 ng/mL IL-36α for 18 h. After the incubation time, supernatant was collected and 20 µL of the supernatant was incubated with 180 µL QUANTI-Blue™ solution (Invivogen) for 30 min at 37 °C. Optical density (OD) was measured at 630 nm with an Infinite F50 plate reader (Tecan).

3.2.20 Boiling assay

In a 96-well flat-bottom plate, $5x10^4$ U937 cells per well were seeded and differentiated as previously described (section 3.2.2). IL-36RA WT, IL-36RA S113L, IL-36α and LPS were boiled at 95 °C for 30 min and afterwards cooled to RT. 100 µg/mL IL-36RA (boiled or native), 100 ng/mL IL-36α (boiled or native) or 100 ng/ml LPS (boiled or native) were added to the differentiated U937 cells and incubated for 7 h. Supernatant was collected and analyzed by CBA.

3.2.21 Modeling of IL-36RA by AlphaFold

The modeled structure of the human IL-36RA was downloaded as PDB files from AlphaFold (https://AlphaFold.ebi.ac.uk/), which was last updated in AlphaFold DB version 2022-11-01 and created with the AlphaFold Monomer v2.0 pipeline [107, 108]. The file was loaded into the PDB viewer (https://www.rcsb.org/3d-view) and loop domains and critical residues for receptor interactions were annotated based on Dunn et al. [109] and Onoufriadis et al., 2011 [110].

3.2.22 Statistics

Statistical tests were performed with either GraphPad Prism or R. The statistical test used and the number of replicates are stated in the figure legends. Significant p-values are indicated as **** $p < 0.0001$, *** $p < 0.001$, ** $p < 0.01$, * $p < 0.05$.

4 Results

4.1 Aim 1: Understand pathomechanisms of auto-inflammatory symptoms in ROSAH patients

In the first part of this thesis, we characterized the immune cell composition and function of a patient with the rare ROSAH syndrome in order to understand the mechanisms of auto-inflammatory symptoms in ROSAH patients and to identify targets for treatment.

Results of this part of the thesis have been published:
Hecker J, Letizia M, Loescher BS, Siegmund B, Weidinger C. Early Onset of TNFα-Driven Arthritis, Auto-inflammation, and Progressive Loss of Vision in a Patient with ALPK1 Mutation. J Clin Immunol. 2022;42(4):880-884. doi:10.1007/s10875-022-01214-8

4.1.1 Deep immune cell profiling of a patient with ROSAH syndrome reveals major differences in the immune cell composition

A 47-year-old female patient presented with a history of therapy-refractory, early-onset arthritis, lymphopenia, hypogammaglobulinemia and loss of vision. The patient began losing vision at the age of 11 and developed arthritis symptoms shortly thereafter. Over the years, the vision loss worsened until the patient was completely blind when she presented herself to our clinic. The arthritis symptoms were treated with several different therapeutic options, including TNFα inhibitors, the anti-CD20 antibody rituximab and JAK inhibitors, but these did not result in long-term improvement of the symptoms (**Figure 8A**). Suspecting a genetic syndrome, we performed whole exome sequencing (WES) and identified a de novo heterozygous missense mutation in the *ALPK1* gene (*ALPK1* T237M 710C>T), which we subsequently confirmed by Sanger sequencing (**Figure 8B-C**). The identified mutation has been recently described as a cause of the so-called ROSAH syndrome, which is characterized by retinal dystrophy, optic nerve edema, splenomegaly, anhidrosis and migraine headaches [35]. Worldwide, only a very small number of patients with ROSAH syndrome has been reported and, to our knowledge, we have here identified the first patient with ROSAH syndrome in Germany.

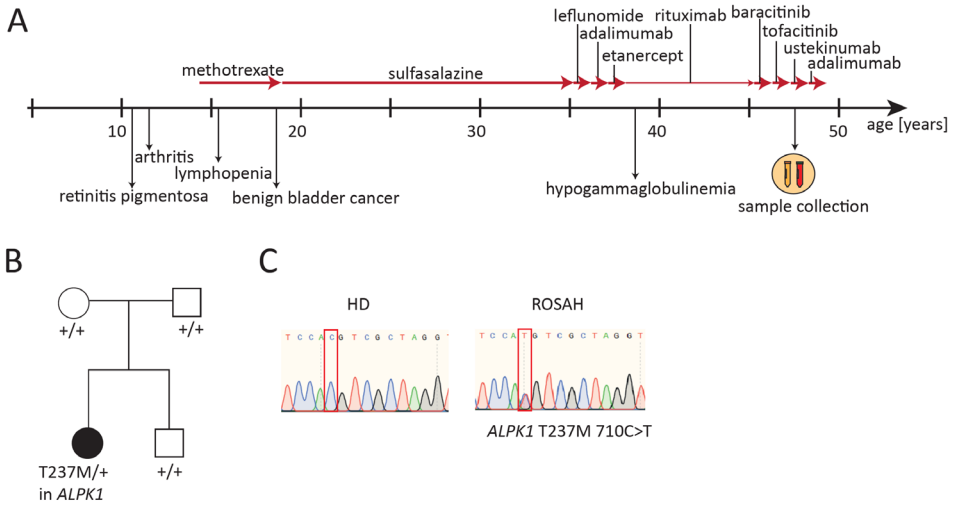

Figure 8: Identification of a mutation in *ALPK1* in a patient with vision loss and therapy-refractory arthritis. **(A)** Summary of the clinical history of the ROSAH patient. **(B)** Variant status in the *ALPK1* gene in the ROSAH patient, her parents and her brother as assessed by whole exome sequencing, " + " indicating the wild type allele, T237M indicating the mutated allele with missense mutation (p.T237M). **(C)** Sanger sequencing of EDTA blood of the ROSAH patient and an unrelated healthy donor (HD). The red square indicates the position of the mutation (c.710C) in the *ALPK1* gene.

As ALPK1 is a kinase involved in NFκB activation in response to Gram-negative bacteria [26], we hypothesized that the mutation in *ALPK1* could affect immune cell composition and function. Therefore, we analyzed PBMCs of our *ALPK1*-mutated patient (hereafter referred to as ROSAH patient) by mass cytometry. For mass cytometry analysis, PBMCs of the ROSAH patient and two healthy donors (HD) were *in vitro* stimulated with PMA/Iono or LPS. The samples were barcoded and pooled to reduce batch effects. The pooled sample was then stained with a panel of 35 markers, including lineage and functional markers and acquired by mass cytometry. After acquisition, the cells were gated on single, live $CD45^+$ cells and de-barcoded to obtain individual files for each sample. The files were then compensated to remove spillover between the different metal isotopes. For the analysis of $CD45^+$ PBMCs, a FlowSom clustering was performed using 16 lineage markers (CD19, CD45RA, CD4, CD11c, CD25, CD3, CD56, CCR7, CD27, CD8α, CD33, CD45RO, HLA-DR, CD14, IL-7R, CD11b). For visualization, a t-Distributed Stochastic Neighbor Embedding (t-SNE) plot was generated. The frequency of the 14 identified clusters was compared between the ROSAH patient and the HDs (**Figure 9A-C**).

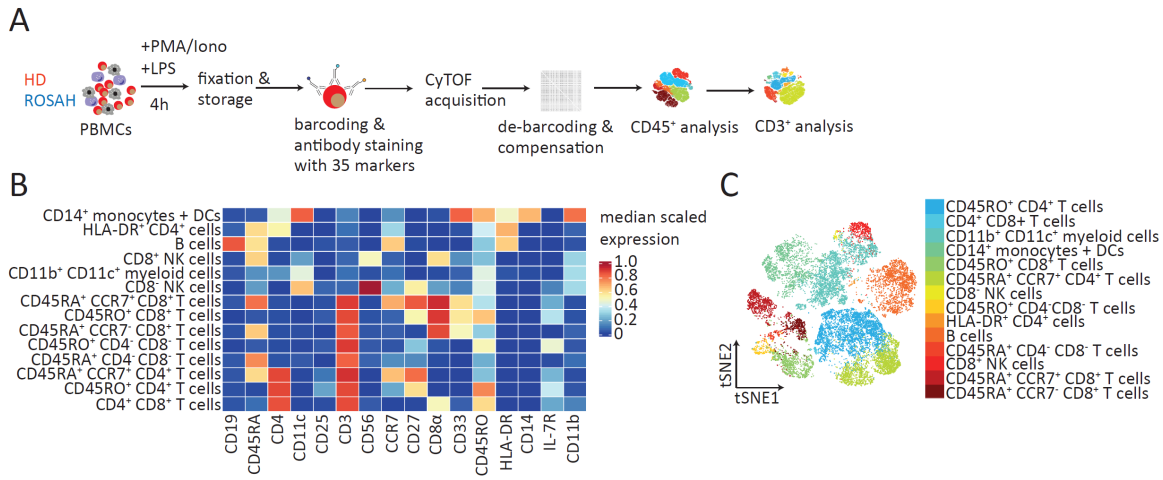

Figure 9: In-depth immune cell characterization of PBMCs of the ROSAH patient by mass cytometry.
(A) Schematic summary of the immune cell characterization of the ROSAH patient by mass cytometry. Peripheral blood mononuclear cells (PBMCs) of the ROSAH patient and two healthy donors (HD) were *in vitro* stimulated with phorbol 12-myristate 13-acetate (PMA)/ionomycin (Iono) or lipopolysaccharide (LPS) for 4 h and fixed. Subsequently, PBMCs were stained with 35 metal-conjugated antibodies and acquired by mass cytometry (CyTOF). Resulting FCS files were debarcoded, compensated and gated on $CD45^+$ cells. Following, reduced-dimensional (2D) t-SNE maps were generated, clusters were identified and differential expression and abundance was analyzed. **(B)** Heat map showing the expression of 16 selected markers used for clustering of $CD45^+$ PBMCs. **(C)** t-SNE plot colored by the 14 identified clusters.

In PBMCs of the ROSAH patient, we observed an almost complete absence of $CD19^+$ B cells and a pronounced reduction of $CD8^+$ T cells, as both the frequency of naive ($CD45RA^+$ $CCR7^+$) and activated ($CD45RO^+$) $CD8^+$ T cells was reduced. In contrast, the frequency of myeloid cell clusters ($CD11b^+$ $CD11c^+$ myeloid cells and $CD14^+$ monocytes + DCs) was increased in PBMCs of the ROSAH patient (**Figure 10A-C**). We also found that myeloid cells of the ROSAH patient produced more TNFα and IL-6 after LPS stimulation, whereas $CD4^+$ and $CD8^+$ T cells produced less TNFα and IFNγ after PMA/Iono stimulation (**Figure 10C-E**).

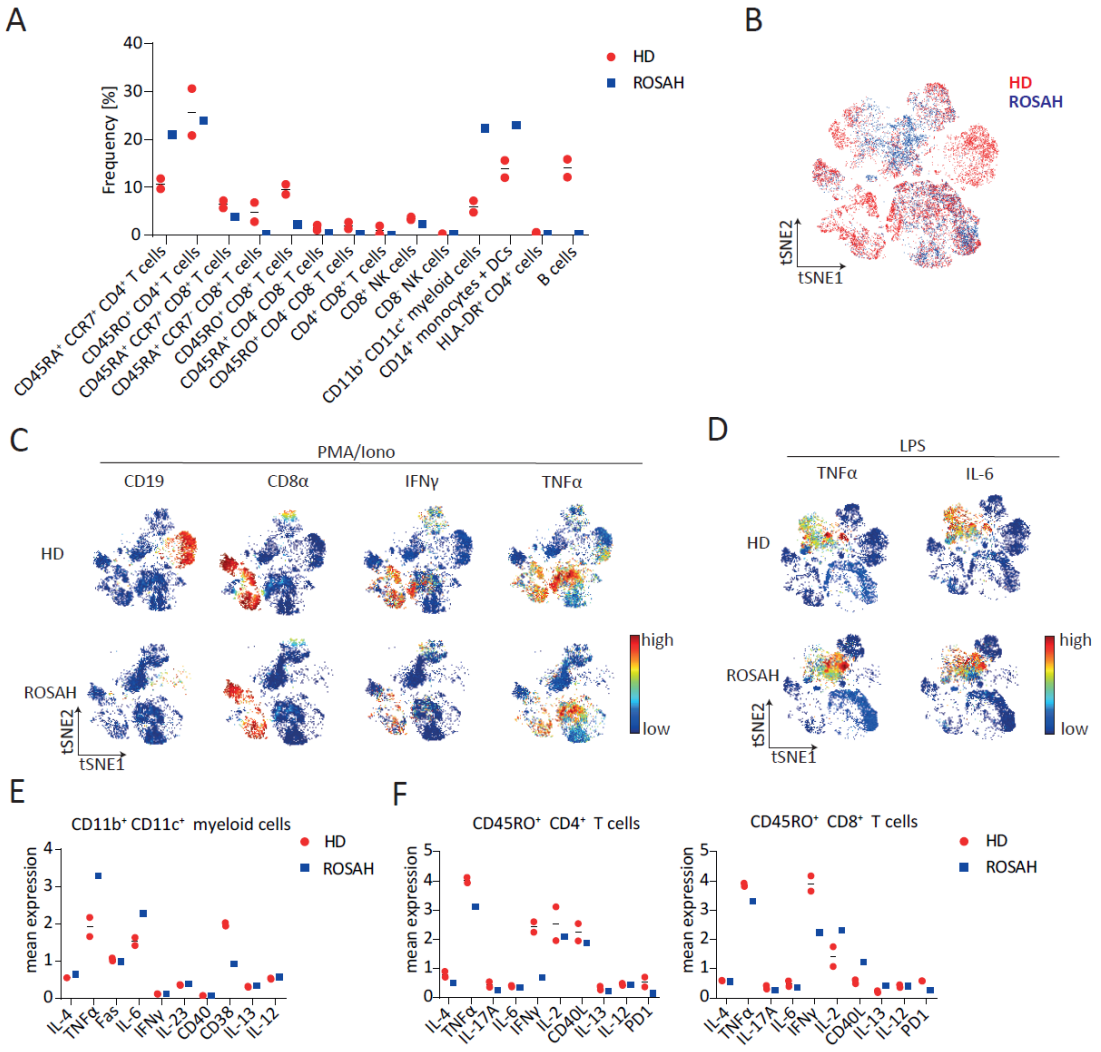

Figure 10: Mass cytometry reveals differences in B cells, T cells and myeloid cells of the ROSAH patient.
(A) Frequency of the 14 different cell clusters in phorbol 12-myristate 13-acetate (PMA)/ionomycin (Iono)-stimulated peripheral blood mononuclear cells (PBMCs). **(B)** t-SNE plot displaying the cellular distribution of CD45$^+$ cells of the ROSAH sample (blue) and two healthy donor (HD) samples (red). **(C-D)** t-SNE plots of **(C)** PMA/Iono-stimulated PBMCs or **(D)** lipopolysaccharide (LPS)-stimulated PBMCs colored by the expression of selected markers. **(E)** Mean expression of selected markers in CD11b$^+$CD11c$^+$ myeloid cells of LPS-stimulated PBMCs. **(F)** Mean expression of selected markers in CD45RO$^+$ CD4$^+$ and CD8$^+$ T cells of PMA/Iono-stimulated PBMCs. Line in the plots indicates the median.

4.1.2 Myeloid cells of the ROSAH patient show an increased expression of pro-inflammatory cytokines

To further characterize the myeloid compartment of the ROSAH patient, blood derived monocytes of the ROSAH patient and a HD were polarized *in vitro* into M1 and M2 macrophages (**Figure 11A**). Successful polarization was confirmed by flow cytometry and microscopy. No differences in polarization were found between the ROSAH patient and the HD (**Figure 11B-C**). On day 7 of differentiation, macrophages were incubated with LPS or the Gram-negative bacteria *H. hepaticus* for 24 h and cytokines in the supernatant were subsequently analyzed by CBA. We observed that M2 macrophages

of the ROSAH patient produced more IL-10 after incubation with *H. hepaticus* when compared to macrophages of the HD. We also found that macrophages of the ROSAH patient produced more IL-6 and TNFα after LPS stimulation compared to macrophages of the HD (**Figure 11D**). In conclusion, our mass cytometry and *in vitro* data suggest that the identified mutation in *ALPK1* leads to an increased production of TNFα and IL-6 in myeloid cells upon LPS stimulation, as well as to an increased production of IL-10 upon stimulation with *H. hepaticus*.

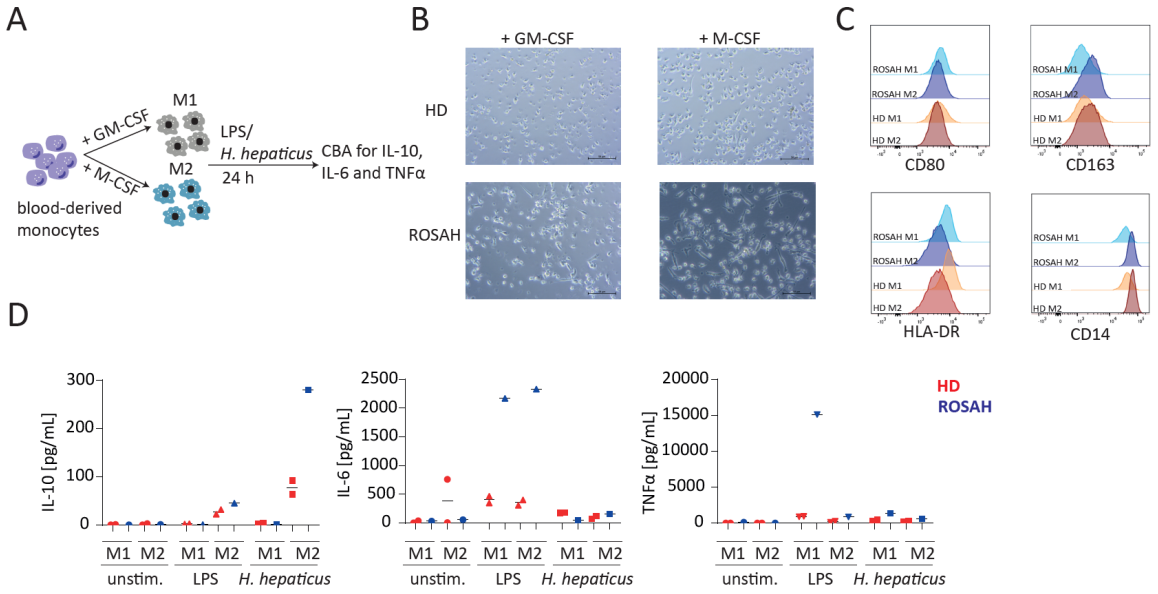

Figure 11: *In vitro* differentiated macrophages of the ROSAH patient produce higher levels of pro-inflammatory cytokines.
(A-D) Blood-derived monocytes of the ROSAH patient and one healthy donor (HD) were differentiated into M1 or M2 macrophages by supplementation of GM-CSF or M-CSF respectively for 7 days and subsequently stimulated with lipopolysaccharide (LPS) or *Helicobacter hepaticus (H. hepaticus)*. **(B)** Microscopic pictures of differentiated macrophages 6 days after start of polarization. Scale bar depicts 50 µm. **(C)** Analysis of differentiated macrophages 6 days after start of polarization by flow cytometry. **(D)** Concentrations of IL-10, TNFα and IL-6 in the supernatant of LPS- or *H.hepaticus*-stimulated or unstimulated (unstim.) macrophages. Duplicates represent technical replicates from the same HD. Line in the plots indicates the median.

4.1.3 Reduced frequencies of TNFα and IFNγ producing T cells in PBMCs of the ROSAH patient

As we had also observed differences in the T cell compartment of the ROSAH patient in the initial analysis of our mass cytometry data, we performed an additional in-depth analysis of the $CD3^+$ cells in this dataset. For this, we clustered $CD3^+$ PBMCs with 15 markers (CD45RA, IL-4, CD4, TNFα, IL-17A, CD25, IL-6, IFNγ, CCR7, CD27, CD8α, CD45RO, IL-2, IL-13, IL-7R) and identified by this 17 T cell clusters (**Figure 12A-B**). When we compared cluster abundances between the ROSAH patient and the HDs, we found that all clusters of TNFα and IFNγ expressing $CD4^+$ and $CD8^+$ T cells were reduced in the ROSAH patient (**Figure 12C-D**).

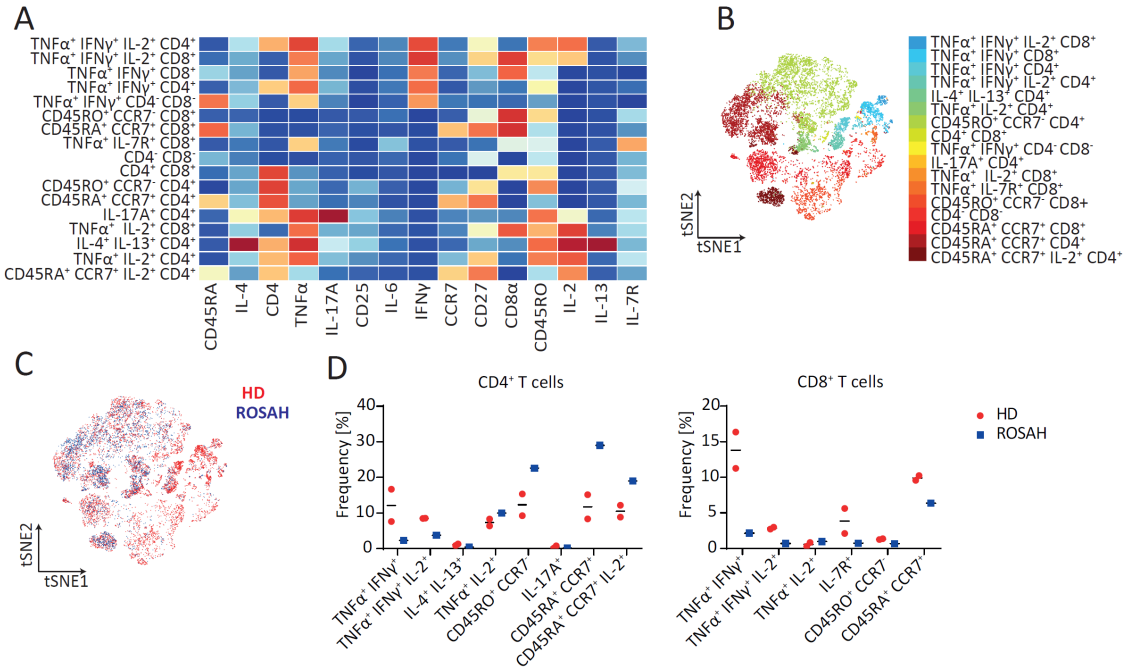

Figure 12: Analysis of the T cell compartment by mass cytometry reveals a reduced frequency of effector T cells in the ROSAH patient.

(A) Heat map showing the expression of 15 selected markers used for clustering of CD3$^+$ peripheral blood mononuclear cells PBMCs. **(B)** t-SNE plot colored by the 17 identified clusters. **(C)** t-SNE plot displaying the cellular distribution of CD3$^+$ cells of the ROSAH sample (blue) and two healthy donor (HD) samples (red). **(D)** Frequency of the CD4$^+$ and CD8$^+$ T cell clusters in phorbol 12-myristate 13-acetate (PMA)/ionomycin (Iono)-stimulated PBMCs. Line in the plots indicates the median.

To independently validate these findings, we analyzed PBMCs of the ROSAH patient and five additional HDs by flow cytometry. Similar to our mass cytometry data, we detected a decreased frequency of CD8$^+$ T cells in PBMCs of the ROSAH patient compared to HDs (**Figure 13A**). In addition, we also observed a reduced frequency of TNFα$^+$ IFNγ$^+$ CD4$^+$ and TNFα$^+$ IFNγ$^+$ CD8$^+$ T cells and a reduced expression of TNFα and IFNγ within these cells (**Figure 13B-D**). Thus, our data suggest that the identified mutation in *ALPK1* could affect T cell differentiation and cytokine production. Of note, the patient was receiving the JAK inhibitor tofacitinib at the time of sampling, which could potentially affect T cell proliferation and function [111].

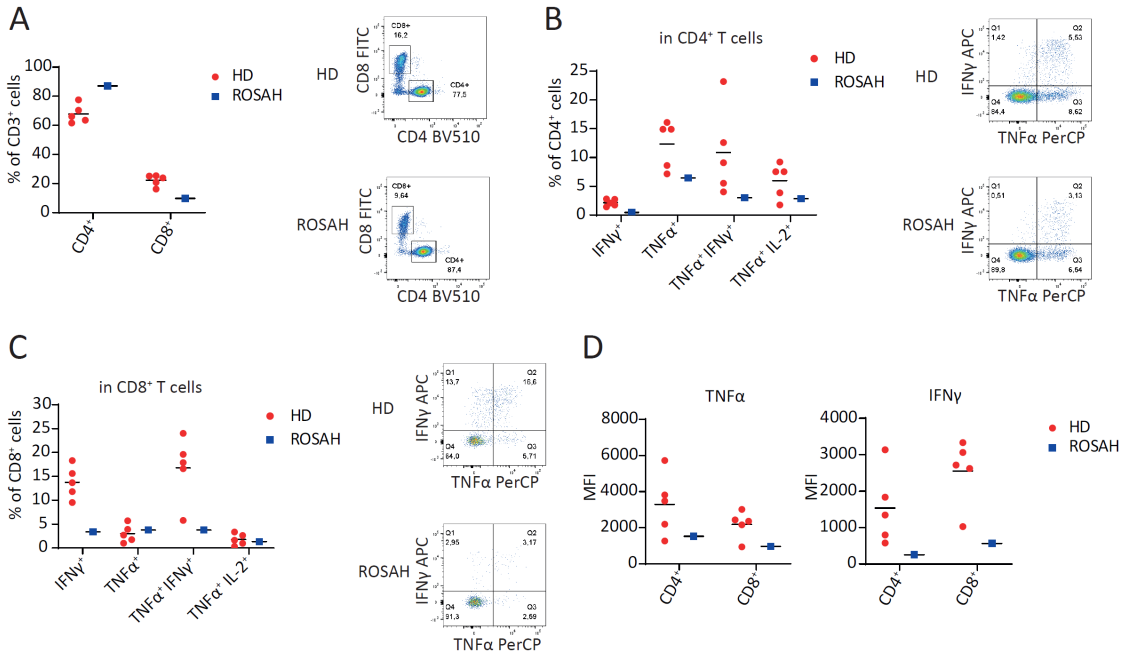

Figure 13: Confirmation of differences in the T cell compartment of the ROSAH patient by flow cytometry.
(A-D) Frozen peripheral blood mononuclear cells (PBMCs) of the ROSAH patient and healthy donors (HD) were thawed and subsequently stimulated with phorbol 12-myristate 13-acetate (PMA)/ionomycin (Iono) and analyzed by flow cytometry. **(A)** Frequency of $CD4^+$ and $CD8^+$ T cells among $CD3^+$ T cells. Representative flow cytometry plots are depicted next to the graph. **(B)** Frequency of $IFN\gamma^+$, $TNF\alpha^+$, $TNF\alpha^+$ $IFN\gamma^+$ and $TNF\alpha^+$ $IL\text{-}2^+$ cells among $CD4^+$ T cells. Representative flow cytometry dot plots are depicted next to the graph. **(C)** Frequency of $IFN\gamma^+$, $TNF\alpha^+$, $TNF\alpha^+$ $IFN\gamma^+$ and $TNF\alpha^+$ $IL\text{-}2^+$ cells among $CD8^+$ T cells. Representative flow cytometry dot plots are depicted next to the graph. **(D)** Mean fluorescence intensity (MFI) of TNFα and IFNγ in $CD4^+$ and $CD8^+$ T cells.

4.1.4 Summary aim 1

Using mass cytometry, we have here performed an in-depth characterization of the immune cell composition of a patient with ROSAH syndrome carrying a heterozygous mutation in *ALPK1* (T237M). We observed an increased expression of TNFα and IL-6 in myeloid cells of the ROSAH patient, which we subsequently confirmed by *in vitro* experiments. Direct targeting of TNFα by administration of an anti-TNFα antibody resulted in reduced joint inflammation and pain in the ROSAH patient. Based on our data, we therefore hypothesize that the *ALPK1* T237M mutation is a gain-of-function mutation leading to the overactivation of the NFκB pathway and increased pro-inflammatory cytokine production by myeloid cells, which in turn causes the auto-inflammatory symptoms observed in ROSAH patients (**Figure 14A**).

A

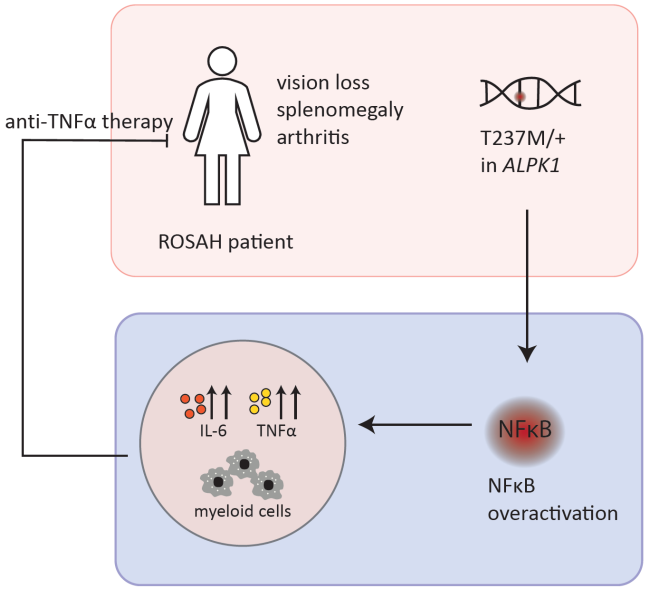

Figure 14: Summary aim 1
(A) In a patient with ROSAH syndrome caused by a heterozygous mutation in *ALPK1* (T237M), we observed an increased expression of TNFα and IL-6 in myeloid cells. Direct targeting of TNFα by administration of an anti-TNFα antibody resulted in reduced joint inflammation and pain in the ROSAH patient. Therefore, we hypothesize that the identified mutation is a gain-of-function mutation leading to the overactivation of the NFκB pathway.

4.2 Aim 2: Investigate the role of *IL36RN* mutations in Crohn's disease

In the second part of this thesis, we investigated the role of *IL36RN* mutations in Crohn' disease and explored if blocking IL-36R signaling represents a personalized therapeutic approach for patients with *IL36RN* mutations.

4.2.1 Immune cell characterization of a therapy-refractory Crohn's disease patient with a heterozygous *IL36RN* mutation

A 27-year-old female patient presented with a severe and therapy refractory form of Crohn's disease. Based on the Montreal classification, her disease was classified as A2 L3 B3p, indicating a disease onset in early adulthood (A2), a disease manifestation in ileum and colon (L3) with the development of fistulas, perianal abscesses (B3p) and intestinal stenoses. The patient was treated with all available therapeutic options for IBD patients, including immunomodulators such as azathioprine and methotrexate, biologics such as TNFα and IL-23/IL-12 antibodies and small molecules such as JAK inhibitors. The patient also underwent several bowel resections and received an autologous hematopoietic stem cell transplantation (**Figure 15A**). However, none of these interventions resulted in a long-term improvement of symptoms. In order to understand the pathogenesis of her disease and to identify targets for therapy, we performed WES of EDTA blood of this patient. By this, we identified a heterozygous missense mutation in the IL-36 receptor antagonist (*IL36RN* S113L 338C>T), which we subsequently confirmed by Sanger sequencing (**Figure 15B**). This mutation has been described in patients with pustular psoriasis, however, these patients carry either the homozygous *IL36RN* S113L variant or compound-heterozygous variants [110].

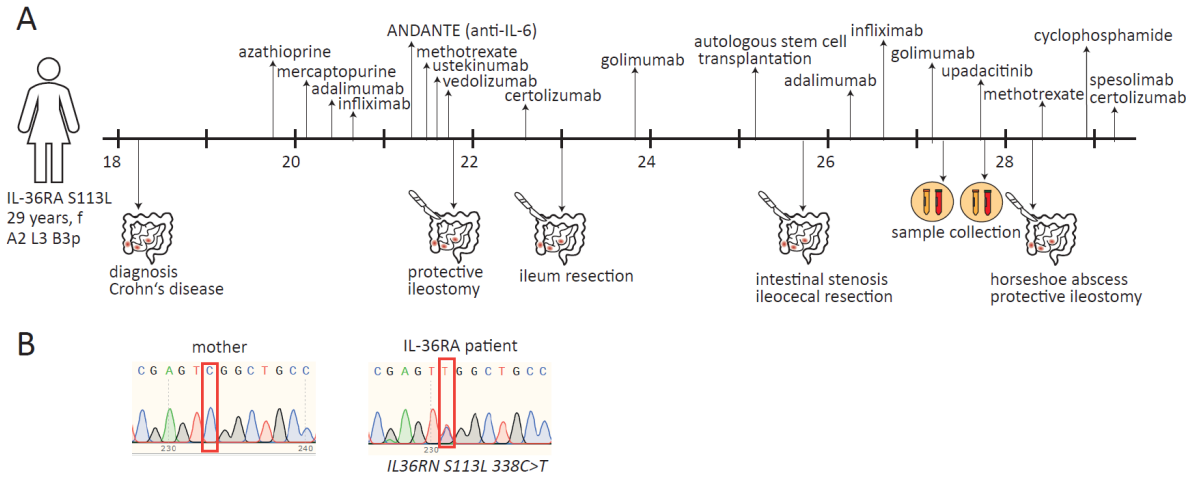

Figure 15: Identification of an *IL36RN* mutation in a therapy-refractory Crohn's disease patient.
(A) Summary of the clinical history of the *IL36RN*-mutated patient (IL-36RA patient). **(B)** Sanger sequencing of EDTA blood of the IL-36RA patient and her mother. The red square indicates the position of the mutation (c.338C) in the *IL36RN* gene. f = female.

To understand if the identified mutation causes an altered function of IL-36RA in our patient, we stimulated PBMCs of the *IL36RN*-mutated patient (hereafter referred to as IL-36RA patient) with IL-36α *in vitro* and subsequently measured cytokines in the supernatant (**Figure 16A**). In the first experiment, we found that PBMCs of the IL-36RA patient produced strongly increased levels of IL-8, IL-6 and TNFα compared to PBMCs from a HD (**Figure 16B**). However, when we repeated the experiment at a different time point, we were unable to reproduce these findings. Instead, we observed that PBMCs of the IL-36RA patient produced less pro-inflammatory cytokines compared to PBMCs from CD patients and HDs (**Figure 16C**). An important difference between the two experiments was the treatment of the IL-36RA patient. At the first time point, the patient received the anti-TNFα antibody golimumab, while at the second time point the patient was being treated with the JAK inhibitor upadacitinib.

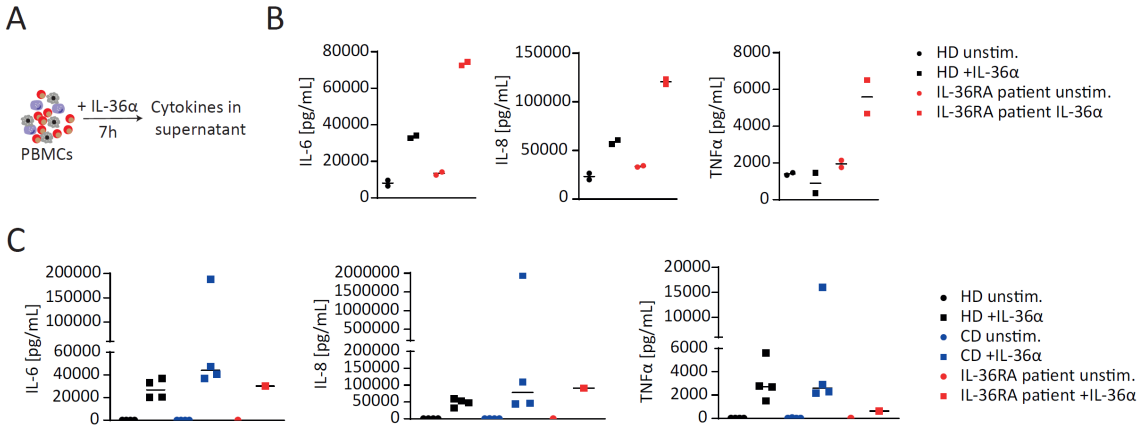

Figure 16: *In vitro* stimulation of PBMCs of the IL-36RA patient with IL-36α.
(A-C) Peripheral blood mononuclear cells (PBMCs) of the *IL36RN*-mutated patient (IL-36RA patient), healthy donors (HD) and Crohn's disease patients (CD) were *in vitro* stimulated with IL-36α for 7 h and subsequently cytokine levels in the supernatant were analyzed. **(B)** Results from experiment 1 showing concentrations of IL-6, IL-8 and TNFα in the supernatant of IL-36α-stimulated or unstimulated (unstim.) PBMCs. Duplicates represent technical replicates. **(C)** Results from experiment 2 showing concentrations of IL-6, IL-8 and TNFα in the supernatant of IL-36α-stimulated or unstim. PBMCs. Replicates represent individual patients. Line in the plots indicates the median.

Since IL-36 signaling is known to affect immune cell differentiation and function [51, 59], we hypothesized that the identified *IL36RN* mutation leads to alterations in the IL-36 signaling pathway, resulting in changes in immune cell composition and function. Therefore, we collected PBMCs and serum of the IL-36RA patient and analyzed them by mass cytometry and ELISA or CBA, respectively. In the serum, we found elevated levels of IL-36RA, IL-18 and IL-23 (**Figure 17A**). IL-36α, IL-36β and IL-36γ were also measured by ELISA, but could not be detected in any sample (data not shown). When we stimulated PBMCs from HDs with IL-36α *in vitro,* the cells secreted IL-18 and IL-23, suggesting that

these cytokines may be elevated in the IL-36RA patient due to increased IL-36 signaling (**Figure 17B-C**).

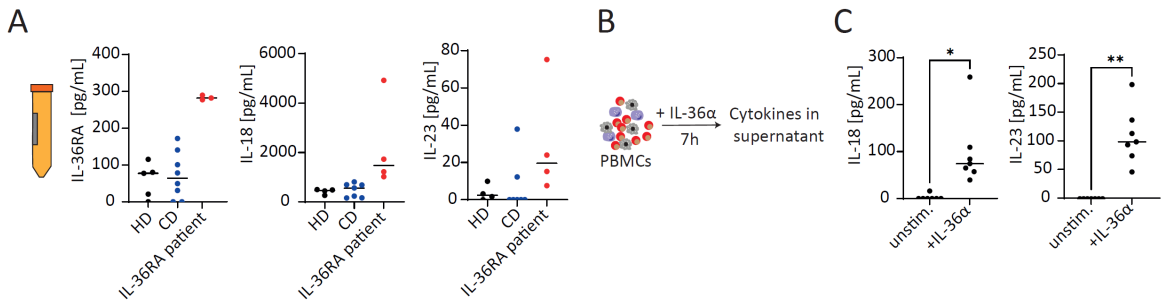

Figure 17: Increased levels of IL-36RA, IL-18 and IL-23 in the serum of the IL-36RA patient.
(A) Cytokine levels in the serum of healthy donors (HD), Crohn's disease patients (CD) and the *IL36RN*-mutated patient (IL-36RA patient) at different time points. **(B-C)** Peripheral blood mononuclear cells (PBMCs) of HDs were stimulated with IL-36α for 7 h or left unstimulated (unstim.) Subsequently, cytokine levels in the supernatant were analyzed. Line in the plots indicates the median. Statistical significance in panel C was determined by paired student's t-test. ****p<0.0001, ***p<0.001, **p<0.01, *p<0.05.

For mass cytometry analysis, PBMCs of the IL-36RA patient, three CD patients and four HDs were *in vitro* stimulated with PMA/Iono, LPS or IL-36α. The samples were acquired by mass cytometry, resulting files were gated on single, live $CD45^+$ cells, de-barcoded and compensated as previously described (**Figure 18A**). For the $CD45^+$ analysis, a FlowSom clustering was performed using 10 lineage markers (CD19, CD4, CD11c, CD16, CD3, CD56, CD8α, CD68, CD14, CD11b) (**Figure 18B-C**). The frequency of the 10 identified clusters was compared between the IL-36RA patient and the control groups. While we did not find any differences in the T cell and myeloid cell compartment of the IL-36RA patient, we detected an increased frequency of B cells and a decreased frequency of NK cells in PBMCs of the IL-36RA patient compared to HDs and CD patients (**Figure 18D**).

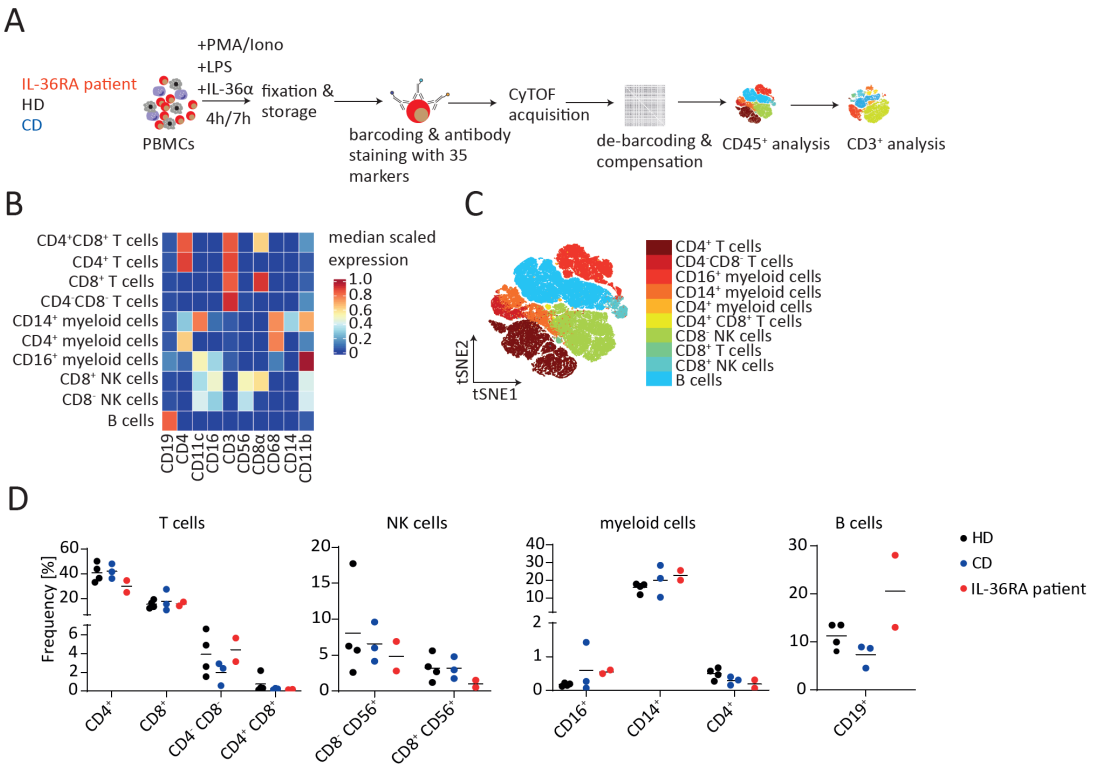

Figure 18: Mass cytometry reveals no major differences in the immune cell composition of the IL-36RA patient. **(A)** Schematic summary of the immune cell characterization of the *IL36RN*-mutated patient (IL-36RA patient) by mass cytometry. Peripheral blood mononuclear cells (PBMCs) of the IL-36RA patient at two different time points, three Crohn's disease patients (CD) and four healthy donors (HD) were *in vitro* stimulated with phorbol 12-myristate 13-acetate (PMA)/ionomycin (Iono) or lipopolysaccharide (LPS) for 4 h or with IL-36α for 7 h and fixed. Subsequently, PBMCs were stained with 35 metal-conjugated antibodies and acquired by CyTOF. Resulting FCS files were debarcoded, compensated and gated on CD45⁺ cells. Following, reduced-dimensional (2D) t-SNE maps were generated, clusters were identified, and differential expression and abundance was analyzed. **(B)** Heat map showing the expression of 10 selected markers used for clustering of CD45⁺ PBMCs. **(C)** t-SNE plot colored by the 10 identified clusters. **(D)** Frequency of the 10 different clusters in unstimulated PBMCs. Line in the plots indicates the median.

Recent literature highlights that IL-36 signaling affects the polarization of T cells by promoting the differentiation of Th17 and Th1 cells [51, 60]. Therefore, we performed a more in-depth analysis of T cells and identified 13 clusters within the CD3⁺ T cells by clustering them with 14 T cell markers (CD45RA, IL-4, CD4, TNFα, CD25, IFNγ, CCR7, CD27, CD8α, CD45RO, IL-2, IL-13, IL-17, IL-7R) (**Figure 19A-B**). Among those clusters, we detected an increased frequency of naïve CD45RA⁺ CCR7⁺ CD8⁺ T cells and CD4⁻ CD8⁻ cells in the IL-36RA patient compared to the control groups. Furthermore, we observed a slightly increased frequency of Th17 cells in the IL-36RA patient (**Figure 19C**).

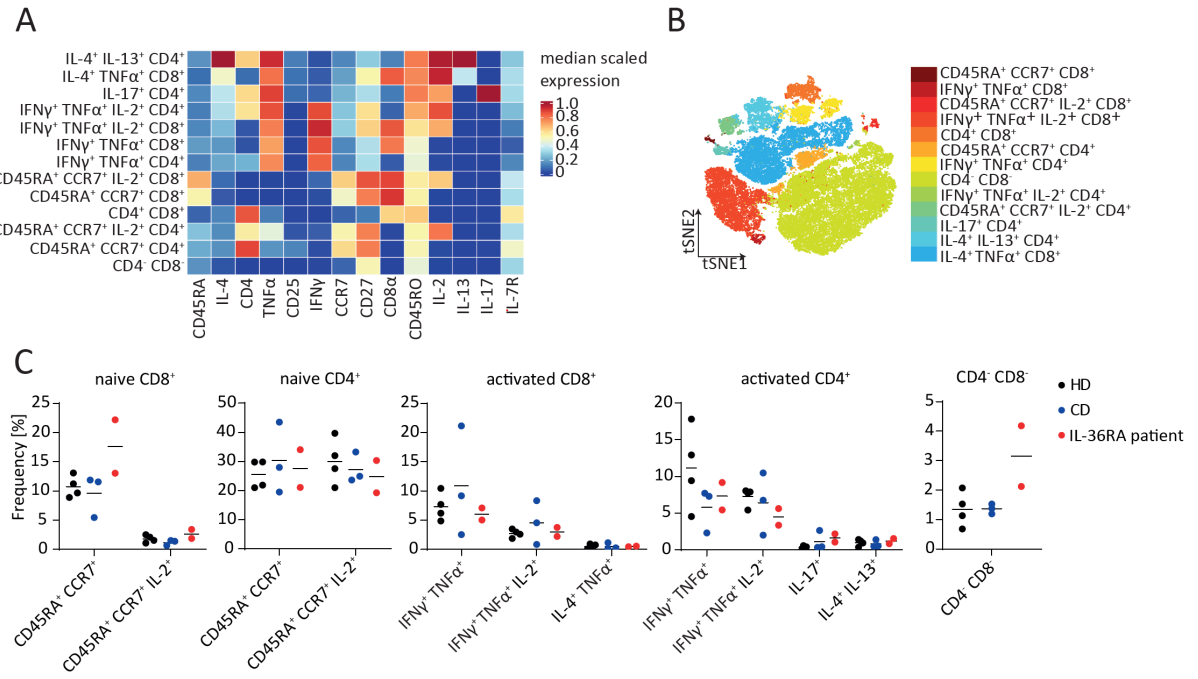

Figure 19: Characterization of the T cell compartment in the blood of the IL-36RA patient by mass cytometry. **(A)** Heat map showing the expression of 14 selected markers used for clustering of CD3$^+$ peripheral blood mononuclear cells (PBMCs). **(B)** t-SNE plot colored by the 13 identified clusters. **(C)** Frequency of the 13 different clusters in phorbol 12-myristate 13-acetate (PMA)/ionomycin (Iono)-stimulated PBMCs. Line in the plots indicates the median.

4.2.2 *IL36RN* S113L leads to a reduced protein expression

To explain how the identified *IL36RN* mutation contributes to the disease pathogenesis of the patient, it is crucial to understand how the mutation affects protein expression and function. To this end, we first analyzed the location of the mutation within the protein. We used the three dimensional structure of the human IL-36RA modeled by AlphaFold and annotated critical binding sites and loop domains according to Dunn et al. [109] and Onoufriadis et al. [110]. We found that *IL36RN* S113L is not directly located at a critical binding site, but in close proximity (**Figure 20A**). Additionally, the modeling showed that Ser113 forms hydrogen bonds with Cys70, Ala115 and Tyr116, which cannot be formed if serine is substituted with leucine (**Figure 20B**). Overall, these data suggest that the S113L mutation in *IL36RN* likely affects the protein stability.

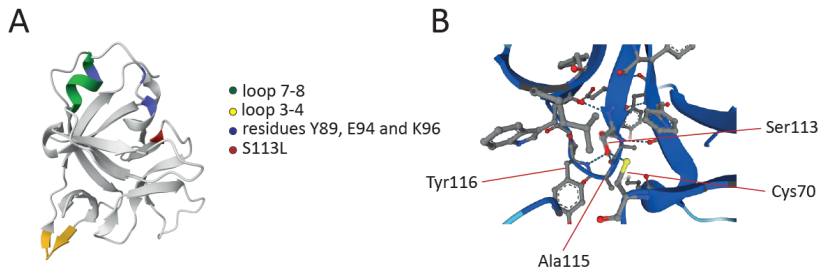

Figure 20: Modeling of IL-36RA by AlphaFold suggests effect of S113L on protein stability.
(A) Three-dimensional structure of wild type human IL-36RA modeled by AlphaFold. Loops and residues important for receptor interaction are labeled in green, yellow and blue. The location of the mutated residue Ser113 is labeled in red. **(B)** Detailed view of the structure of wild type human IL-36RA, zoomed in on the mutated residue Ser113. Important amino acids interacting with Ser113 are labeled, and dotted lines indicate hydrogen bonds.

In order to investigate the effect of the *IL36RN* S113L mutation on the protein expression of IL-36RA, we overexpressed *IL36RN* WT and *IL36RN* S113L in HEK 293T cells. For this, we used the mammalian expression vector pCMV-Entry-*IL36RN* in which IL-36RA is expressed with a C-terminal Myc-DDK tag. The construct was transiently transfected into HEK 293T cells and after 48 h supernatant and cell pellet were collected and analyzed for protein expression (**Figure 21A**). By ELISA, we found a significantly reduced concentration of IL-36RA in the supernatant of cells transfected with pCMV-Entry-*IL36RN* S113L compared to cells transfected with pCMV-Entry-*IL36RN* WT (**Figure 21B**). Since a reduced IL-36RA concentration in the supernatant could be explained either by defects in protein secretion or by low expression of IL-36RA, we also analyzed the protein content within the cells by Western blot. Here, we also found a strongly reduced expression of IL-36RA in cells transfected with pCMV-Entry-*IL36RN* S113L compared to cells transfected with pCMV-Entry-*IL36RN* WT (**Figure 21C**). In summary, these data indicate that the S133L mutation in *IL36RN* leads to a reduced protein expression.

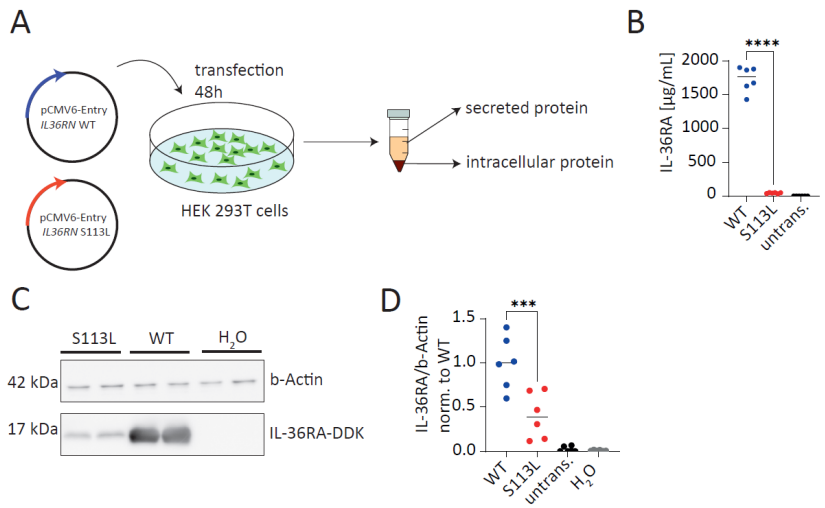

Figure 21: *IL36RN* S113L leads to a reduced protein expression.[1]

(A-C) Identified mutations were introduced into the C-terminal Myc-DDK-tagged pCMV6-Entry *IL36RN* plasmid by site-directed mutagenesis and the generated plasmids were transfected into HEK 293T cells. HEK 293T cells were either transfected with *IL36RN* wild type (WT), *IL36RN* S113L (S113L), water (H_2O) or left untransfected (untrans.) IL-36RA expression was analyzed 48 h after transfection **(B)** in the supernatant by ELISA and **(C-D)** in the cells by Western blot. The line in the plots indicates the median. Data represent three independent experiments. Statistical significance in panels B and D was determined by one-way ANOVA with Tukey's multiple comparisons test. ****p<0.0001, ***p<0.001, **p<0.01, *p<0.05.

4.2.3 Successful expression of recombinant IL-36RA S113L and IL-36RA WT

To investigate whether *IL36RN* S113L affects not only the protein expression, but also the protein function of IL-36RA, we wanted to perform functional assays with IL-36RA S113L. For this, we produced IL-36RA WT and IL-36RA S113L recombinantly in *E. coli*. In detail, we first optimized the codon sequence of human *IL36RN* for *E. coli* and removed the first base triplet coding for methionine, as it had been previously described that the removal of methionine is important for protein activity [53]. Then, we synthesized a pET vector, in which the codon optimized sequence of *IL36RN* with an N-terminal His6-SUMO-tag was introduced. The S113L mutation was introduced into the plasmid by site-directed mutagenesis. IL-36RA WT and IL-36RA S113L were then expressed in ClearColi BL21, a special strain of *E. coli*, which has a genetically modified LPS that does not induce an endotoxin response in human cells [112]. After expression, the proteins were purified and the His6-SUMO Tag was cleaved off. Protein identity was verified by SDS-page and mass spectrometry (**Figure 22A**). SDS-PAGE showed a single distinct band of the expected size of 16 kDa for both proteins produced. The exact molecular mass of the proteins was determined by mass spectrometry. IL-36RA WT had a molecular mass of 16831.28 Da and IL-36RA S113L had a molecular mass of 16857.36 Da, which can be explained by the difference in mass of serine and leucine (105 Da vs. 131 Da) (**Figure 22B-C**).

[1] Experiments in Figure 21A-D were performed by Judith Saurenbach as part of her master's thesis.

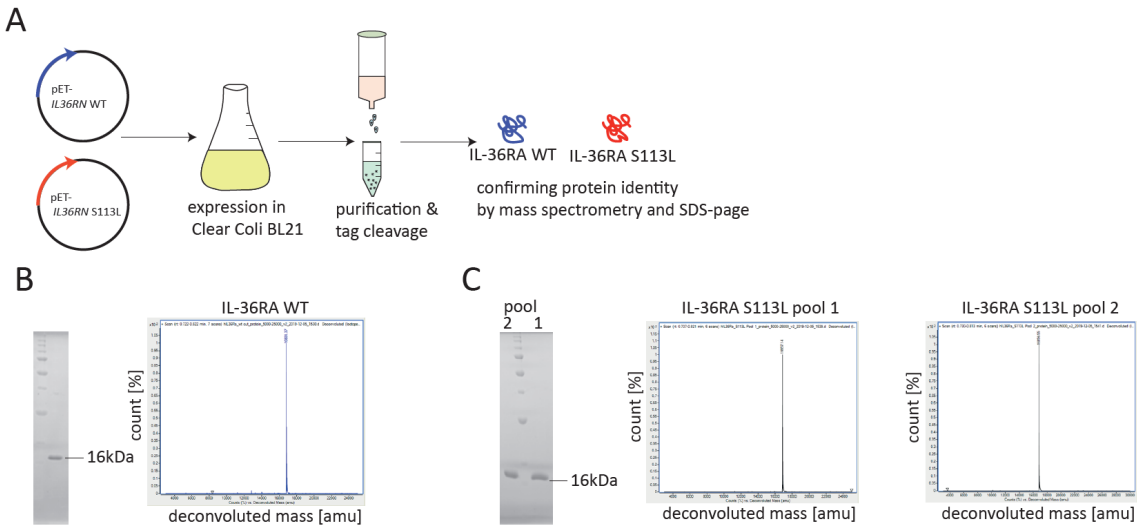

Figure 22: Successful expression of recombinant IL-36RA WT and IL-36RA S113L.[2]
(A) Experimental workflow showing the expression and purification of IL-36RA wild type (IL-36RA WT) and IL-36RA S113L. **(B)** Confirmation of the protein identity of IL-36RA WT by SDS page (left) and mass spectrometry (right). **(C)** Confirmation of the protein identity of IL-36RA S113L by SDS page (left) and mass spectrometry (right).

4.2.4 *In vitro* assays show pro-inflammatory function of recombinantly produced IL-36RA S113L

After the successful production of IL-36RA WT and IL-36RA S113L, we looked for a suitable experimental setup to test the function of IL-36RA S113L *in vitro*. Since it was not known in detail which cells respond to IL-36 stimulation and to what extent, we re-analyzed our CyTOF data and looked for cell types that respond to IL-36α stimulation. We found that only myeloid cells showed differences in marker expression after a 7 h stimulation period with IL-36α *in vitro* by upregulating IL-6 and TNFα (**Figure 23A-B**). Therefore, we decided to use primary human PBMCs and the myeloid cell line U937 for initial experiments and focused our analysis on myeloid cell markers and the pro-inflammatory cytokines IL-6 and TNFα.

[2] Experiments in Figure 22A-C were performed in collaboration with Anja Schütz and the team of the Protein Production & Characterization Technology Platform of the Max-Delbrück-Center for Molecular Medicine in the Helmholtz Association (MDC), Berlin, Germany.

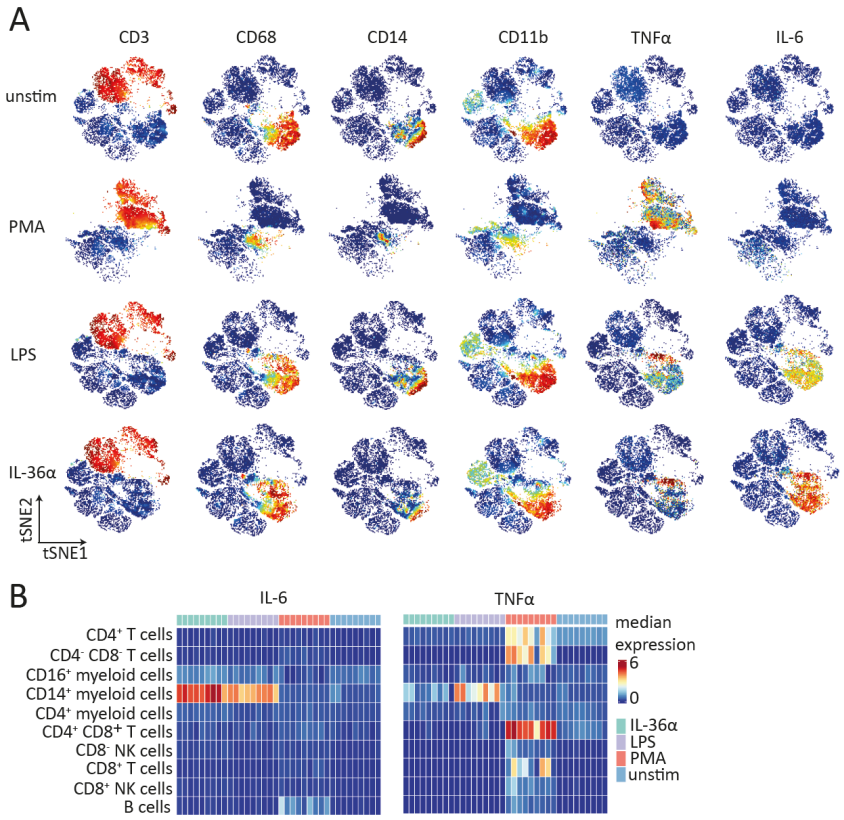

Figure 23: Myeloid cells are the main responders to IL-36α stimulation in the blood.
(A-B) Peripheral blood mononuclear cells (PBMCs) of healthy donors (HD) and Crohn's disease patients (CD) were stimulated *in vitro* with phorbol 12-myristate 13-acetate (PMA)/ionomycin (Iono), lipopolysaccharide (LPS) or IL-36α and then analyzed by mass cytometry. **(A)** t-SNE plots colored by the expression of different markers. **(B)** Heat map showing the expression of selected markers in different clusters identified in $CD45^+$ PBMCs.

Based on our CyTOF data, the following experimental setup was used to test the function of IL-36RA S113L *in vitro*. PBMCs were isolated from HDs and then pre-incubated with 100 µg/mL IL-36RA WT or IL-36RA S113L for 15 min before the addition of 100 ng/mL IL-36α. After 7 h, cells were harvested and the frequency of $TNFα^+$ $IL\text{-}6^+$ myeloid cells was determined by flow cytometry (**Figure 24A**). We found that both IL-36RA WT and IL-36RA S113L reduced the frequency of $TNFα^+$ $IL\text{-}6^+$ myeloid cells after IL-36α stimulation compared to the control with IL-36α alone. Surprisingly, we also observed that myeloid cells produced TNFα and IL-6 when IL-36RA S113L alone was added to the cells (**Figure 24B-C**). This would suggest that either IL-36RA S113L has an agonistic function similar to IL-36α or that the protein we produced was contaminated.

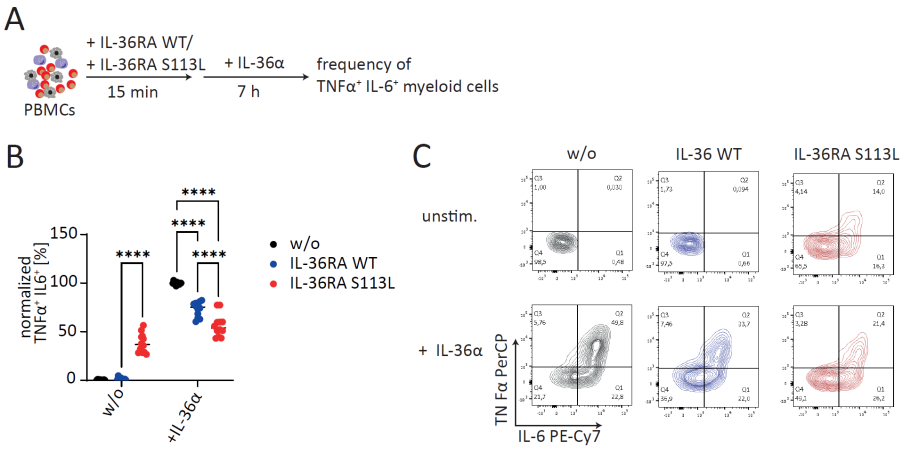

Figure 24: Recombinantly produced IL-36RA S113L has a pro-inflammatory effect.
(A-C) Peripheral blood mononuclear cells (PBMCs) of healthy donors (HD) were pre-incubated with 100 µg/mL IL-36RA wild type (IL-36RA WT) or IL-36RA S113L for 15 min and subsequently stimulated with 100 ng/mL IL-36α for 7 h. Then, the frequency of TNFα$^+$ IL-6$^+$ myeloid cells was assessed by flow cytometry. **(B)** Plot showing the frequency of TNFα$^+$ IL-6$^+$ myeloid cells measured in six HDs with technical duplicates per patient. The line in the plot indicates the median. **(C)** Representative dot plot showing the TNFα and IL-6 expression in myeloid cells. Statistical significance in panel B was determined by two-way ANOVA with Tukey's multiple comparisons test. ****p<0.0001, ***p<0.001, **p<0.01, *p<0.05.

4.2.5 Investigation of a potential contamination of recombinant IL-36RA S113L

To verify that the observed agonistic effect of IL-36RA S113L was not due to bacterial contamination with LPS in our recombinantly produced protein, we carried out two validation steps. First, an experiment was conducted in which we boiled our produced protein at 95 °C for 30 min and then tested the ability of the boiled protein to induce TNFα and IL-6 expression in the myeloid cell line U937 (**Figure 25A**). Because bacterial LPS is heat stable at high temperatures, whereas proteins denature and become non-functional [113], this experiment allowed us to determine if the observed effect is caused by LPS. We found that after boiling, IL-36RA S113L was unable to induce IL-6 production in U937 cells, whereas the boiled control LPS remained active (**Figure 25B**). These data indicate that the observed effect is not caused by an LPS contamination. As a second approach, we produced a second batch of IL-36RA S113L and compared its function to the first batch. We performed the same experiment in PBMCs as described in Figure 24. We found that the second batch of IL-36RA S113L did not induce the expression of TNFα and IL-6 in myeloid cells as observed for the first batch (**Figure 25C-D**), suggesting a contamination of the first batch with a factor other than LPS.

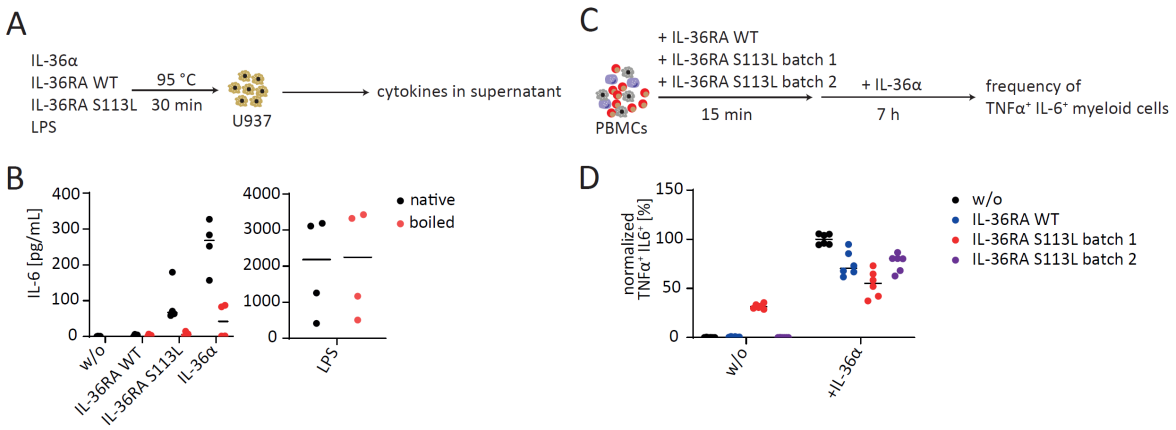

Figure 25: Investigation of a potential LPS contamination of recombinant IL-36RA S113L.
(A-B) IL-36α, IL-36RA wild type (IL-36RA WT), IL-36RA S113L and lipopolysaccharide (LPS) were boiled for 30 min at 95 °C and subsequently added to differentiated U937 cells. After 7 h, supernatant was collected and the concentration of cytokines was measured. **(B)** Plot showing the concentration of IL-6 in the supernatant of U937 cells. Data represent two independent experiments. **(C-D)** Peripheral blood mononuclear cells (PBMCs) of healthy donors (HD) were pre-incubated with 100 µg/mL IL-36RA WT or IL-36RA S113L from batch 1 or batch 2 for 15 min and subsequently stimulated with 100 ng/mL IL-36α for 7 h. Then, the frequency of TNFα$^+$ IL-6$^+$ myeloid cells was assessed by flow cytometry. **(D)** Plot showing the frequency of TNFα$^+$ IL-6$^+$ myeloid cells measured in three HDs with technical duplicates per patient. The line in the plots indicates the median.

As the data of the validation experiments remained inconclusive, we decided to test our proteins in a different experimental setup. We used HEK-Blue IL-36 cells, which overexpress the IL-36R and have an NFκB-inducible secreted alkaline phosphatase (SEAP) as reporter (**Figure 26A**). We first tested the reactivity of HEK-Blue IL-36 cells to stimulation with IL-36α and LPS. We found that increased concentrations of IL-36α led to increased NFκB activation as measured by optical density (OD) and that 10 ng/mL was the optimal concentration for the activation of HEK-Blue IL-36 cells (**Figure 26B**). Furthermore, we observed that HEK-Blue IL-36 cells did not respond to LPS stimulation. To construct a dose-response curve, HEK-Blue IL-36 cells were pre-incubated with different concentrations of IL-36RA WT or IL-36RA S113L and then stimulated with 10 ng/mL IL-36α for 18 h. After incubation of the cell supernatant with QUANTI-Blue solution, the OD representing the NFκB activity in the cells was measured and the half maximal inhibitory concentration (IC_{50}) was calculated. For IL-36RA WT and IL-36RA S113L, the NFκB activity decreased with increasing concentrations of the antagonist (**Figure 26C**). The IC_{50} was comparable between the mutant and the wild type antagonist, with 102 ng/mL for IL-36RA WT, 97.14 ng/mL for IL-36RA S113 batch 1 and 85.85 ng/mL for IL-36RA S113L batch 2 (**Figure 26D**). Furthermore, we did not detect any NFκB activation by IL-36RA S113L alone, as we had observed in PBMCs. In summary, our data show that IL-36RA S113L has a similar function to IL-36RA WT and that the effects observed in batch 1 were most likely caused by a contamination of the produced protein.

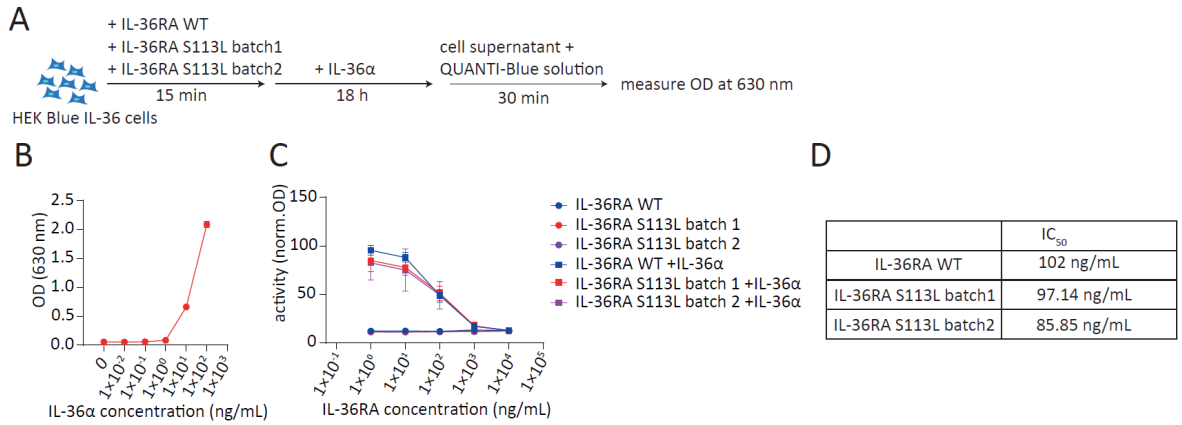

	IC_{50}
IL-36RA WT	102 ng/mL
IL-36RA S113L batch1	97.14 ng/mL
IL-36RA S113L batch2	85.85 ng/mL

Figure 26: IL-36 reporter assay shows similar function of IL-36RA WT and IL-36RA S113L.
(A-D) HEK Blue IL-36 cells were pre-incubated with different concentrations of IL-36RA wild type (IL-36RA WT) or IL-36RA S113L for 15 min and then stimulated with 10 ng/mL IL-36α for 18 h. Afterwards, the cell supernatant was incubated with QUANTI-Blue solution and the optical density (OD) was measured at 630 nm. **(B)** Graph showing the NFκB activity of HEK Blue IL-36 cells incubated with different concentrations of IL-36α for 18 h. Data are represented as mean ± SD (n = 6). **(C)** Graph showing the NFκB activity of HEK Blue IL-36 cells incubated with IL-36RA WT or IL-36RA S113L. OD values were normalized to the cells stimulated with IL-36α only. Data represent four independent experiments. Data are represented as mean ± SD (n = 8). **(D)** Half maximal inhibitory concentration (IC_{50}) for IL-36RA WT and IL-36RA S113L.

4.2.6 Anti-IL-36R therapy leads to a reduced intestinal inflammation in the IL-36RA patient

Based on the experiments, we hypothesize that the *IL36RN* S113L mutation leads to a reduced expression of IL-36RA, resulting in an overactivity of the IL-36R signaling pathway and thus to a pro-inflammatory state in our patient. We therefore contacted Boehringer Ingelheim, a company that had developed an IL-36R blocking antibody called spesolimab for the treatment of generalized pustular psoriasis and got the approval to treat our patient with spesolimab on the basis of an “individueller Heilversuch”. The patient was first treated with three cycles of cyclophosphamide followed by monthly treatment with spesolimab and biweekly treatment with certolizumab pegol, a PEGylated Fab' fragment of a humanized TNF inhibitor monoclonal antibody. Clinical data as well as PBMCs, serum and intestinal biopsies before and during the therapy were collected to assess clinical response and molecular changes caused by the treatment (**Figure 27A**). Stool levels of calprotectin, a marker for intestinal inflammation, decreased during the therapy and remained low until week 18 of treatment (**Figure 27B**). Furthermore, the simple endoscopic score for Crohn’s disease (SES-CD), which measures ulcerations and inflamed areas of the intestine, was reduced by half at week 12 of treatment compared to pre-treatment (**Figure 27C**). We also found that the concentration of IL-18 and IL-23 in the serum, which had been elevated before treatment, decreased during spesolimab treatment (**Figure 27D**).

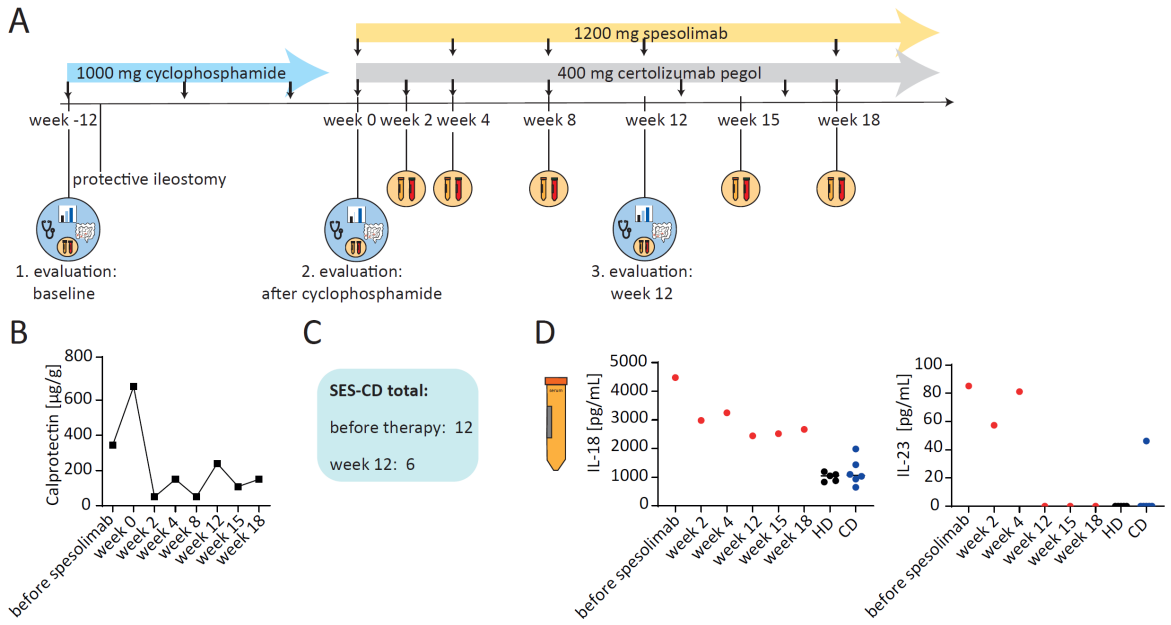

Figure 27: Anti-IL-36R therapy leads to a reduced intestinal inflammation in the IL-36RA patient.
(A) Therapy plan of the *IL36RN*-mutated patient (IL-36RA patient). **(B)** Calprotectin in the stool of IL-36RA patient during the spesolimab therapy. **(C)** Simple endoscopic score for Crohn's disease (SES-CD) measured during colonoscopy. **(D)** Cytokine levels in the serum of healthy donors (HD), Crohn's disease patients (CD) and the IL-36RA patient at different timepoints during spesolimab therapy. The line in the plots indicates the median.

4.2.7 Anti-IL-36R therapy results in a decreased frequency of pro-inflammatory monocytes

To further investigate the molecular changes induced by the therapy, we analyzed PBMCs of the IL-36RA patient before and during spesolimab therapy by mass cytometry. The experiment was performed as previously described and 11 clusters were identified within $CD45^+$ cells (**Figure 28A-B**). After cyclophosphamide treatment (week 0), the frequency of B cells decreased while the frequency of T cells increased (**Figure 28C**). From week 8 of treatment with spesolimab and certolizumab, the frequency of $CD11b^+CD11c^+$ myeloid cells and $CD16^+CD11b^+$ myeloid cells decreased and the frequency of $CD56^+$ NK cells and $CD56^+$ $CD16^+$NK cells increased (**Figure 28D**). In addition, the expression of the pro-inflammatory cytokines IL-6, IL-8 and TNFα in $CD11b^+$ $CD11c^+$ myeloid cells after IL-36α stimulation was reduced starting from week 8 of treatment (**Figure 28E**). These data demonstrate that the therapy especially targeted myeloid cells in the blood that produced less pro-inflammatory cytokines, which could contribute to the reduced intestinal inflammation observed in our *IL36RN*-mutated patient.

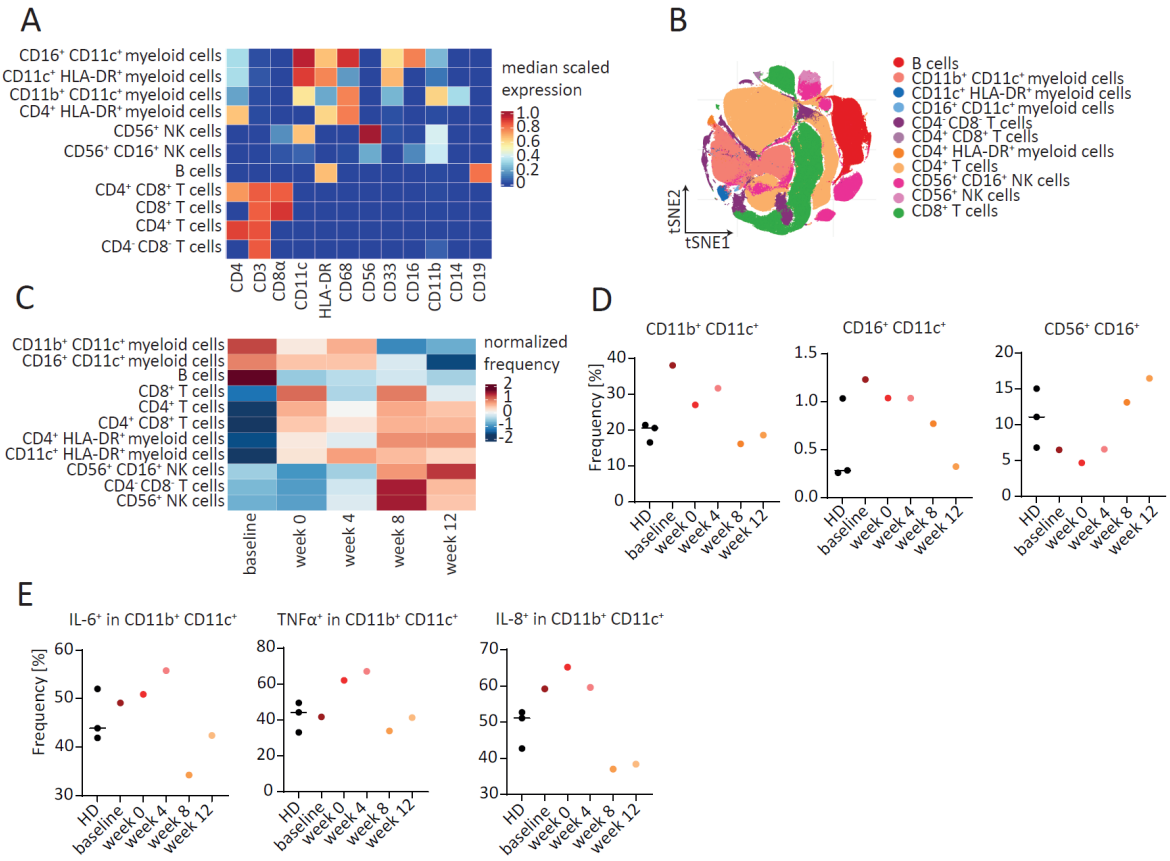

Figure 28: Anti-IL-36R therapy *in-vivo* results in a decreased expression of pro-inflammatory cytokines in myeloid cells.

(A-E) Peripheral blood mononuclear cells (PBMCs) of the *IL36RN*-mutated patient (IL-36RA patient) at different time points before and during spesolimab therapy and of three healthy donors (HD) were *in vitro* stimulated with phorbol 12-myristate 13-acetate (PMA)/ionomycin (Iono) or lipopolysaccharide (LPS) for 4 h or with IL-36α for 7 h and subsequently analyzed by mass cytometry **(A)** Heat map showing the expression of 12 selected markers used for clustering of CD45$^+$ PBMCs. **(B)** t-SNE plot colored by the 11 identified clusters. **(C)** Heat map showing the frequency of the 11 identified clusters in unstimulated PBMCs. **(D)** Frequency of selected clusters in unstimulated PBMCs. **(E)** Frequency of pro-inflammatory cytokine producing myeloid cells in IL-36α-stimulated samples. Line in the plots indicates the median.

In analogy to our previous analyses, we subsequently analyzed the T cell compartment in more detail by performing an additional clustering of CD3$^+$ T cells (**Figure 29A-B**). Surprisingly, we found that the frequency of most T effector subsets increased during the treatment. For example, the frequency of IL-17$^+$ T cells, IL-4$^+$ IL-13$^+$ T cells and CD4$^+$ TNFα$^+$ IL-2$^+$ T cells increased, whereas the frequency of naïve T cells clusters (CD4$^+$ CD45RA$^+$ CCR7$^+$ and CD8$^+$ CD45RA$^+$ CCR7$^+$) decreased during therapy (**Figure 29C-D**). Of note, these clusters already showed differences after cyclophosphamide treatment (week 0), suggesting that the expansion of effector T cell subsets is most likely caused by the cyclophosphamide treatment.

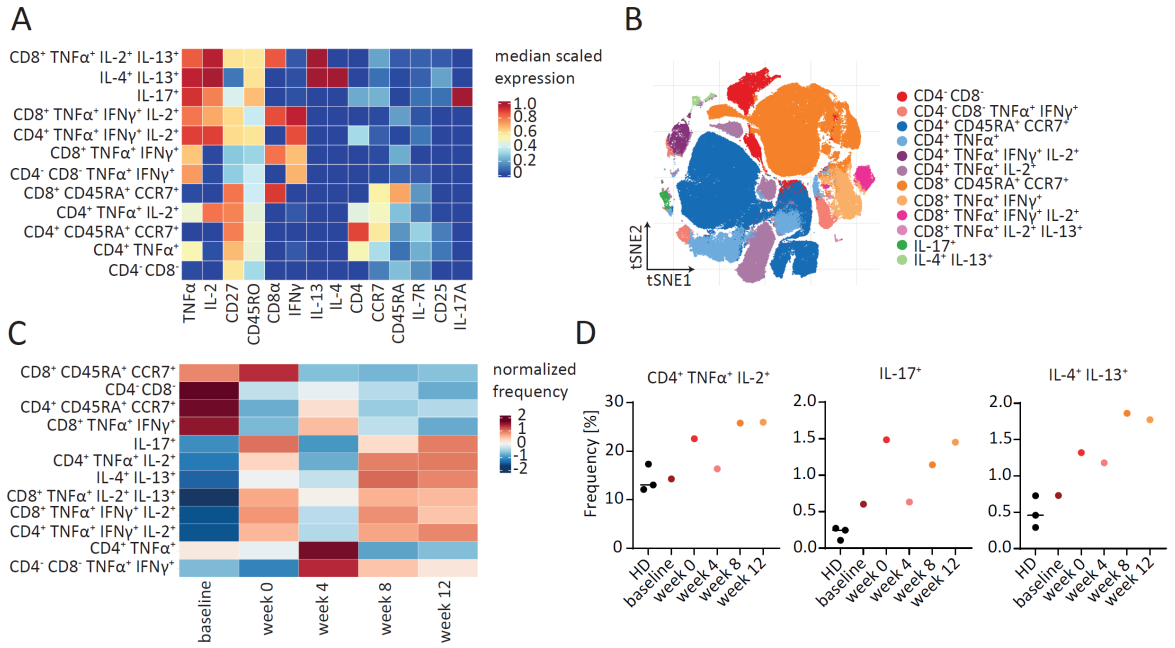

Figure 29: Increased frequency of effector T cells during anti-IL-36R therapy.
(A) Heat map showing the expression of 14 selected markers used for clustering of CD3⁺ peripheral blood mononuclear cells (PBMCs). **(B)** t-SNE plot colored by the 12 identified clusters. **(C)** Heat map showing the frequency of the 12 identified clusters in phorbol 12-myristate 13-acetate (PMA)/ionomycin (Iono)-stimulated PBMCs. **(D)** Frequency of selected clusters in PMA/Iono-stimulated PBMCs. Line in the plot indicates the median.

4.2.8 Identification of three additional Crohn's disease patients with heterozygous missense mutations in *IL36RN*

To determine whether *IL36RN* mutations are present in other IBD patients, we searched within a previously generated WES dataset of a cohort of 86 UC patients, 244 CD patients and 45 controls for pathogenic *IL36RN* mutations. Within this cohort, we identified three additional patients with heterozygous missense mutations in *IL36RN*. The first patient was a 45-year-old man who was diagnosed with CD at the age of 40, exhibited inflammation mainly in the terminal ileum and developed intestinal fistulae and stenoses (Montreal classification A3 L1 B2). The second patient was a 55-year-old man, who was diagnosed with CD at the age of 17, experienced inflammation only in the ileum and neither developed intestinal fistulas nor stenoses (Montreal classification A2 L1 B1). The third patient was a 46-year-old woman who was diagnosed with CD at the age of 42 and presented with inflammation mainly in the terminal ileum and the presence of intestinal stenoses. (Montreal classification A3 L1 B2). In the first patient we detected the *IL36RN* P76L 227C>T variant, in the second patient we found the previously identified *IL36RN* S113L 338C>T variant and the third patient carries the *IL36RN* L133I 397C>A variant (**Figure 30A**). Based on the Polymorphism Phenotyping v2 (PolyPhen-2) tool, all identified mutations were predicted to be probably damaging, meaning that they probably affect protein structure and function [114].

To understand if *IL36RN* mutations might be enriched in CD patients, we determined the frequency of the identified mutations in the healthy population using the Genome Aggregation Database (gnomAD) [115]. The allele frequency of *IL36RN* S113L was estimated to be 0.0028, that of *IL36RN* P76L was 0.000265 and *IL36RN* L133I had no database entry. However, larger cohorts of IBD patients need to be analyzed to conclude whether *IL36RN* mutations are more common in CD patients.

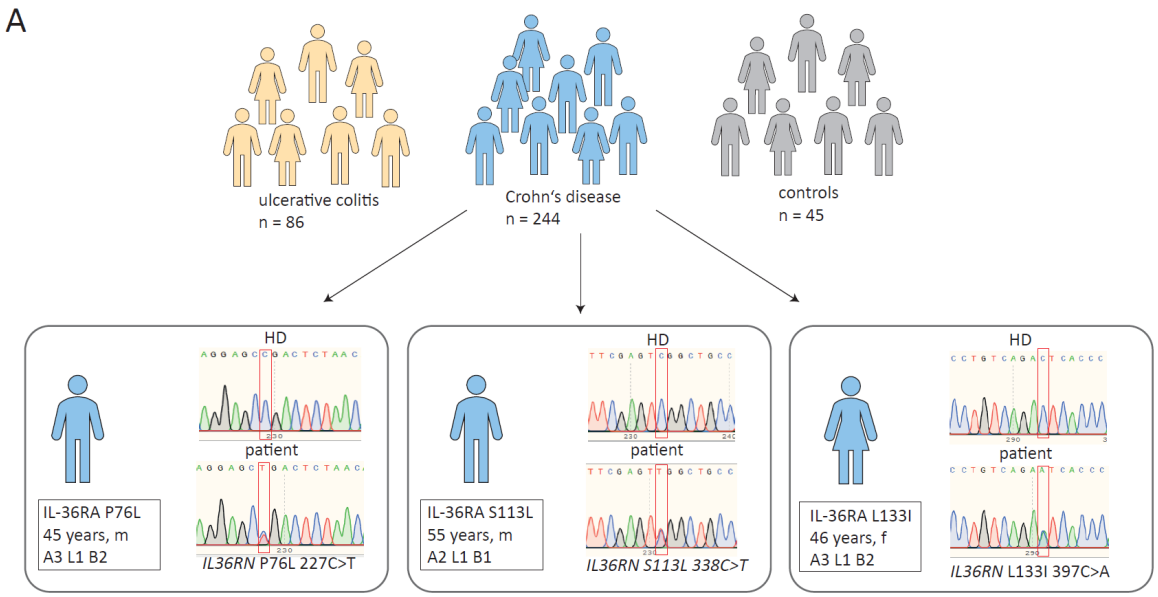

Figure 30: Identification of additional *IL36RN*-mutated patients in the IBDome cohort.
(A) In the whole-exome sequencing dataset of the IBDome cohort, mutations in *IL36RN* were identified by searching for mutations predicted by PolyPhen-2 to be probably damaging. Subsequently, mutations were confirmed by targeted Sanger sequencing. Age, sex, Montreal classification and Sanger sequencing results are depicted for all identified patients carrying mutations in *IL36RN*. The red square indicates the position of the mutation in the *IL36RN* gene. f = female, m = male, HD = healthy donor.

4.2.9 Effect of *IL36RN* P76L and *IL36RN* L133I on protein expression and function

Similar to *IL36RN* S113L, we also characterized the effect of *IL36RN* P76L and *IL36RN* L133I on the protein expression and function. We first analyzed the location of the mutation within the protein by using the three-dimensional structure of human IL-36RA generated by AlphaFold. We found that both affected residues, Pro76 and Leu133, are not located in critical binding sites and do not form bonds that are important for the protein structure and stability (**Figure 31A-B**). Nevertheless, the amino acid change could affect the structure of the protein and therefore the stability or expression of the protein.

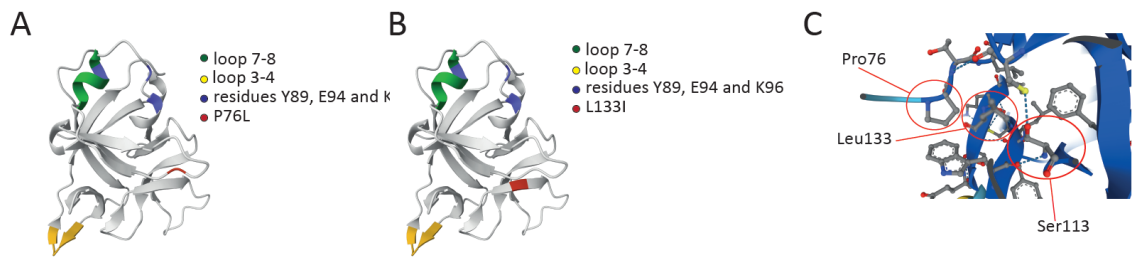

Figure 31: Location of mutated residues Pro76 and Leu133 within the 3D structure of IL-36RA.
(A-B) Three-dimensional structure of wild type human IL-36RA modeled by AlphaFold. Loops and residues important for receptor interaction are labeled in green, yellow and blue. The location of the mutated residues **(A)** Pro76 and **(B)** Leu133 are labeled in red. **(C)** Detailed view of the structure of wild type human IL-36RA, zoomed in on the mutated residues P76 and L133. Selected amino acids are labeled, and dotted lines indicate hydrogen bonds.

We then overexpressed *IL36RN* P76L and *IL36RN* L133I in HEK 293T as described in section 4.2.2. Similar to the effects observed for IL-36RA S113L, we found that cells transfected with pCMV-Entry-*IL36RN* P76L showed a significantly reduced IL-36RA expression compared to cells transfected with pCMV-Entry-*IL36RN* WT. In contrast, we detected a significantly increased concentration of IL-36RA in the supernatant of cells transfected with pCMV-Entry-*IL36RN* L133I (**Figure 32A-B**). Finally, we also produced IL-36RA P76L and IL-36RA L133I recombinantly and tested their function in *in vitro* assays using HEK-Blue IL-36 cells as described in section 4.2.5. HEK-Blue IL-36 cells were pre-incubated with different concentrations of IL-36RA WT, IL-36RA P76L or IL-36RA L133I and then stimulated with 10 ng/mL IL-36α for 18 h. Subsequently, the NFκB activity was measured and the IC_{50} calculated. For P76L (49.23 ng/mL) and L133I (53.96 ng/mL) the IC_{50} was slightly lower compared to WT (87.09 ng/mL and 86.43 ng/mL) indicating that both mutations do not affect the antagonistic function of IL-36RA (**Figure 32C-E**). In summary, our data indicate that the *IL36RN* P76L mutation leads to a decrease in protein expression, whereas the *IL36RN* L133I mutation did not appear to have a significant effect on protein expression or function.

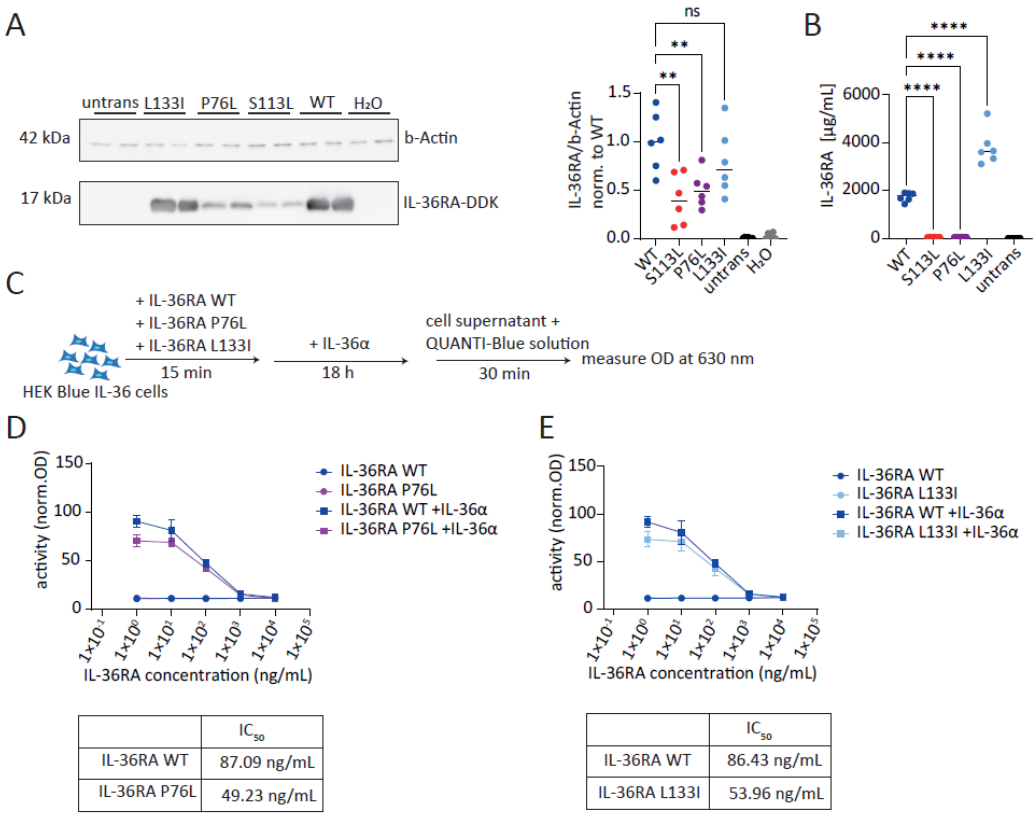

	IC_{50}
IL-36RA WT	87.09 ng/mL
IL-36RA P76L	49.23 ng/mL

	IC_{50}
IL-36RA WT	86.43 ng/mL
IL-36RA L133I	53.96 ng/mL

Figure 32: Functional characterization of *IL36RN* P76L and L133I.[3]

(A-B) Identified mutations were introduced into the C-terminal Myc-DDK-tagged pCMV6-Entry *IL36RN* plasmid by site-directed mutagenesis and the generated plasmids were transfected into HEK 293T cells. HEK 293T cells were either transfected with *IL36RN* wild type (WT), *IL36RN* P76L (P76L), *IL36RN* L133I (L133I), water (H_2O) or left untransfected (untrans.) IL-36RA expression was analyzed 48 h after transfection **(A)** in the cells by Western blot and **(B)** in the supernatant by ELISA. The line in the plots indicates the median. Data represent three independent experiments. **(C-E)** HEK Blue IL-36 cells were pre-incubated with different concentrations of IL-36RA WT, IL-36RA P76L or IL-36RA L133I for 15 min and then stimulated with 10 ng/mL IL-36α for 18 h. Afterwards, the cell supernatant was incubated with QUANTI-Blue solution and the optical density (OD) was measured at 630 nm. **(D-E)** Graph showing the NFκB activity of HEK Blue IL-36 cells incubated with **(D)** IL-36RA P76L or **(E)** IL-36RA L133I. OD values were normalized to the cells stimulated with IL-36α only. Data are represented as mean ± SD (n = 10). Data represent three independent experiments. The half maximal inhibitory concentration (IC_{50}) for the respective proteins is listed in the table below. Statistical significance in panels A and B was determined by one-way ANOVA with Tukey's multiple comparisons test. ****p<0.0001, ***p<0.001, **p<0.01, *p<0.05.

[3] Experiments in Figure 32A-B were performed by Judith Saurenbach as part of her master's thesis.

4.2.10 Summary aim 2

In a therapy-refractory CD patient, we have here identified a heterozygous missense mutation in the gene encoding IL-36RA (*IL36RN*). Through *in vitro* assays, we studied the effect of the identified *IL36RN* S113L mutation on protein expression and function and found that the mutation causes a reduced expression of IL-36RA, which could lead to the overactivation of the IL-36R signaling pathway. As animal studies have recently linked IL-36R signaling to intestinal inflammation and fibrosis [55], we thus hypothesize that the identified mutation contributes to the development of intestinal inflammation and fibrosis observed in our patient. Consequently, anti-IL36R therapy resulted in a reduced intestinal inflammation in our patient (**Figure 33A**). Finally, we identified three other CD patients with heterozygous missense mutations in *IL36RN*, highlighting that *IL36RN* mutations are present in a subset of CD patients with ileal disease who could benefit from anti-IL-36R therapy.

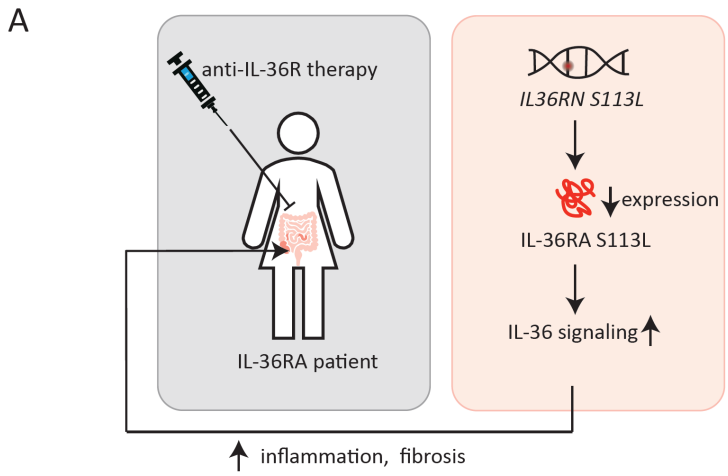

Figure 33: Summary aim 2
(A) In a therapy-refractory Crohn's disease patient, we identified a heterozygous missense mutation in the *IL36RN* gene, which encodes IL-36RA. *In vitro* assays revealed that the identified *IL36RN* S113L mutation leads to a reduced expression of IL-36RA. Therefore, we hypothesize that the identified mutation leads to the overactivation of the IL-36R signaling pathway, thereby contributing to the intestinal inflammation and fibrosis observed in the *IL36RN*-mutated patient. Consequently, anti-IL-36R therapy resulted in a reduced intestinal inflammation in the patient.

4.3 Aim 3: Analyze the function of the leptin-melanocortin signaling pathway in immune regulation

In the third part of this thesis, we aimed to analyze the role of POMC, LEPR, PC1/3 and MC4R in the human immune system by characterizing the immune cell composition and function of patients with monogenic obesity, who carry loss of function mutations in the respective genes.

4.3.1 Deep immune cell profiling of patients with mutations in the leptin-melanocortin signaling pathway

To analyze the impact of the leptin-melanocortin signaling pathway on immune cell composition and function, we collected PBMCs and serum of a cohort of patients with mutations in *LEPR*, *MC4R, PCSK1* and *POMC*, as well as lean and obese controls. For adults, obesity was defined as a BMI greater than or equal to 30, while for children a BMI greater than or equal to the 95th age and sex specific percentile was considered obese. Specifically, we collected samples from four patients with mutations in *LEPR*, either homozygous for p.W664R or compound heterozygous for p.W664R and p.E657* or p.W664R and 2674-3564del. All these mutations result in a strongly reduced function of LEPR and severe obesity in all individuals [81]. We also included three patients with heterozygous mutations in *MC4R*, carrying either the p.I251L or the p.T112M variant. These heterozygous mutations lead to a milder form of obesity compared to homozygous mutations [85]. Furthermore, we sampled six patients with homozygous mutations in *POMC*, carrying either the p.K51*, the p.Q102* or the p.E105* variant, resulting in POMC deficiency and severe obesity in the affected individuals [116]. In addition, one patient with a homozygous deletion in exons 1-9 of *PCSK1* (encoding PC1/3) was included. In order to have age-, sex- and BMI-matched controls, we collected samples from seven obese adults and six obese children, as well as six lean adults and five lean children to also analyze the effect of obesity on the immune system. All patients except one *LEPR*-mutated patient and the *PCSK1*-mutated patient were treated with the MC4R agonist setmelanotide and all *POMC*-mutated patients were receiving hydrocortisone at the time of sample collection (**Figure 34A**).

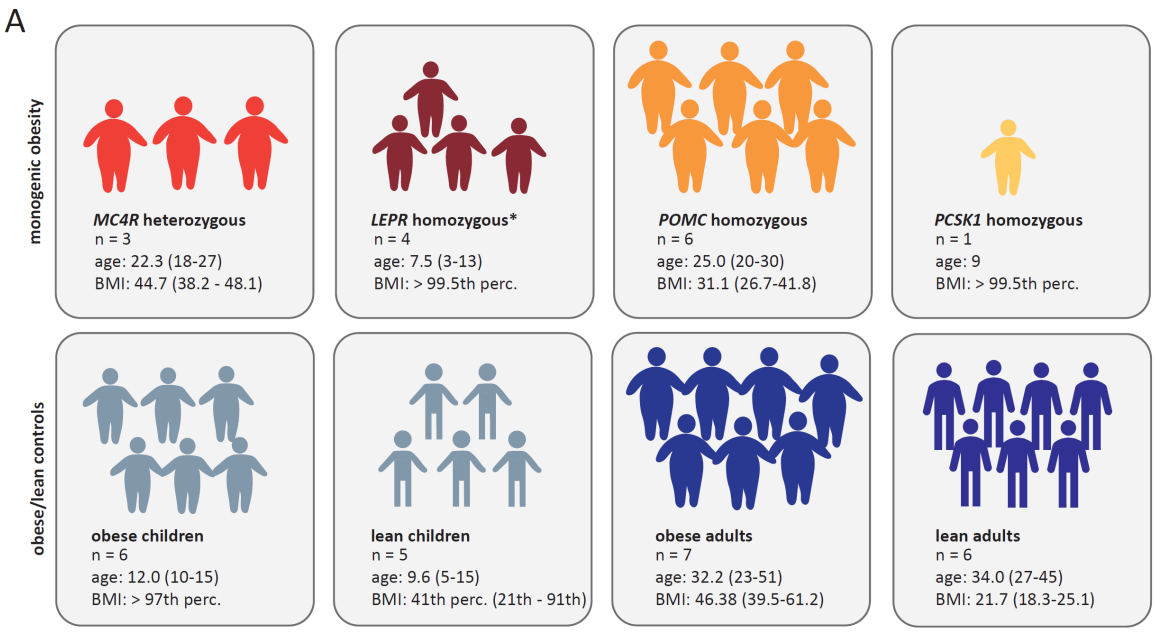

Figure 34: Characteristics of the cohort of patients with monogenic obesity analyzed by mass cytometry.
(A) Overview of patients included in the mass cytometry analysis of PBMCs. For all groups, the number of patients (n), mean age and age range, and mean and range of body mass index (BMI) for adults or the sex and age specific percentile of the BMI for children are given. * = homozygous or compound heterozygous, MC4R = melanocortin 4 receptor, LEPR = leptin receptor, POMC = proopiomelanocortin, PCSK1 = proprotein convertase subtilisin/kexin type 1.

Freshly isolated PBMCs of all included subjects were stimulated *in vitro* for 4 h with PMA/Iono or LPS. Samples were barcoded and pooled and subsequently stained with a panel of 35 markers and analyzed by mass cytometry. The analysis was performed as previously described and consisted of a general analysis of $CD45^+$ cells followed by sub-cluster analysis of T, B, NK and myeloid cells (**Figure 35A**).

A

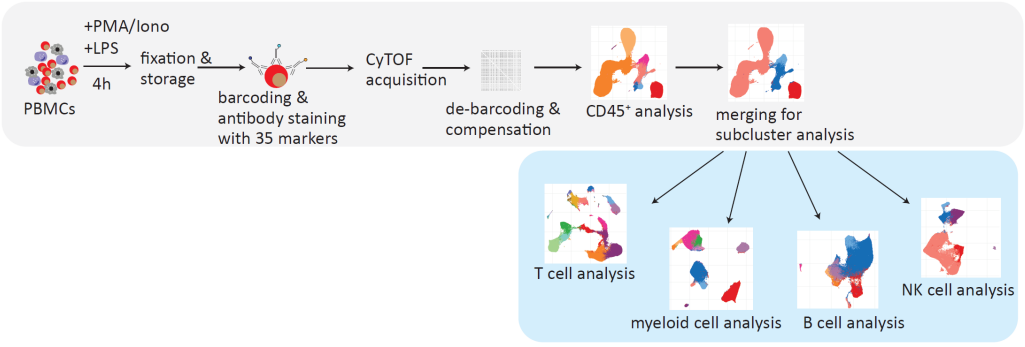

Figure 35: Schematic representation of the mass cytometry workflow.
(A) Schematic summary of the immune cell characterization of patients with leptin-melanocortin pathway mutations by mass cytometry. Peripheral blood mononuclear cells (PBMCs) of all patients were *in vitro* stimulated with phorbol 12-myristate 13-acetate (PMA)/ionomycin (Iono) or lipopolysaccharide (LPS) for 4 h and fixed. Subsequently, PBMCs were stained with 35 metal-conjugated antibodies and acquired by CyTOF. Resulting FCS files were debarcoded, compensated and gated on $CD45^+$ cells. Following, reduced-dimensional (2D) UMAP plots were generated, clusters were identified, and differential expression and abundance was analyzed. Afterwards, all clusters of T, B, NK and myeloid cells were merged and subcluster analysis was performed.

4.3.2 Increased frequency of B cells in PBMCs of *MC4R*-mutated patients

For the initial analysis of $CD45^+$ cells, a FlowSom clustering was performed using 11 lineage markers (CD3, CD4, CD8α, CD68, CD11c, CD11b, HLA-DR, CD19, CD14, CD16, CD56) and 10 distinct clusters were identified. For visualization and annotation of the clusters a Uniform Manifold Approximation and Projection (UMAP) plot was generated. The cluster frequencies were then compared between the different groups (**Figure 36A-B**).

In *LEPR*-mutated patients, we observed a significantly reduced frequency of $CD14^+$ myeloid cells compared to lean children. However, obese children also showed a reduced frequency of $CD14^+$ myeloid cells compared to lean children, suggesting that a reduction of $CD14^+$ myeloid cells in the blood may be associated with obesity rather than defects in LEPR. In contrast to previous publications [80], we did not detect a reduced frequency of $CD4^+$ T cells in *LEPR*-mutated patients.

MC4R-mutated patients had an increased frequency of B cells in the blood when compared to lean and obese adults. In *POMC*-mutated patients, we detected a significantly reduced frequency of NK cells compared to lean adults and a significantly reduced frequency of $CD11b^+$ $CD11c^+$ myeloid cells compared to obese adults. The *PCSK1*-mutated patient showed a reduced frequency of $CD4^+$ T cells and an increased frequency of $CD8^+$ T cells, as well as a strongly increased frequency of $CD11c^+$ $HLA\text{-}DR^+$ dendritic cells. Of note, because we analyzed only one *PCSK1*-mutated patient, no statistical analysis could be performed (**Figure 36C**).

For a more detailed analysis of the different cell subsets, we merged all clusters of T, B, NK and myeloid cells and performed additional FlowSom clustering of these (**Figure 36D**).

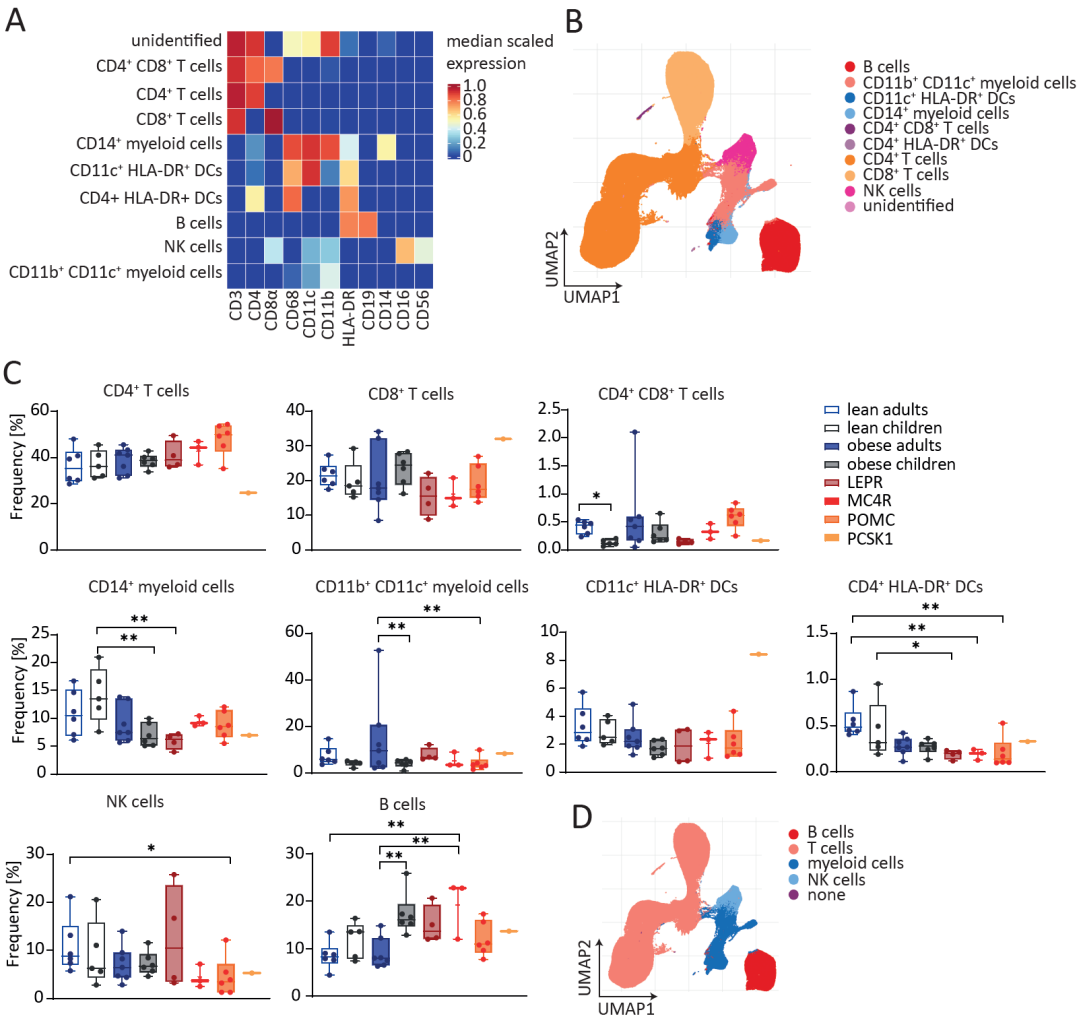

Figure 36: Immune cell phenotyping of CD45⁺ PBMCs of patients with leptin-melanocortin pathway mutations. **(A)** Heat map showing the expression of 11 selected markers used for clustering of CD45⁺ peripheral blood mononuclear cells (PBMCs). **(B)** UMAP plot colored by the 10 identified clusters. **(C)** Frequency of nine different clusters in unstimulated PBMCs of patients with mutations in the melanocortin 4 receptor (*MC4R*), the leptin receptor (*LEPR*), proopiomelanocortin (*POMC*) and proprotein convertase subtilisin/kexin type (*PCSK1*). Boxes extend from the 25th to the 75th percentile. Whiskers extend to the minimum and maximum. The line in the box indicates the median. **(D)** UMAP plot colored by the merged clusters for subcluster analysis. Statistical significance in panel C was determined by diffcyt-DA-edgeR with Benjamini-Hochberg adjustment. *padjust <0.05, **padjust <0.01, ***padjust <0.001 and ****padjust <0.0001.

4.3.3 Increased frequency of effector T cell subsets in PBMCs of *POMC*-mutated patients

For the subcluster analysis of T cells, we used a panel of 14 markers (CD8α, CD27, CD45RO, TNFα, IL-2, IFNγ, CD45RA, CCR7, CD4, IL-7R, CD25, IL-17, IL-4, IL-13) for FlowSom clustering and detected 20 different clusters within PMA/Iono-stimulated and unstimulated samples. When annotating these clusters, we found that several clusters of T cells that expressed cytokines were negative for CD4 and CD8 (**Figure 37A-B**). Since it is known that PMA/Iono stimulation leads to CD4 internalization [117] and the frequency of CD4⁻ CD8⁻ T cells in the blood is usually very low [118], we conclude that these CD4⁻ CD8⁻ cytokine expressing clusters are activated CD4⁺ T cells.

When comparing the cluster frequencies between our groups, we found that several clusters of effector T cells were significantly increased in *POMC*-mutated patients. In particular, the frequencies of $CD8^+$ $TNF\alpha^+$ $IFN\gamma^+$ T cells, $CD8^+$ $TNF\alpha^+$ $IL\text{-}2^+$ T cells and $CD4^-$ $CD8^-$ $TNF\alpha^+$ $IL\text{-}2^+$ T cells were increased in *POMC*-mutated patients, whereas the frequency of $CD8^+$ $CD45RA^+$ T cells was decreased (**Figure 37C**). Consistent with this, we also observed significantly increased expression of IFNγ in $CD4^+$ and $CD8^+$ effector T cell clusters of *POMC*-mutated patients (**Figure 37D**).

In contrast to *POMC*-mutated patients, there were no major differences in the T cell composition of *LEPR*- and *MC4R*-mutated patients. However, in the *PCSK1*-mutated patient, we found a relatively low frequency of several effector T cell clusters ($CD8^+$ $TNF\alpha^+$ $IFN\gamma^+$ T cells, $CD8^+$ $TNF\alpha^+$ $IL\text{-}2^+$ T cells, $CD4^-$ $CD8^-$ $TNF\alpha^+$ $IFN\gamma^+$ $IL\text{-}2^+$ T cells) (**Figure 37C**).

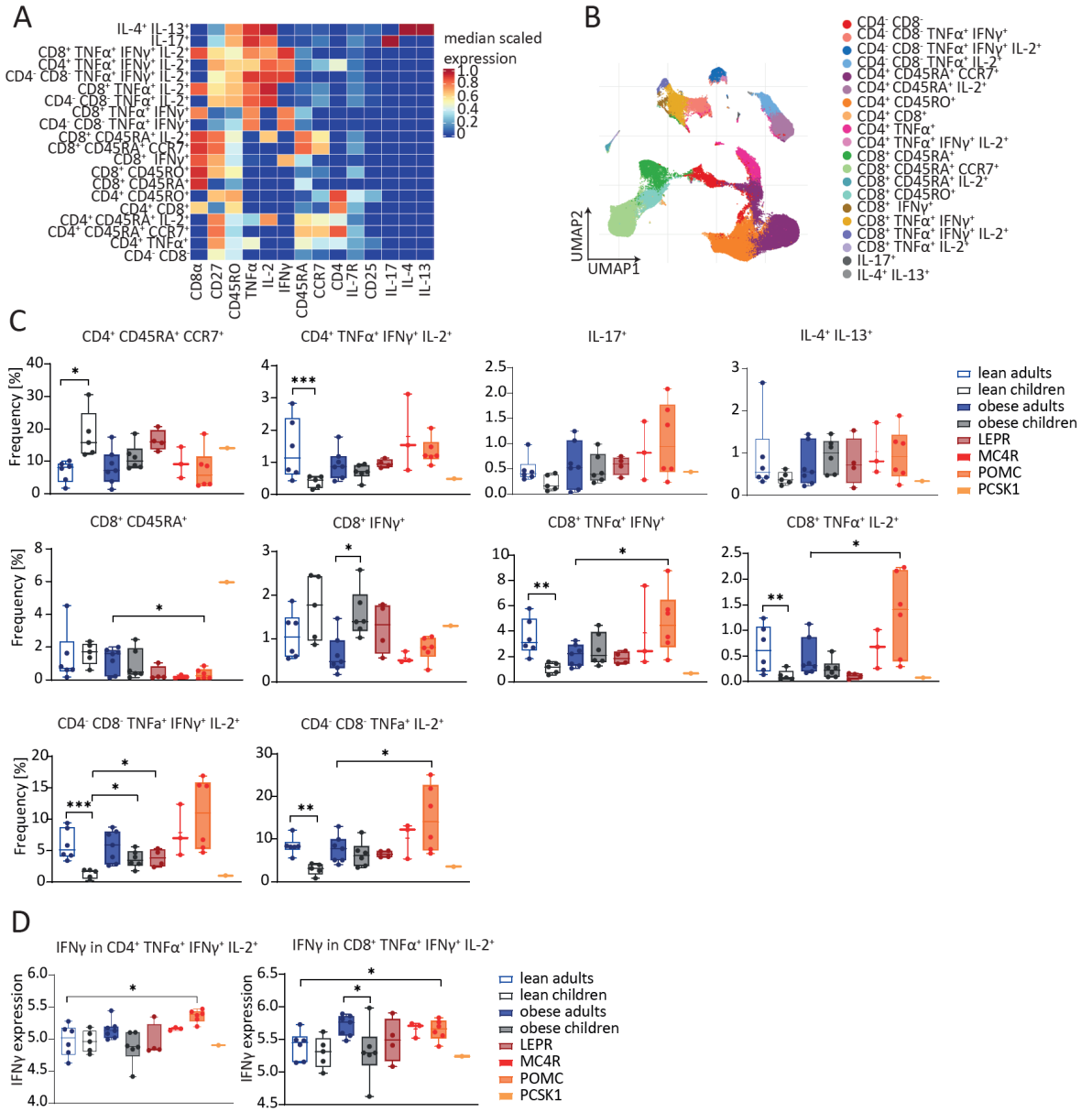

Figure 37: Subcluster analysis of CD3⁺ T cells reveals increased frequency of effector T cells in patients with *POMC* mutations.

(A) Heat map showing the expression of 14 selected markers used for clustering of T cells. **(B)** UMAP plot colored by the 20 identified clusters. **(C)** Frequency of the 10 selected clusters in phorbol 12-myristate 13-acetate (PMA)/ionomycin (Iono)-stimulated peripheral blood mononuclear cells (PBMCs) of patients with mutations in the melanocortin 4 receptor (*MC4R*), the leptin receptor (*LEPR*), proopiomelanocortin (*POMC*) and proprotein convertase subtilisin/kexin type (*PCSK1*). **(D)** Mean expression of selected markers within selected clusters in PMA/Iono-stimulated PBMCs. Boxes extend from the 25th to the 75th percentile. Whiskers extend to the minimum and maximum. The line in the box indicates the median. Statistical significance in panel C was determined by diffcyt-DA-edgeR with Benjamini-Hochberg adjustment. Statistical significance in panel D was determined by diffcyt-DS-limma with Benjamini-Hochberg adjustment. *padjust <0.05, **padjust <0.01, ***padjust <0.001 and ****padjust <0.0001.

4.3.4 Reduced frequency of pro-inflammatory monocytes in PBMCs of *LEPR*-mutated patients

In analogy to our T cell analysis, we performed an in-depth analysis of myeloid cells. Using a panel of 15 markers (CD11b, HLA-DR, CD38, CD4, CD68, IL-8, TNFα, IL-6, CD11b, IL-23, IL-12, CD16, CD14, IFNγ, CD8α), we identified 11 clusters within LPS-stimulated and unstimulated samples (**Figure 38A-B**). When frequencies of the identified clusters were compared, no differences were found in the myeloid cell composition of *POMC*-, *MC4R*- and *PCSK1*-mutated patients. However, *LEPR*-mutated patients showed a significantly reduced frequency of IL-8$^+$ IL-6$^+$ TNFα$^+$ monocytes and a significantly increased frequency of IL-12$^+$ IL-23$^+$ monocytes compared to lean children (**Figure 38C**).

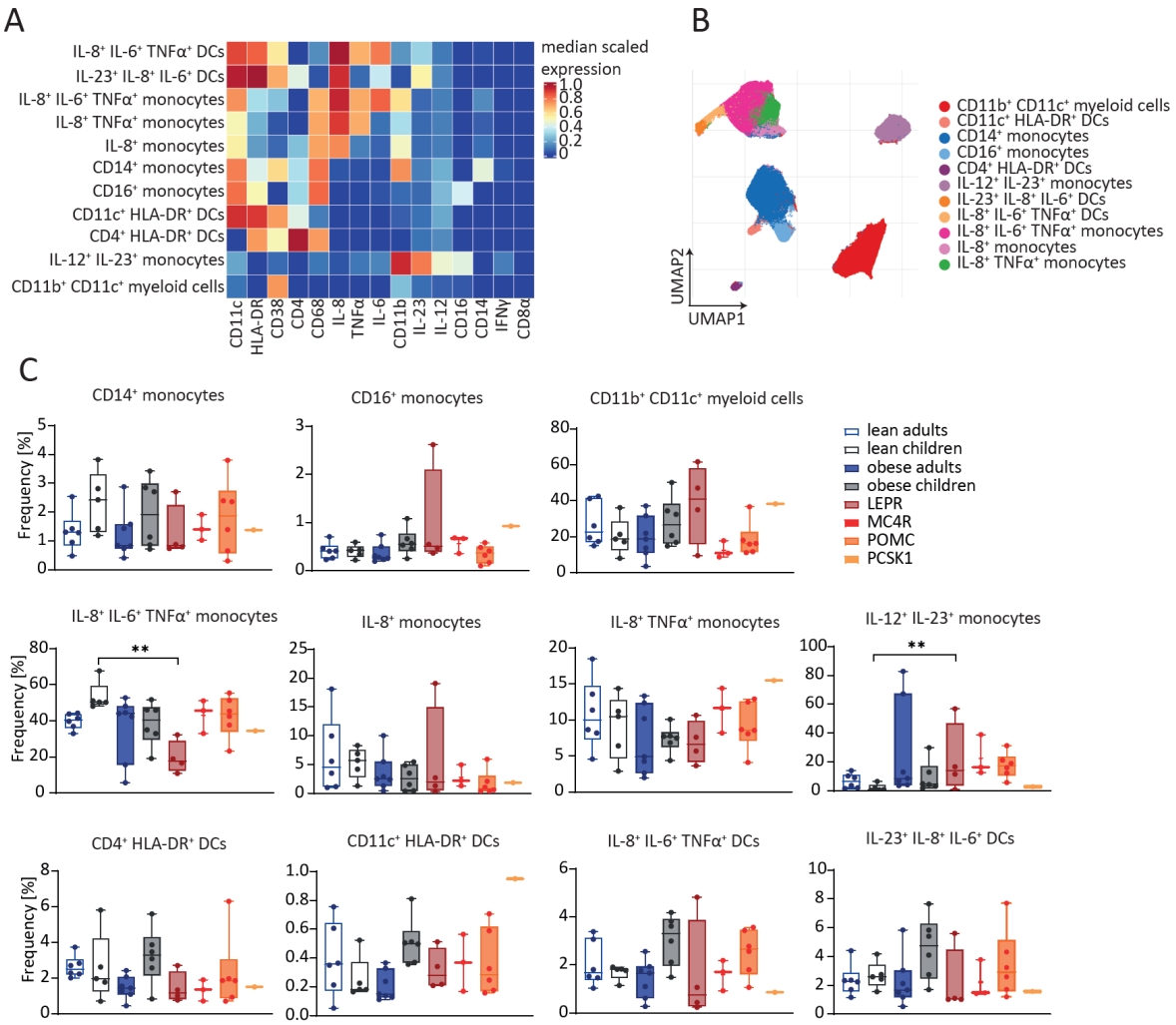

Figure 38: Reduced frequency of pro-inflammatory monocytes in patients with *LEPR* mutations.
(A) Heat map showing the expression of 15 selected markers used for clustering of myeloid cells. **(B)** UMAP plot colored by the 11 identified clusters. **(C)** Frequency of the 11 different clusters in lipopolysaccharide (LPS)-stimulated peripheral blood mononuclear cells (PBMCs) of patients with mutations in the melanocortin 4 receptor (*MC4R*), the leptin receptor (*LEPR*), proopiomelanocortin (*POMC*) and proprotein convertase subtilisin/kexin type (*PCSK1*). Boxes extend from the 25th to the 75th percentile. Whiskers extend to the minimum and maximum. The line in the box indicates the median. Statistical significance in panel C was determined by diffcyt-DA-edgeR with Benjamini-Hochberg adjustment. *padjust <0.05, **padjust <0.01, ***padjust <0.001 and ****padjust <0.0001.

4.3.5 Reduced frequency of TNFα⁺ B cells in PBMCs of *MC4R*-mutated patients

For an in-depth analysis of B cells, we used a panel of 14 markers (CD45RA, CD45RO, HLA-DR, CD19, IgM, CD38, CD27, TNFα, IL-6, CD40, IL-23, IL-12, IFNγ, IL-8) for FlowSom clustering and detected nine different clusters within PMA/Iono-stimulated, LPS-stimulated and unstimulated samples (**Figure 39A-B**). When we compared the cluster frequencies, we noticed that lean and obese children had a significantly reduced frequency of TNFα⁺ B cells compared to adults. Furthermore, we found that *LEPR*-mutated patients had a significantly increased frequency of both plasma cell clusters. In *MC4R*-mutated patients, we detected a reduced frequency of TNFα⁺ B cells compared to lean and obese adults (**Figure 39C**).

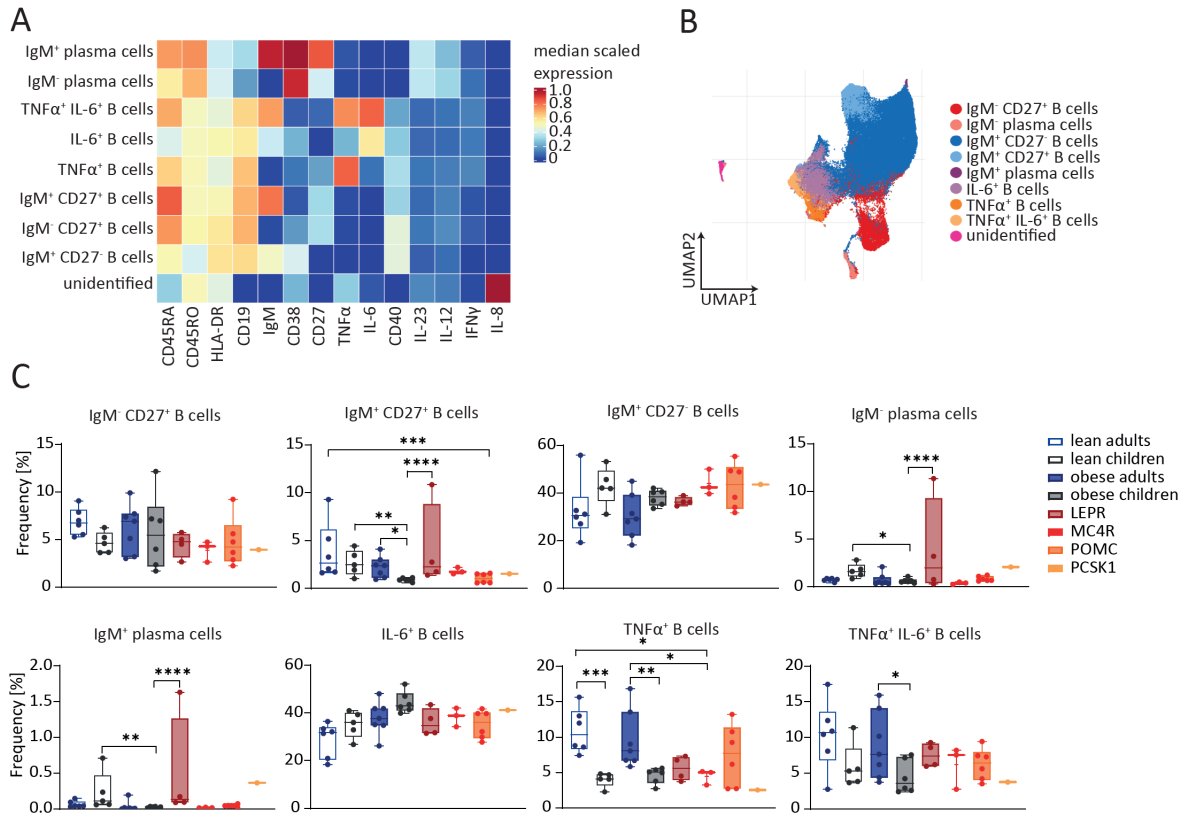

Figure 39: Subcluster analysis of B cells reveals reduced frequency of TNFα⁺ B cells in patients with *MC4R* mutations.

(A) Heat map showing the expression of 14 selected markers used for clustering of B cells. **(B)** UMAP plot colored by the nine identified clusters. **(C)** Frequency of the eight different clusters in phorbol 12-myristate 13-acetate (PMA)/ionomycin (Iono)-stimulated peripheral blood mononuclear cells (PBMCs) of patients with mutations in the melanocortin 4 receptor (*MC4R*), the leptin receptor (*LEPR*), proopiomelanocortin (*POMC*) and proprotein convertase subtilisin/kexin type (*PCSK1*). Boxes extend from the 25th to the 75th percentile. Whiskers extend to the minimum and maximum. The line in the box indicates the median. Statistical significance in panel C was determined by diffcyt-DA-edgeR with Benjamini-Hochberg adjustment. *padjust <0.05, **padjust <0.01, ***padjust <0.001 and ****padjust <0.0001.

4.3.6 No differences in NK cell frequency in patients with leptin-melanocortin pathway mutations

Finally, we analyzed the NK cells in more detail by clustering them with a panel of 13 markers (IFNγ, CD11b, CD11c, CD56, CD8α, CD16, CCR7, CD27, CD25, CD3, TNFα, IL-8, CD68). Thus, we identified five distinct clusters of NK cells, which we subsequently compared between groups (**Figure 40A-B**). However, no significant differences were found in patients with *MC4R*, *LEPR*, *POMC* and *PCSK1* mutations (**Figure 40C**).

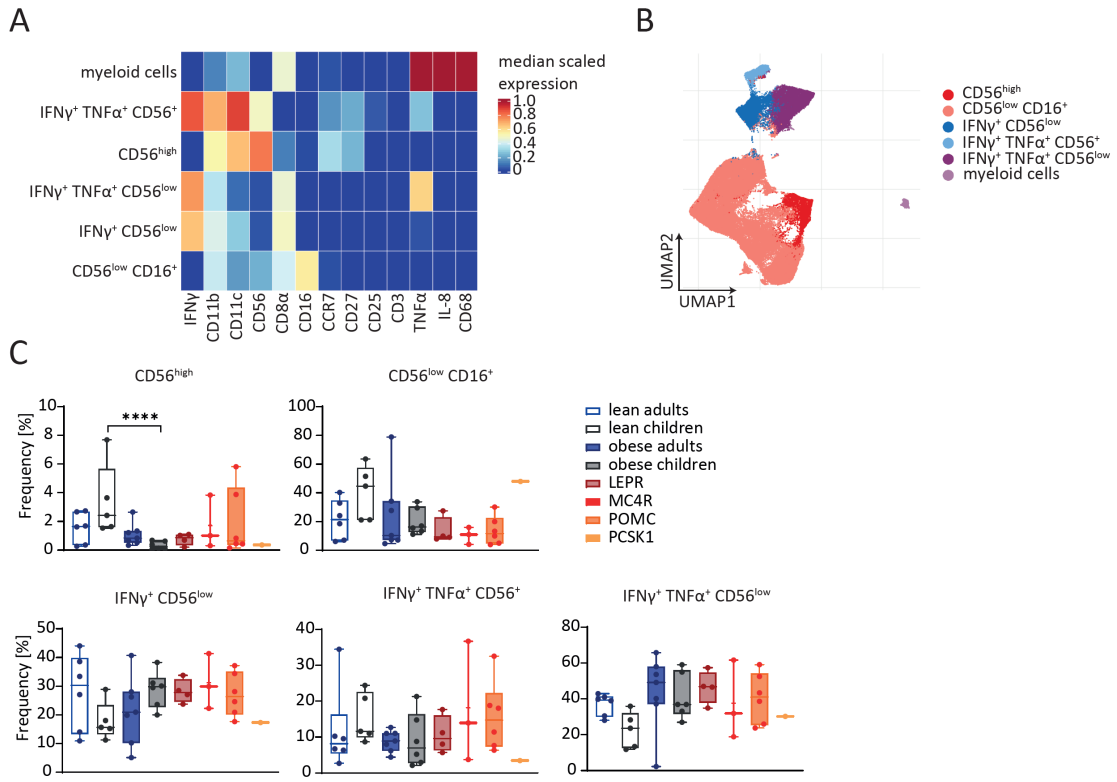

Figure 40: No differences in the NK cell composition in patients with leptin-melanocortin pathway mutations. **(A)** Heat map showing the expression of 13 selected markers used for clustering of NK cells. **(B)** UMAP plot colored by the six identified clusters. **(C)** Frequency of the five different clusters in phorbol 12-myristate 13-acetate (PMA)/ionomycin (Iono)-stimulated peripheral blood mononuclear cells (PBMCs) of patients with mutations in the melanocortin 4 receptor (*MC4R*), the leptin receptor (*LEPR*), proopiomelanocortin (*POMC*) and proprotein convertase subtilisin/kexin type (*PCSK1*). Boxes extend from the 25th to the 75th percentile. Whiskers extend to the minimum and maximum. The line in the box indicates the median. Statistical significance in panel C was determined by diffcyt-DA-edgeR with Benjamini-Hochberg adjustment. *padjust <0.05, **padjust <0.01, ***padjust <0.001 and ****padjust <0.0001.

4.3.7 Differentiation and function of *in vitro* polarized macrophages of *LEPR*-mutated patients

By mass cytometry, we observed a decreased frequency of IL-8⁺ IL-6⁺ TNFα⁺ monocytes in *LEPR*-mutated patients, suggesting a potential defect in the myeloid compartment of *LEPR*-mutated patients. To validate these findings, we polarized blood-derived monocytes of *LEPR*-mutated patients

and HDs *in vitro* in the presence or absence of leptin into M1 macrophages (**Figure 41A**). Flow cytometry and microscopy analysis revealed no differences in the polarization of M1 macrophages between *LEPR*-mutated patients and HDs (**Figure 41B**). On day 6 of differentiation, macrophages were incubated with LPS for 4 h and cytokines in the supernatant were subsequently analyzed by CBA. We detected no differences in IL-6 and TNFα production between macrophages of the first *LEPR*-mutated patient (hereafter referred to as LEPR 1) and HDs. However, in the second *LEPR*-mutated patient (hereafter referred to as LEPR 2), we found that macrophages produced less TNFα and IL-6 than macrophages of HDs, similar to what we had observed in our mass cytometry data (**Figure 41C**). Due to the different results obtained in both *LEPR*-mutated patients, we cannot conclude whether *LEPR*-mutated patients have a defect in the myeloid cells compartment or not. Therefore, it is necessary to repeat and validate these experiments in other *LEPR*-mutated patients to gain a better understanding of how leptin signaling affects myeloid cell function in humans.

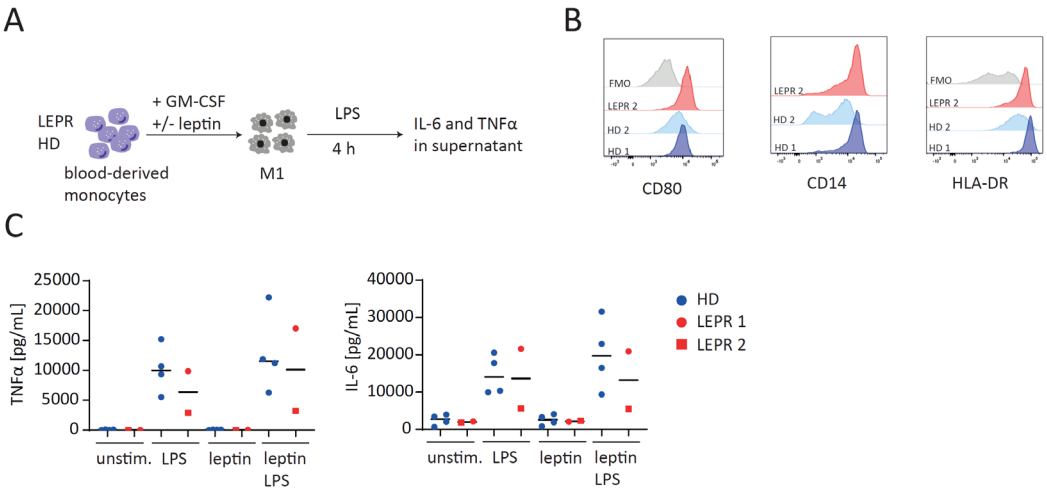

Figure 41: Differentiation and function of *in vitro* polarized macrophages of *LEPR*-mutated patients.
(A-C) Blood-derived monocytes of leptin receptor (*LEPR*)-mutated patients and healthy donors (HD) were differentiated into M1 macrophages by supplementation of GM-CSF in the presence or absence of leptin for 6 days and subsequently stimulated with lipopolysaccharide (LPS) or left unstimulated (unstim.). **(B)** Analysis of differentiated macrophages 6 days after start of polarization by flow cytometry exemplary shown for LEPR 2. FMO = fluorescence minus one **(C)** Concentrations of TNFα and IL-6 in the supernatant of stimulated macrophages. Line in the plots indicates the median.

4.3.7 Summary aim 3

In conclusion, we have here performed the first in-depth characterization of the immune cell composition and function of patients with monogenic obesity and identified specific changes associated with mutations in *LEPR*, *MC4R* and *POMC*. In *LEPR*-mutated patients, we observed a reduced frequency of IL-8$^+$ IL-6$^+$ TNFα$^+$ monocytes, in *POMC*-mutated patients, we detected an increased frequency of pro-inflammatory T cell subsets and in *MC4R*-mutated patients, we found an increased frequency of B cells (**Figure 42A**). These findings indicate that these proteins are not only important for appetite regulation via the leptin-melanocortin signaling pathway, but are also involved in immune cell regulation and function.

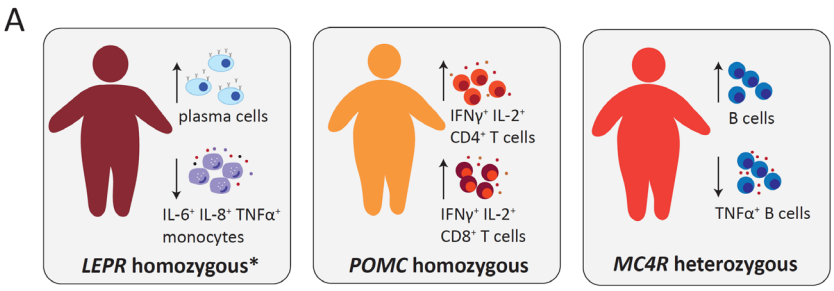

Figure 42: Summary aim 3
(A) We have here performed an in-depth characterization of the immune cell composition and function of patients with monogenic obesity and identified specific changes associated with mutations in leptin receptor (*LEPR)*, melanocortin 4 receptor (*MC4R*) and proopiomelanocortin (*POMC*). In *LEPR*-mutated patients, we observed a reduced frequency of IL-8$^+$ IL-6$^+$ TNFα$^+$ monocytes, in *POMC*-mutated patients, we detected an increased frequency of pro-inflammatory T cell subsets and in *MC4R*-mutated patients, we found an increased frequency of B cells. * = homozygous or compound heterozygous.

5 Discussion

In this thesis, three different rare diseases were investigated to study principle mechanisms of immune regulation and function. To better characterize individual diseases and their underlying molecular mechanisms, we performed genetic analyses, deep immune cell profiling by mass cytometry and functional *in vitro* assays and combined these data with clinical observations to link identified mutations to altered cell states. This allowed us not only to better understand the function of the affected and mutated genes and their respective proteins in the immune system, but also enabled us to identify targeted therapies for affected patients.

5.1 Aim 1: Understand pathomechanisms of auto-inflammatory symptoms in ROSAH patients

The pathogenesis of the ROSAH syndrome, which is caused by mutations in the *ALPK1* gene and leads to symptoms such as vision loss, splenomegaly, anhidrosis and migraine headache, is still incompletely understood. The fact that patients also suffer from various auto-inflammatory symptoms such as episodic fevers, uveitis and arthritis [35, 36] and that ALPK has recently been identified as PRR [26], suggests that ALPK1 is involved in immune regulation. However, the exact role of ALPK1 in different immune subsets and the mechanism of auto-inflammatory symptoms in ROSAH patients remains unclear. Therefore, it is also currently unknown which anti-inflammatory therapy should be used to treat auto-inflammatory symptoms in ROSAH patients. To our knowledge, we have here identified the first ROSAH patient in Germany and performed the first in-depth immune cell profiling of a ROSAH patient, identifying specific changes in the immune system and targets for therapy [119].

5.1.1 Role of ALPK1 in immune regulation and function

When we compared the immune cell composition of PBMCs of the ROSAH patient to HDs, we observed differences in several immune cell subsets of the ROSAH patient. Most strikingly was the almost complete absence of B cells in PBMCs. Upon reviewing the clinical history, we found that the ROSAH patient had been receiving rituximab for eight years until two years prior to sample collection. Rituximab is a monoclonal antibody that targets the pan-B cell marker CD20, resulting in the depletion of B cells. However, studies indicate that B cell repopulation typically occurs 6-8 months after the end of rituximab treatment and B cell depletion longer than 12 months is very rare [120, 121]. Therefore, the complete absence of B cells two years after therapy, detected in the ROSAH patient, may indicate defects in the B cell compartment of the ROSAH patient and a potential role of ALPK1 in B cell homeostasis. Nevertheless, further validation in other ROSAH patients is needed to determine if the observed differences were caused by the mutation in *ALPK1* or by the rituximab treatment.

In T cells, we found a reduced frequency of both naïve CD45RA$^+$ CCR7$^+$ CD8$^+$ T cells and activated CD45RO$^+$ CD8$^+$ T cells in PBMCs of the ROSAH patient. Further analysis of the T cell compartment also revealed a decreased frequency of IFNγ$^+$ and TNFα$^+$ CD4$^+$ and CD8$^+$ T cells, as well as a reduced expression of IFNγ and TNFα in T cells of the ROSAH patient. However, the patient was receiving the JAK inhibitor tofacitinib at the time of sample collection, which has been shown to affect proliferation and cytokine production of T cells [111]. Therefore, it cannot be excluded that the observed differences in the T cell compartment were at least partly caused by the treatment with tofacitinib.

In contrast to B and T cells, the frequency of monocytes was increased in PBMCs of the ROSAH patient and monocytes and *in vitro* differentiated macrophages expressed increased levels of TNFα and IL-6 after LPS stimulation. This is of particular interest since ALPK1 has recently been identified as a PRR for LPS-derived metabolites, which initiates the activation of the NFkB pathway and the production of pro-inflammatory cytokines [26]. The increased production of TNFα and IL-6 by myeloid cells of the ROSAH patient might therefore indicate that the T273M mutation in *ALPK1* is a gain-of-function mutation leading to enhanced activity of ALPK1 in response to microbial stimuli and subsequently to an overactivation of the NFkB pathway. This conclusion is supported by recent studies showing that HEK cells overexpressing the *ALPK1* T273M variant exhibit an increased ADPH-induced kinase activity [122].

5.1.2 Therapy of auto-inflammatory symptoms in ROSAH patients

Based on our data, we therefore hypothesized that the auto-inflammatory symptoms observed in ROSAH patients are caused by the increased cytokine expression of myeloid cells due to an enhanced activity of ALPK1. However, since the JAK inhibitors tofacitinib and baricitinib, which target the signaling of several cytokines including IL-6 [123], were ineffective in the ROSAH patient ,we considered the non-JAK/STAT regulated cytokine TNFα to be the key player in the pathogenesis of arthritis symptoms in our ROSAH patient. Consequently, anti-TNFα therapy with adalimumab and low-dose corticosteroids was initiated in our ROSAH patient, which resulted in a reduction in joint inflammation and pain. Furthermore, also other studies suggest that TNFα blockers effectively treat auto-inflammatory symptoms in ROSAH patients [36, 124]. Thus, we propose that blocking TNFα should be considered as primary therapy for auto-inflammatory symptoms in ROSAH patients.

We could not assess the effect of anti-TNFα therapy on vision loss, as our ROSAH patient was already completely blind when she presented herself to our clinic. However, other studies showed that anti-TNFα therapy does not affect the progression of vision loss [124], indicating that inflammation is not the only cause of vision loss in ROSAH patients. In addition, the abundant expression of ALPK1 in various tissues and cell types, as well as the diverse symptoms of ROSAH patients suggests that ALPK1 might has distinct functions in different cell types. For instance, Williams et al. demonstrated that ALPK1 is highly expressed in cilia and that the *ALPK1* T237M mutation results in abnormal cilia function

[35], which has also been observed in other ocular diseases, such as retinitis pigmentosa and Leber congenital amaurosis [125].

5.1.3 Limitations and outlook

As our data is based on the characterization of a single patient with ROSAH syndrome, generalization of the results might be limited and validation in other patients is needed. However, due to the rarity of the ROSAH syndrome and the small number of patients known worldwide, access to patient samples is extremely limited. Furthermore, the various immune modulatory treatments that our ROSAH patient received in the past are known to affect immune cell differentiation and function and we cannot exclude the possibility that these treatments influenced our results. Despite these limitations, we provide here the first in-depth characterization of the immune cell composition and function of a ROSAH patient and identify increased TNFα expression of myeloid cells as the main cause for auto-inflammatory symptoms in our ROSAH patient. Whether ALPK1 also plays a role in the function of other immune cells such as B and T cells requires further validation, for example by overexpressing the *ALPK1* T237M variant in different immune cell subsets and studying cell differentiation and function.

While blocking TNFα signaling appears to be a suitable therapy for auto-inflammatory symptoms of ROSAH patients, there is currently no effective treatment for the vision loss caused by the ROSAH syndrome. Therefore, DF-003, an ALPK1 inhibitor, has been recently developed and is currently undergoing safety and pharmacokinetic evaluation in a phase 1 clinical trial [126]. Finally, it is important to note that the number of patients with ROSAH syndrome might be significantly higher than currently reported due to misdiagnoses of ROSAH patients. Hence, it is crucial to screen patients with ocular disorders and auto-inflammatory symptoms for mutations in *ALPK1* to enable an early diagnosis of patients.

5.2 Aim 2: Investigate the role of *IL36RN* mutations in Crohn's disease

IL-36R signaling has recently been shown to play a role in the development of intestinal inflammation and fibrosis [56]. While missense mutations in the gene encoding IL-36RA (*IL36RN*) have been associated with severe skin inflammation [110], their role in CD is currently unknown. Here, we identified three different heterozygous missense mutations in *IL36RN* in four CD patients with primarily ileal disease manifestation, investigated their role in intestinal inflammation and explored whether anti-IL-36R therapy represents a targeted treatment option for CD patients with *IL36RN* mutations.

5.2.1 In-depth analysis of the immune cell composition and function of an *IL36RN*-mutated Crohn's disease patient

The first patient in whom we identified an *IL36RN* mutation was a patient with a severe and therapy refractory course of CD. The patient carries the heterozygous missense mutation *IL36RN S113L*, which had previously been described in the context of generalized pustular psoriasis [110]. To determine if the identified mutation can be linked to a distinct immune cell state that may contribute to intestinal inflammation, we performed an in-depth analysis of the immune cell composition and function in PBMCs obtained from the IL-36RA patient.

To assess if the mutation affects the function of IL-36RA and leads to changes in IL-36R regulation in the patient, we stimulated PBMCs of the IL-36RA patient *in vitro* with IL-36α and subsequently analyzed the secretion of pro-inflammatory cytokines. We observed that PBMCs of the IL-36RA patient produced highly elevated levels of IL-6, IL-8 and TNFα compared to those of a HD. These findings are in line with data from patients with generalized pustular psoriasis, who carry homozygous mutations in *IL36RN* [110] and suggest defects in IL-36R regulation in the IL-36RA patient. However, when we repeated the experiment at a different time point, we were unable to reproduce these findings and instead found that PBMCs of the IL-36RA patient produced less pro-inflammatory cytokines. A possible reason for the different results in the two experiments is that the patient was receiving different anti-inflammatory treatments at both time points. In the first experiment, the patient was treated with the anti-TNFα antibody golimumab, while in the second experiment the patient was receiving the JAK inhibitor upadacitinib, which has been shown to affect cytokine production of various immune cells [127].

In addition, we found elevated levels of IL-36RA in the serum of the IL36RA patient when compared to CD patients and HDs. IL-36α, IL-36β and IL-36γ were not measurable in the serum, which is consistent with previous reports showing that their concentrations in serum are typically very low [128]. Furthermore, we detected elevated levels of IL-23 and IL-18 and demonstrated that both cytokines can be induced by IL-36α stimulation. However, also various other stimuli such as LPS or TNFα can cause the expression of IL-23 and IL-18 [129, 130].

When we compared the immune cell composition of PBMCs of the IL-36RA patient to that of CD patients and HDs, we detected an increased frequency of B cells and naïve $CD8^+$ T cells and a decreased frequency of NK cells in PBMCs of the IL-36RA patient. Although we had also expected to observe an increase in Th1 and Th17 cells, as IL-36 signaling has been shown to promote Th1 and Th17 differentiation [60, 61], we only found a slight increase in Th17 cells and no difference in Th1 cells.

In summary, we have here detected changes in immune cell composition and function of the IL-36RA patient that may be associated with increased IL-36 signaling. However, we could not identify a distinct immune cell state that would clearly link the identified mutation to the intestinal inflammation

observed in our patient. Possible reasons for this include the multiple treatments that the patient was receiving in the past and at the time of sample collection, which are known to affect immune cell differentiation and function and the fact that we only analyzed immune cells from the periphery and not directly from the site of inflammation.

5.2.2 Effect of the *IL36RN* S113L mutation on the expression and function of IL-36RA

To further understand the role of the identified mutation in the disease pathogenesis of the IL-36RA patient, we analyzed the effect of the *IL36RN* S113L mutation on the expression and function of IL-36RA.

Thus, we overexpressed *IL36RN* S113L in HEK 293T cells and compared the expression and secretion of IL-36RA to cells transfected with *IL36RN* WT. In line with previous reports [131], we observed that overexpression of *IL36RN* S113L led to a reduced expression and secretion of IL-36RA. In addition, *in silico* data revealed that Ser113 forms three hydrogen bonds that cannot be formed when serine is substituted by leucine. Since hydrogen bonds are important for the three-dimensional structure of proteins [132], it is likely that the S113L mutation leads to changes in protein structure and protein stability, which result in a reduced expression of IL-36RA observed in the overexpression experiments. However, further experiments are needed to study the exact impact of *IL36RN* S113L on the protein structure.

To investigate whether *IL36RN* S113L also affects the function of IL-36RA, we recombinantly produced IL-36RA S113L. Based on previous publications, we decided to produce IL-36RA in *E. coli* and to remove the first base triplet encoding the amino acid methionine, as this has been shown to be important for protein activity [53]. Because residual endotoxin contamination is a known problem in proteins produced in *E. coli* and even low concentrations can induce a pro-inflammatory response by myeloid cells [133], we used the special *E. coli* strain ClearColi BL21 for the production of IL-36RA, which has a mutant LPS that cannot trigger an endotoxin response in human cells [112].

When we tested the function of the successfully produced IL-36RA S113L in *in vitro* assays using primary human PBMCs, we surprisingly found that IL-36RA S113L showed a pro-inflammatory function similar to IL-36α. Since we had used the ClearColi BL21 strain to ensure an endotoxin free production of IL-36RA and IL-36RA WT produced with the same protocol did not show similar effects, we assumed that the pro-inflammatory effect was caused by IL-36RA S113L itself and not by an endotoxin contamination. This was further supported by boiling experiments showing that the pro-inflammatory effect of IL-36RA S113L was abolished by boiling and therefore must be caused by a protein and not by LPS, since LPS is heat stable whereas proteins denature and become non-functional at high temperatures [113]. However, when we produced a second batch of IL-36RA S113L and tested it in a special IL-36 reporter cell line we could not detect any pro-inflammatory effect of IL-36RA S113L, but

rather found that IL-36RA S113L had a similar function as IL-36RA WT. This suggests that the effects observed in the first batch were likely caused by a contamination with a factor other than LPS and that *IL36RN* S113L does not impair the antagonistic function of IL-36RA.

In summary, our findings indicate that the identified *IL36RN* S113L mutation is a pathogenic mutation that leads to a reduced expression of IL-36RA. Yet it remains unclear how these results relate to the elevated levels of IL-36RA in the serum of the IL-36RA patient. Measuring the expression of IL-36RA at other sites, such as the colon, could provide more insight.

5.2.3 Prevalence of *IL36RN* mutations in Crohn's disease

Upon literature review, we found no reports about *IL36RN* mutations in IBD patients nor was *IL36RN* listed as a risk locus for IBD in GWAS [134]. To investigate the prevalence of *IL36RN* mutations in IBD patients, we searched within an existing WES dataset of 86 UC patients, 244 CD patients and 45 controls for additional IBD patients with pathogenic *IL36RN* mutations. Surprisingly, we identified three other CD patients with heterozygous missense mutations in *IL36RN* in this cohort. However, only one patient carries the previously identified *IL36RN* S113L mutation, while the other two patients have different mutations (P76L and L133I). All identified patients developed CD in adulthood, experienced inflammation mainly in the terminal ileum and had no reported skin phenotype.

We also investigated the impact of the P76L and L133I mutations on the protein expression and function and found that *IL36RN* P76L had a similar effect as *IL36RN* S113L, resulting in a reduced protein expression. For *IL36RN* L133I, we did not detect any changes in protein expression or function, although the mutation was predicted to be damaging by PolyPhen. Nevertheless, it is possible that the mutation has other effects that we could not assess with the assays used.

Given the high number of CD patients with *IL36RN* mutations identified in the relatively small WES dataset, we hypothesized that *IL36RN* mutations are enriched in CD patients. In order to investigate this, we determined the frequency of the identified mutations in the healthy population by using the gnomAD database. We found that the identified *IL36RN* mutations are not very frequent in the healthy population as the allele frequency of *IL36RN* S113L was estimated to be 0.0028, that of *IL36RN* P76L was 0.000265 and *IL36RN* L133I had no entry. However, since the identified *IL36RN*-mutated patients had different *IL36RN* mutations, larger cohorts of IBD patients need to be analyzed to conclude if *IL36RN* mutations are enriched in CD patients.

Of note, all identified patients carry heterozygous mutations in *IL36RN*. Although homozygous mutations are more likely to result in an altered phenotype due to the presence of pathogenic mutations in both alleles, heterozygous mutations have also been found to cause diseases, for example the ROSAH syndrome described in this thesis. Mechanisms underlying these so-called dominant diseases include dominant negative mutations, where the mutant allele interferes with the wild type

allele and haploinsufficiency, where the amount of gene-product produced by the wild type allele is not enough to ensure the normal phenotype [135]. Furthermore, heterozygous mutations often result in milder forms of the disease compared to homozygous mutations and show an incomplete clinical penetrance, meaning that not all individuals who carry the mutation exhibit clinical symptoms. This incomplete penetrance indicates that also other factors such as other genetic or epigenetic mechanisms or environmental or infectious stimuli are involved in the onset of the disease [136]. A similar mechanism may also underlie the development of CD in *IL36RN*-mutated patients, where the combination of the *IL36RN* mutation with environmental or microbial factors could result in the disease phenotype. This could also explain why the identified *IL36RN*-mutated patients developed CD in adulthood and not in their early childhood, as it typically is the case in monogenic IBD [45].

5.2.4 Anti-IL-36R therapy as personalized therapy for Crohn's disease patients with *IL36RN* mutations

The implication of the IL-36R signaling pathway in various inflammatory conditions has led to the development of therapies targeting the IL-36R. Spesolimab, an IL-36R blocking antibody, has been shown to be effective in treating generalized pustular psoriasis and was recently approved in the European Union [137]. Since studies also suggest the involvement of IL-36R signaling in intestinal inflammation, the use of spesolimab for the treatment of UC and CD has also been evaluated. However, phase 2 clinical trials were unsuccessful as the efficacy endpoints were not met [138]. Although these trials showed that anti-IL-36R therapy had no positive effect on the overall study population, it is possible that it may be effective in a subgroup of IBD patients.

Based on our data, we hypothesized that CD patients with pathogenic *IL36RN* mutations represent a distinct group of CD patients in whom the IL-36R pathway is involved in the development and progression of intestinal inflammation and who may therefore benefit from anti-IL36R therapy.

Given that the first identified *IL36RN*-mutated patient experienced severe, therapy-refractory inflammation, we applied for treatment with spesolimab on the basis of an "individueller Heilversuch". As the patient was steroid-refractory, she was first treated with three cycles of cyclophosphamide to rapidly treat her severe ongoing inflammation. Following, the patient received a combination therapy of spesolimab and certolizumab pegol to achieve long-term clinical remission. Spesolimab and certolizumab were combined because it was expected that both agents would have a synergistic effect and would thus result in a higher efficacy compared to treatment with spesolimab alone.

At week 12 of treatment, we observed a decrease in stool levels of calprotectin and a reduced SES-CD score measured by endoscopy, indicating that the therapy resulted in reduced intestinal inflammation in the IL-36RA patient and a partial clinical response. Additionally, we found that serum levels of IL-18 and IL-23, which were elevated prior to therapy, decreased during therapy.

Furthermore, we observed in PBMCs an increased frequency of pro-inflammatory T cells and a reduced expression of the pro-inflammatory cytokines by myeloid cells after IL-36α stimulation. Since studies have shown that cyclophosphamide treatment can lead to the expansion of pro-inflammatory T cells [139, 140], we mainly attributed the changes in T cells to the cyclophosphamide treatment. In contrast, we hypothesize that the reduced expression of pro-inflammatory cytokines in myeloid cells is caused by the spesolimab treatment and contributes to the reduced intestinal inflammation observed in the IL-36RA patient. However, we cannot exclude the possibility that the here reported molecular changes and the clinical outcome were at least partly caused by treatment with cyclophosphamide or certolizumab pegol or by the combination of all three treatments. In addition, the long-term efficacy of the treatment in our patient could not be evaluated as the therapy had to be discontinued at week 22 due to the development of a perianal abscess.

In conclusion, our data demonstrate that pathogenic *IL36RN* mutations are present in a subgroup of CD patients with ileal disease and that blocking IL-36 signaling may represent a personalized therapeutic approach for this rare subset of patients. To validate our findings, it is necessary to analyze the prevalence of *IL36RN* mutations in larger cohorts and to evaluate the efficacy of anti-IL-36R therapy in other *IL36RN*-mutated patients.

5.3 Aim 3: Analyze the function of the leptin-melanocortin signaling pathway in immune regulation

The leptin-melanocortin signaling pathway plays an important role in body weight regulation, and defects in the pathway such as mutations in *LEPR*, *POMC* and *MC4R* can lead to monogenic obesity. Although the effects of these mutations on the metabolism have been extensively studied, their impact on the immune system has not been analyzed in detail. We here identified specific changes associated with mutations in *LEPR*, *POMC* and *MC4R*, indicating that these proteins are not only involved in body weight regulation but also in immune regulation.

5.3.1 Deep immune cell profiling of patients with mutations in the leptin-melanocortin signaling pathway

To analyze the function of LEPR, POMC and MC4R in immune regulation, we performed deep immune cell profiling by mass cytometry of PBMCs of patients with monogenic obesity and compared the frequency of several T cell, myeloid cell, B cell and NK cell clusters to BMI- and age-matched control groups.

In patients with *LEPR* mutations, we detected a significantly decreased frequency of IL-8^+ IL-6^+ TNFα^+ monocytes and a significantly increased frequency of IL-12^+ IL-23^+ monocytes. These findings are in line with previous studies in mice, which demonstrated that leptin enhances the LPS-induced

production of pro-inflammatory cytokines in macrophages and that *LEPR*-deficient db/db mice have an impaired bacterial phagocytosis and killing [96, 141]. Similarly, it has been observed that leptin induces the proliferation, activation and secretion of pro-inflammatory cytokines of human monocytes *in vitro* [142, 143].

To further analyze the myeloid cell compartment of our *LEPR*-mutated patients, we differentiated blood-derived monocytes into macrophages and measured LPS-induced cytokine production. Interestingly, only the macrophages of one *LEPR*-mutated patient (LEPR 2) produced reduced levels of TNFα and IL-6 similar to the findings obtained by mass cytometry, whereas macrophages of the other *LEPR*-mutated patient (LEPR 1) showed no differences compared to the controls. These findings may reflect the impact of the different *LEPR* mutations identified in these patients on LEPR function. While the LEPR 2 patient was compound heterozygous for the missense mutation p.W664R and the large deletion 2674-3564del, the LEPR 1 patient was homozygous for the p.W664R mutation. Functional studies of the p.W664R variant revealed that the mutation does not lead to a complete loss of function of LEPR, but only reduces the activity of LEPR by half compared to the wild type [81]. Therefore, it is possible that the remaining activity of LEPR in the LEPR 1 patient carrying the homozygous p.W664R mutation is sufficient to maintain the normal phenotype of macrophages. In contrast, the large deletion in *LEPR* identified in the LEPR 2 patient is likely to have a more severe impact on the LEPR function and consequently on the myeloid cell function. However, to conclude how defects in leptin signaling affect myeloid cell function in humans, it is necessary to repeat and validate these experiments in other *LEPR*-mutated patients.

Furthermore, we observed an increased frequency of plasma cells in *LEPR*-mutated patients, which could indicate that leptin signaling is involved in plasma cell differentiation.

Research in mice and humans suggests that leptin signaling also plays an important role in T cell differentiation and function. In humans, it has been demonstrated that the addition of leptin leads to an enhanced T cell proliferation and to an increased production of pro-inflammatory cytokines by T cells *in vitro* [94, 144]. Additionally, it has been reported that *LEPR*-mutated patients have a reduced frequency of $CD4^+$ T cells [88]. Moreover, studies in mice have shown that leptin signaling is an important regulator of Th1 and Th17 differentiation [93, 95]. However, we did not observe any differences in the T cell frequency or the cytokine expression in T cells in our *LEPR*-mutated patients.

Given that studies in mice have mainly analyzed the function of leptin signaling in the context of acute or chronic inflammation, differences in Th1 and Th17 differentiation in *LEPR*-mutated patients might only be apparent in inflammation and not in the healthy state, which we have studied here. Furthermore, more subtle differences in cytokine expression and proliferation might not be detectable by mass cytometry. Consequently, *in vitro* experiments should be performed to analyze the proliferation and cytokine production of T cells of *LEPR*-mutated patients in more detail.

In *POMC*-mutated patients, we found a significantly increased frequency of several effector $CD4^+$ and $CD8^+$ T cells subsets producing TNFα, IFNγ and IL-2. POMC is a precursor peptide that can be cleaved into eight different peptides. The *POMC*-mutated patients analyzed here carry homozygous nonsense mutations in *POMC* that lead to a premature stop codon and presumably to the absence of nearly all POMC-derived peptides (**Figure 43**). Therefore, these patients lack the expression of the hormone ACTH, which is crucial for the production and secretion of glucocorticoid hormones [83]. Since glucocorticoid hormones, such as cortisol have anti-inflammatory properties [99], the lack of ACTH could result in increased pro-inflammatory responses. However, as all analyzed *POMC*-mutated patients were receiving hydrocortisone replacement therapy, it is unlikely that the observed effects were caused by a lack of cortisol. Studies have shown that α-MSH has also anti-inflammatory properties and can downregulate pro-inflammatory cytokines *in vitro* [100]. Consequently, the increased frequency of effector T cells could be the result of α-MSH deficiency. However, further experiments are needed to determine the mechanisms causing the increased frequency of effector T cells subsets observed in *POMC*-mutated patients.

In *MC4R*-mutated patients, we observed a significantly increased frequency of B cells and a significantly decreased frequency of $TNF\alpha^+$ B cells. Since MC4R expression is also upregulated in plasma cells [104], these findings could indicate that MC4R plays a role in B cell differentiation and function. Importantly, we here only analyzed patients with heterozygous *MC4R* mutations, who have a milder form of monogenic obesity, which is assumed to be caused by a reduced expression of functional MC4R [145]. Therefore, characterizing patients with rare, homozygous mutations in *MC4R* could provide more information on the role of MC4R in immune regulation.

Finally, we also analyzed the immune cell composition of one *PCSK1*-mutated patient. *PCSK1* encodes PC1/3, a peptidase essential for the processing of several proteins, including POMC, NPY, AgRP, proinsulin and proglucagon [146]. Consequently, PC1/3 deficiency leads to a number of symptoms including severe obesity, hyperphagia, adrenal insufficiency and malabsorptive diarrhea. In PC1/3-deficient mice, it has been observed that macrophages produce increased levels of pro-inflammatory cytokines and that *in vivo* administration of LPS leads to an increased expression of pro-inflammatory cytokines [103]. In our *PCSK1*-mutated patient, we detected an increased frequency of DCs but no other differences in myeloid cell frequency and function. Furthermore, we found a decreased frequency of $CD4^+$ T cells and several effector T cell subsets in PBMCs of the *PCSK1*-mutated patient, indicating that PC1/3 might also play a role in T cell differentiation and function. However, as these findings are based on a single patient, generalization of the results might be limited and require validation in other *PCSK1*-mutated patients.

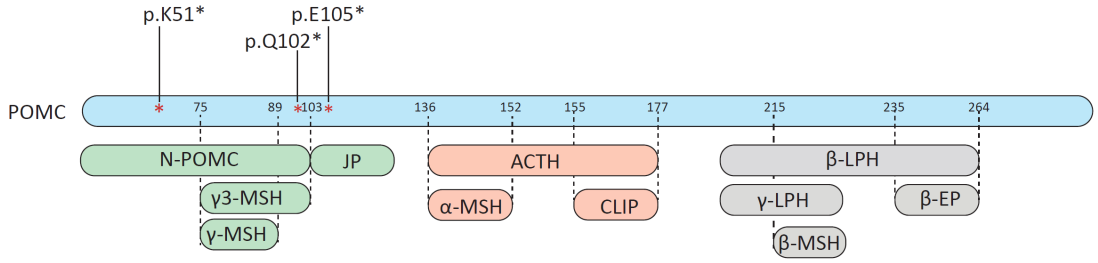

Figure 43: Location of mutations in proopiomelanocortin.
Schematic representation of proopiomelancortin (POMC) and POMC-derived peptides. Cleavage sites are marked by the number of the respective amino acid. * indicates the position of mutations identified in patients analyzed in this thesis. N-POMC = N-terminal peptide of POMC, JP = joining peptide, MSH = melanocyte-stimulating hormone, ACTH = adrenocorticotropic hormone, CLIP = corticotropin-like intermediate [lobe] peptide, LPH = lipotropic hormone, β-EP = β-endorphin. Adapted from Harno et al. 2018 [147].

5.3.2 Limitations and outlook

All analyzed patients with monogenic obesity, except for one *LEPR*-mutated patient and the *PCSK1*-mutated patient were treated with setmelanotide. Setmelanotide is an eight amino acid cyclic peptide analogue of the endogenous MC4R ligand α-MSH [148]. Since studies have shown that α-MSH has anti-inflammatory properties [100, 101], it is possible that setmelanotide has similar functions. Therefore, setmelanotide treatment could have affected the immune cell composition and function in patients with monogenic obesity analyzed here. To determine the exact effects of setmelanotide treatment on the immune system, we are currently performing an in-depth immune cell profiling of PBMCs of patients before and after setmelanotide treatment. In addition, functional assays are needed to validate our findings and to investigate underlying mechanisms leading to the immune cell alterations observed in patients with monogenic obesity.

Despite these limitations, the data presented here, provide the first in-depth characterization of the immune cell composition of patients with monogenic obesity and further supports data from mice and humans indicating that LEPR, POMC and MC4R are not only important for appetite regulation but also have specific functions in the immune system.

5.4 Development of a pipeline for the characterization of rare autoimmune diseases

Linking identified mutations to the clinical phenotype of a patient remains a major challenge in the field of rare diseases. Consequently, the underlying mechanisms of rare diseases are often not understood and patients are treated based on symptoms rather than the molecular phenotype, leading to inadequate management of disease symptoms [149]. By studying three rare autoimmune diseases, we here developed a pipeline for the characterization of rare autoimmune diseases in order to improve diagnosis and therapy of patients. We demonstrated that a combination of whole-exome sequencing, deep immune cell profiling by mass cytometry and functional assays facilitates the

identification of altered cell states in patients and the selection of treatments that specifically target these cell states (**Figure 44**). Similarly, studies in the field of pediatrics have shown that combining clinical data with molecular data improves diagnosis and leads to a better understanding of genetic disorders [150, 151]. We suggest that the pipeline developed here cannot only be used for the characterization of classical rare diseases such as the ROSAH syndrome, but also for common auto-inflammatory diseases such as IBD, where subgroups of patients have distinct molecular phenotypes requiring different treatment strategies. Finally, our work highlights that applying this pipeline does not only improve diagnosis and therapy of patients, but also allows us to investigate molecular mechanisms of immune regulation and function in humans.

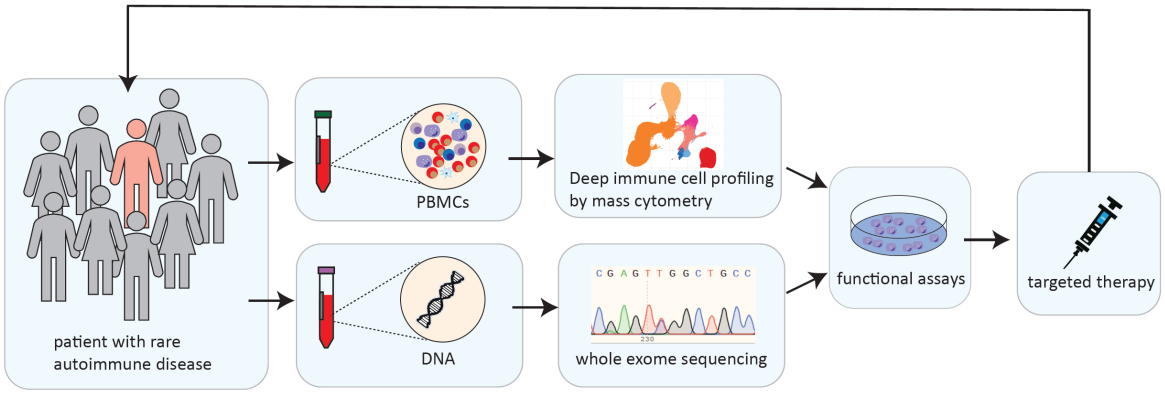

Figure 44: Pipeline for characterizing patients with rare autoimmune diseases.
We propose that patients with rare autoimmune diseases and patients with rare subtypes of common autoimmune diseases should undergo whole exome sequencing (WES) to identify disease causing variants and deep immune cell profiling by mass cytometry to identify differences in immune cell composition and function. Based on the results obtained by WES and mass cytometry, specific functional assays should be performed to identify functional alterations in specific immune cell subsets and consequently selecting treatments specifically targeting these alterations.

6 References

1. Fugger, L., L.T. Jensen, and J. Rossjohn, *Challenges, Progress, and Prospects of Developing Therapies to Treat Autoimmune Diseases.* Cell, 2020. **181**(1): p. 63-80.
2. Rosenblum, M.D., K.A. Remedios, and A.K. Abbas, *Mechanisms of human autoimmunity.* J Clin Invest, 2015. **125**(6): p. 2228-33.
3. Wright, C.F., D.R. FitzPatrick, and H.V. Firth, *Paediatric genomics: diagnosing rare disease in children.* Nat Rev Genet, 2018. **19**(5): p. 325.
4. Haendel, M., et al., *How many rare diseases are there?* Nat Rev Drug Discov, 2020. **19**(2): p. 77-78.
5. Gambineri, E., T.R. Torgerson, and H.D. Ochs, *Immune dysregulation, polyendocrinopathy, enteropathy, and X-linked inheritance (IPEX), a syndrome of systemic autoimmunity caused by mutations of FOXP3, a critical regulator of T-cell homeostasis.* Curr Opin Rheumatol, 2003. **15**(4): p. 430-5.
6. Fischer, A., *Gene therapy for inborn errors of immunity: past, present and future.* Nat Rev Immunol, 2023. **23**(6): p. 397-408.
7. Notarangelo, L.D., et al., *Human RAG mutations: biochemistry and clinical implications.* Nat Rev Immunol, 2016. **16**(4): p. 234-46.
8. Wise, A.L., et al., *Genomic medicine for undiagnosed diseases.* Lancet, 2019. **394**(10197): p. 533-540.
9. Splinter, K., et al., *Effect of Genetic Diagnosis on Patients with Previously Undiagnosed Disease.* N Engl J Med, 2018. **379**(22): p. 2131-2139.
10. Landrum, M.J., et al., *ClinVar: public archive of interpretations of clinically relevant variants.* Nucleic Acids Res, 2016. **44**(D1): p. D862-8.
11. Findlay, G.M., *Linking genome variants to disease: scalable approaches to test the functional impact of human mutations.* Hum Mol Genet, 2021. **30**(R2): p. R187-R197.
12. Hartmann, F.J. and S.C. Bendall, *Immune monitoring using mass cytometry and related high-dimensional imaging approaches.* Nat Rev Rheumatol, 2020. **16**(2): p. 87-99.
13. Vivier, E. and B. Malissen, *Innate and adaptive immunity: specificities and signaling hierarchies revisited.* Nat Immunol, 2005. **6**(1): p. 17-21.
14. Jakubzick, C.V., G.J. Randolph, and P.M. Henson, *Monocyte differentiation and antigen-presenting functions.* Nat Rev Immunol, 2017. **17**(6): p. 349-362.
15. Murphy, K. and C. Weaver, *Janeway's immunobiology 9th edition*. 2017: Garland Science, Taylor & Francis Group, LLC,.
16. Abel, A.M., et al., *Natural Killer Cells: Development, Maturation, and Clinical Utilization.* Front Immunol, 2018. **9**: p. 1869.
17. Eberl, G., et al., *Innate lymphoid cells. Innate lymphoid cells: a new paradigm in immunology.* Science, 2015. **348**(6237): p. aaa6566.
18. Sun, L., et al., *T cells in health and disease.* Signal Transduct Target Ther, 2023. **8**(1): p. 235.
19. van den Broek, T., J.A.M. Borghans, and F. van Wijk, *The full spectrum of human naive T cells.* Nat Rev Immunol, 2018. **18**(6): p. 363-373.
20. Koh, C.H., et al., *CD8 T-cell subsets: heterogeneity, functions, and therapeutic potential.* Exp Mol Med, 2023. **55**(11): p. 2287-2299.
21. Sanz, I., et al., *Challenges and Opportunities for Consistent Classification of Human B Cell and Plasma Cell Populations.* Front Immunol, 2019. **10**: p. 2458.
22. Ardito, F., et al., *The crucial role of protein phosphorylation in cell signaling and its use as targeted therapy (Review).* Int J Mol Med, 2017. **40**(2): p. 271-280.
23. Middelbeek, J., et al., *The alpha-kinase family: an exceptional branch on the protein kinase tree.* Cell Mol Life Sci, 2010. **67**(6): p. 875-90.
24. Ryazanov, A.G., K.S. Pavur, and M.V. Dorovkov, *Alpha-kinases: a new class of protein kinases with a novel catalytic domain.* Curr Biol, 1999. **9**(2): p. R43-5.

25. Heine, M., et al., *Alpha-kinase 1, a new component in apical protein transport.* J Biol Chem, 2005. **280**(27): p. 25637-43.
26. Zhou, P., et al., *Alpha-kinase 1 is a cytosolic innate immune receptor for bacterial ADP-heptose.* Nature, 2018. **561**(7721): p. 122-126.
27. Gaudet, R.G., et al., *INNATE IMMUNITY. Cytosolic detection of the bacterial metabolite HBP activates TIFA-dependent innate immunity.* Science, 2015. **348**(6240): p. 1251-5.
28. Zimmermann, S., et al., *ALPK1- and TIFA-Dependent Innate Immune Response Triggered by the Helicobacter pylori Type IV Secretion System.* Cell Rep, 2017. **20**(10): p. 2384-2395.
29. Xue, Y. and S.M. Man, *ALPK1: innate attraction to the sweetness of bacteria.* Cell Res, 2018. **28**(12): p. 1125-1126.
30. Yamada, Y., et al., *Identification of chromosome 3q28 and ALPK1 as susceptibility loci for chronic kidney disease in Japanese individuals by a genome-wide association study.* J Med Genet, 2013. **50**(6): p. 410-8.
31. Shimokata, S., et al., *Association between polymorphisms of the alpha-kinase 1 gene and type 2 diabetes mellitus in community-dwelling individuals.* Biomed Rep, 2013. **1**(6): p. 940-944.
32. Ko, A.M., et al., *ALPK1 genetic regulation and risk in relation to gout.* Int J Epidemiol, 2013. **42**(2): p. 466-74.
33. Lee, C.P., et al., *ALPK1 phosphorylates myosin IIA modulating TNF-alpha trafficking in gout flares.* Sci Rep, 2016. **6**: p. 25740.
34. Ryzhakov, G., et al., *Alpha kinase 1 controls intestinal inflammation by suppressing the IL-12/Th1 axis.* Nat Commun, 2018. **9**(1): p. 3797.
35. Williams, L.B., et al., *ALPK1 missense pathogenic variant in five families leads to ROSAH syndrome, an ocular multisystem autosomal dominant disorder.* Genet Med, 2019. **21**(9): p. 2103-2115.
36. Jamilloux, Y., et al., *ALPK1 Gene Mutations Drive Autoinflammation with Ectodermal Dysplasia and Progressive Vision Loss.* J Clin Immunol, 2021. **41**(7): p. 1671-1673.
37. Kozycki, C.T., et al., *Gain-of-function mutations in ALPK1 cause an NF-kappaB-mediated autoinflammatory disease: functional assessment, clinical phenotyping and disease course of patients with ROSAH syndrome.* Ann Rheum Dis, 2022. **81**(10): p. 1453-1464.
38. Zhao, M., et al., *The Burden of Inflammatory Bowel Disease in Europe in 2020.* J Crohns Colitis, 2021. **15**(9): p. 1573-1587.
39. Neurath, M.F., *Targeting immune cell circuits and trafficking in inflammatory bowel disease.* Nat Immunol, 2019. **20**(8): p. 970-979.
40. D'Alessio, S., et al., *Revisiting fibrosis in inflammatory bowel disease: the gut thickens.* Nat Rev Gastroenterol Hepatol, 2022. **19**(3): p. 169-184.
41. Rogler, G., et al., *Extraintestinal Manifestations of Inflammatory Bowel Disease: Current Concepts, Treatment, and Implications for Disease Management.* Gastroenterology, 2021. **161**(4): p. 1118-1132.
42. Momozawa, Y., et al., *IBD risk loci are enriched in multigenic regulatory modules encompassing putative causative genes.* Nat Commun, 2018. **9**(1): p. 2427.
43. Loddo, I. and C. Romano, *Inflammatory Bowel Disease: Genetics, Epigenetics, and Pathogenesis.* Front Immunol, 2015. **6**: p. 551.
44. Alsoud, D., et al., *Breaking the therapeutic ceiling in drug development in ulcerative colitis.* Lancet Gastroenterol Hepatol, 2021. **6**(7): p. 589-595.
45. Graham, D.B. and R.J. Xavier, *Pathway paradigms revealed from the genetics of inflammatory bowel disease.* Nature, 2020. **578**(7796): p. 527-539.
46. Towne, J.E., et al., *Interleukin (IL)-1F6, IL-1F8, and IL-1F9 signal through IL-1Rrp2 and IL-1RAcP to activate the pathway leading to NF-kappaB and MAPKs.* J Biol Chem, 2004. **279**(14): p. 13677-88.
47. Yi, G., et al., *Structural and Functional Attributes of the Interleukin-36 Receptor.* J Biol Chem, 2016. **291**(32): p. 16597-609.

48. Debets, R., et al., *Two novel IL-1 family members, IL-1 delta and IL-1 epsilon, function as an antagonist and agonist of NF-kappa B activation through the orphan IL-1 receptor-related protein 2.* J Immunol, 2001. **167**(3): p. 1440-6.
49. van de Veerdonk, F.L., et al., *IL-38 binds to the IL-36 receptor and has biological effects on immune cells similar to IL-36 receptor antagonist.* Proc Natl Acad Sci U S A, 2012. **109**(8): p. 3001-5.
50. Elias, M., et al., *IL-36 in chronic inflammation and fibrosis - bridging the gap?* J Clin Invest, 2021. **131**(2).
51. Carrier, Y., et al., *Inter-regulation of Th17 cytokines and the IL-36 cytokines in vitro and in vivo: implications in psoriasis pathogenesis.* J Invest Dermatol, 2011. **131**(12): p. 2428-37.
52. Gresnigt, M.S., et al., *The IL-36 receptor pathway regulates Aspergillus fumigatus-induced Th1 and Th17 responses.* Eur J Immunol, 2013. **43**(2): p. 416-26.
53. Towne, J.E., et al., *Interleukin-36 (IL-36) ligands require processing for full agonist (IL-36alpha, IL-36beta, and IL-36gamma) or antagonist (IL-36Ra) activity.* J Biol Chem, 2011. **286**(49): p. 42594-42602.
54. Sachen, K.L., C.N. Arnold Greving, and J.E. Towne, *Role of IL-36 cytokines in psoriasis and other inflammatory skin conditions.* Cytokine, 2022. **156**: p. 155897.
55. Scheibe, K., et al., *IL-36R signalling activates intestinal epithelial cells and fibroblasts and promotes mucosal healing in vivo.* Gut, 2017. **66**(5): p. 823-838.
56. Scheibe, K., et al., *Inhibiting Interleukin 36 Receptor Signaling Reduces Fibrosis in Mice With Chronic Intestinal Inflammation.* Gastroenterology, 2019. **156**(4): p. 1082-1097 e11.
57. Bridgewood, C., et al., *IL-36gamma has proinflammatory effects on human endothelial cells.* Exp Dermatol, 2017. **26**(5): p. 402-408.
58. Foster, A.M., et al., *IL-36 promotes myeloid cell infiltration, activation, and inflammatory activity in skin.* J Immunol, 2014. **192**(12): p. 6053-61.
59. Dietrich, D., et al., *Interleukin-36 potently stimulates human M2 macrophages, Langerhans cells and keratinocytes to produce pro-inflammatory cytokines.* Cytokine, 2016. **84**: p. 88-98.
60. Vigne, S., et al., *IL-36 signaling amplifies Th1 responses by enhancing proliferation and Th1 polarization of naive CD4+ T cells.* Blood, 2012. **120**(17): p. 3478-87.
61. Miura, S., et al., *IL-36 and IL-17A Cooperatively Induce a Psoriasis-Like Gene Expression Response in Human Keratinocytes.* J Invest Dermatol, 2021. **141**(8): p. 2086-2090.
62. Leon, G., et al., *IL-36 cytokines imprint a colitogenic phenotype on CD4(+) T helper cells.* Mucosal Immunol, 2022. **15**(3): p. 491-503.
63. Schmitt, V., et al., *Interleukin-36 receptor mediates the crosstalk between plasma cells and synovial fibroblasts.* Eur J Immunol, 2017. **47**(12): p. 2101-2112.
64. Johnston, A., et al., *IL-1F5, -F6, -F8, and -F9: a novel IL-1 family signaling system that is active in psoriasis and promotes keratinocyte antimicrobial peptide expression.* J Immunol, 2011. **186**(4): p. 2613-22.
65. Tortola, L., et al., *Psoriasiform dermatitis is driven by IL-36-mediated DC-keratinocyte crosstalk.* J Clin Invest, 2012. **122**(11): p. 3965-76.
66. Marrakchi, S., et al., *Interleukin-36-receptor antagonist deficiency and generalized pustular psoriasis.* N Engl J Med, 2011. **365**(7): p. 620-8.
67. Nishida, A., et al., *Increased Expression of Interleukin-36, a Member of the Interleukin-1 Cytokine Family, in Inflammatory Bowel Disease.* Inflamm Bowel Dis, 2016. **22**(2): p. 303-14.
68. Boutet, M.A., et al., *Distinct expression of interleukin (IL)-36alpha, beta and gamma, their antagonist IL-36Ra and IL-38 in psoriasis, rheumatoid arthritis and Crohn's disease.* Clin Exp Immunol, 2016. **184**(2): p. 159-73.
69. Medina-Contreras, O., et al., *Cutting Edge: IL-36 Receptor Promotes Resolution of Intestinal Damage.* J Immunol, 2016. **196**(1): p. 34-8.
70. Kopelman, P.G., *Obesity as a medical problem.* Nature, 2000. **404**(6778): p. 635-43.
71. Friedman, J.M., *Leptin and the endocrine control of energy balance.* Nat Metab, 2019. **1**(8): p. 754-764.

72. Lee, G.H., et al., *Abnormal splicing of the leptin receptor in diabetic mice.* Nature, 1996. **379**(6566): p. 632-5.
73. Lavoie, O., N.J. Michael, and A. Caron, *A critical update on the leptin-melanocortin system.* J Neurochem, 2023. **165**(4): p. 467-486.
74. Yeo, G.S.H., et al., *The melanocortin pathway and energy homeostasis: From discovery to obesity therapy.* Mol Metab, 2021. **48**: p. 101206.
75. Baldini, G. and K.D. Phelan, *The melanocortin pathway and control of appetite-progress and therapeutic implications.* J Endocrinol, 2019. **241**(1): p. R1-R33.
76. Center for Disease Control and Prevention. *Defining Child BMI Categories* [cited 2024 14.03.]; Available from: https://www.cdc.gov/obesity/basics/childhood-defining.html.
77. World Health Organisation. *Obesity and overweight*. [cited 2024 14.03.]; Available from: https://www.who.int/news-room/fact-sheets/detail/obesity-and-overweight#:~:text=In%202022%2C%202.5%20billion%20adults,age%20of%205%20were%20overweight.
78. World Health Organisation. *Prevalence of obesity among children and adolescents aged 5 to 19 years*. [cited 2024 14.03.]; Available from: https://data.who.int/indicators/i/EF93DDB.
79. Maes, H.H., M.C. Neale, and L.J. Eaves, *Genetic and environmental factors in relative body weight and human adiposity.* Behav Genet, 1997. **27**(4): p. 325-51.
80. Farooqi, I.S., et al., *Clinical and molecular genetic spectrum of congenital deficiency of the leptin receptor.* N Engl J Med, 2007. **356**(3): p. 237-47.
81. Shah, B.P., et al., *Functional characterization of all missense variants in LEPR, PCSK1, and POMC genes arising from single-nucleotide variants.* Expert Rev Endocrinol Metab, 2023. **18**(2): p. 209-219.
82. Clement, K., et al., *A mutation in the human leptin receptor gene causes obesity and pituitary dysfunction.* Nature, 1998. **392**(6674): p. 398-401.
83. Krude, H., et al., *Severe early-onset obesity, adrenal insufficiency and red hair pigmentation caused by POMC mutations in humans.* Nat Genet, 1998. **19**(2): p. 155-7.
84. Jackson, R.S., et al., *Obesity and impaired prohormone processing associated with mutations in the human prohormone convertase 1 gene.* Nat Genet, 1997. **16**(3): p. 303-6.
85. Kuhnen, P., S. Wiegand, and H. Biebermann, *Pharmacological treatment strategies for patients with monogenic obesity.* J Pediatr Endocrinol Metab, 2020.
86. Zatterale, F., et al., *Chronic Adipose Tissue Inflammation Linking Obesity to Insulin Resistance and Type 2 Diabetes.* Front Physiol, 2019. **10**: p. 1607.
87. Han, J.M. and M.K. Levings, *Immune regulation in obesity-associated adipose inflammation.* J Immunol, 2013. **191**(2): p. 527-32.
88. Farooqi, I.S., et al., *Beneficial effects of leptin on obesity, T cell hyporesponsiveness, and neuroendocrine/metabolic dysfunction of human congenital leptin deficiency.* J Clin Invest, 2002. **110**(8): p. 1093-103.
89. Saeed, S., et al., *High morbidity and mortality in children with untreated congenital deficiency of leptin or its receptor.* Cell Rep Med, 2023. **4**(9): p. 101187.
90. Siegmund, B., H.A. Lehr, and G. Fantuzzi, *Leptin: a pivotal mediator of intestinal inflammation in mice.* Gastroenterology, 2002. **122**(7): p. 2011-25.
91. Howard, J.K., et al., *Leptin protects mice from starvation-induced lymphoid atrophy and increases thymic cellularity in ob/ob mice.* J Clin Invest, 1999. **104**(8): p. 1051-9.
92. Mandel, M.A. and A.A. Mahmoud, *Impairment of cell-mediated immunity in mutation diabetic mice (db/db).* J Immunol, 1978. **120**(4): p. 1375-7.
93. Siegmund, B., et al., *Leptin receptor expression on T lymphocytes modulates chronic intestinal inflammation in mice.* Gut, 2004. **53**(7): p. 965-72.
94. Martin-Romero, C., et al., *Human leptin enhances activation and proliferation of human circulating T lymphocytes.* Cell Immunol, 2000. **199**(1): p. 15-24.
95. Reis, B.S., et al., *Leptin receptor signaling in T cells is required for Th17 differentiation.* J Immunol, 2015. **194**(11): p. 5253-60.

96. Mancuso, P., et al., *Ablation of the leptin receptor in myeloid cells impairs pulmonary clearance of Streptococcus pneumoniae and alveolar macrophage bactericidal function.* Am J Physiol Lung Cell Mol Physiol, 2018. **315**(1): p. L78-L86.
97. Kredel, L.I., et al., *Adipokines from local fat cells shape the macrophage compartment of the creeping fat in Crohn's disease.* Gut, 2013. **62**(6): p. 852-62.
98. Kiernan, K. and N.J. MacIver, *The Role of the Adipokine Leptin in Immune Cell Function in Health and Disease.* Front Immunol, 2020. **11**: p. 622468.
99. Padgett, D.A. and R. Glaser, *How stress influences the immune response.* Trends Immunol, 2003. **24**(8): p. 444-8.
100. Rajora, N., et al., *alpha-MSH production, receptors, and influence on neopterin in a human monocyte/macrophage cell line.* J Leukoc Biol, 1996. **59**(2): p. 248-53.
101. Rajora, N., et al., *alpha-MSH modulates experimental inflammatory bowel disease.* Peptides, 1997. **18**(3): p. 381-5.
102. Maaser, C., et al., *Crucial role of the melanocortin receptor MC1R in experimental colitis.* Gut, 2006. **55**(10): p. 1415-22.
103. Refaie, S., et al., *Disruption of proprotein convertase 1/3 (PC1/3) expression in mice causes innate immune defects and uncontrolled cytokine secretion.* J Biol Chem, 2012. **287**(18): p. 14703-17.
104. The Human Protein Atlas. *MC4R*. [cited 2024 14.03.]; Available from: https://www.proteinatlas.org/ENSG00000166603-MC4R/single+cell+type.
105. Srisai, D., et al., *Characterization of the hyperphagic response to dietary fat in the MC4R knockout mouse.* Endocrinology, 2011. **152**(3): p. 890-902.
106. Farooqi, I.S., et al., *Clinical spectrum of obesity and mutations in the melanocortin 4 receptor gene.* N Engl J Med, 2003. **348**(12): p. 1085-95.
107. Jumper, J., et al., *Highly accurate protein structure prediction with AlphaFold.* Nature, 2021. **596**(7873): p. 583-589.
108. Varadi, M., et al., *AlphaFold Protein Structure Database: massively expanding the structural coverage of protein-sequence space with high-accuracy models.* Nucleic Acids Res, 2022. **50**(D1): p. D439-D444.
109. Dunn, E.F., et al., *High-resolution structure of murine interleukin 1 homologue IL-1F5 reveals unique loop conformations for receptor binding specificity.* Biochemistry, 2003. **42**(37): p. 10938-44.
110. Onoufriadis, A., et al., *Mutations in IL36RN/IL1F5 are associated with the severe episodic inflammatory skin disease known as generalized pustular psoriasis.* Am J Hum Genet, 2011. **89**(3): p. 432-7.
111. Weinhold, K.J., et al., *Reversibility of peripheral blood leukocyte phenotypic and functional changes after exposure to and withdrawal from tofacitinib, a Janus kinase inhibitor, in healthy volunteers.* Clin Immunol, 2018. **191**: p. 10-20.
112. Mamat, U., et al., *Endotoxin-free protein production—ClearColi™ technology.* Nat Methods, 2013. **10**: p. 916.
113. Majde, J.A., *Microbial cell-wall contaminants in peptides: a potential source of physiological artifacts.* Peptides, 1993. **14**(3): p. 629-32.
114. Adzhubei, I.A., et al., *A method and server for predicting damaging missense mutations.* Nat Methods, 2010. **7**(4): p. 248-9.
115. Karczewski, K.J., et al., *Author Correction: The mutational constraint spectrum quantified from variation in 141,456 humans.* Nature, 2021. **590**(7846): p. E53.
116. Krude, H., et al., *Obesity due to proopiomelanocortin deficiency: three new cases and treatment trials with thyroid hormone and ACTH4-10.* J Clin Endocrinol Metab, 2003. **88**(10): p. 4633-40.
117. Petersen, C.M., et al., *Internalization, lysosomal degradation and new synthesis of surface membrane CD4 in phorbol ester-activated T-lymphocytes and U-937 cells.* Exp Cell Res, 1992. **201**(1): p. 160-73.

118. Fischer, K., et al., *Isolation and characterization of human antigen-specific TCR alpha beta+ CD4(-)CD8- double-negative regulatory T cells.* Blood, 2005. **105**(7): p. 2828-35.
119. Hecker, J., et al., *Early Onset of TNFalpha-Driven Arthritis, Auto-inflammation, and Progressive Loss of Vision in a Patient with ALPK1 Mutation.* J Clin Immunol, 2022. **42**(4): p. 880-884.
120. Popa, C., et al., *Repeated B lymphocyte depletion with rituximab in rheumatoid arthritis over 7 yrs.* Rheumatology (Oxford), 2007. **46**(4): p. 626-30.
121. Roll, P., et al., *Regeneration of B cell subsets after transient B cell depletion using anti-CD20 antibodies in rheumatoid arthritis.* Arthritis Rheum, 2006. **54**(8): p. 2377-86.
122. Garcia-Weber, D., et al., *In vitro kinase assay reveals ADP-heptose-dependent ALPK1 autophosphorylation and altered kinase activity of disease-associated ALPK1 mutants.* Sci Rep, 2023. **13**(1): p. 6278.
123. Valli, A., et al., *Tofacitinib treatment modulates the levels of several inflammation-related plasma proteins in rheumatoid arthritis and baseline levels of soluble biomarkers associate with the treatment response.* Clin Exp Immunol, 2022. **210**(2): p. 141-150.
124. Zhong, L., et al., *Juvenile Onset Splenomegaly and Oculopathy Due to Germline Mutation in ALPK1.* J Clin Immunol, 2020. **40**(2): p. 350-358.
125. Shivanna, M., et al., *Ocular Ciliopathies: Genetic and Mechanistic Insights into Developing Therapies.* Curr Med Chem, 2019. **26**(17): p. 3120-3131.
126. ClinicalTrials.gov. *Evaluating the Safety, Tolerability, and Pharmacokinetics of DF-003 in Healthy Subjects*. [cited 2024 27.03]; Available from: https://clinicaltrials.gov/study/NCT05997641.
127. Garufi, C., et al., *Affecting the effectors: JAK inhibitors modulation of immune cell numbers and functions in patients with rheumatoid arthritis.* Expert Rev Clin Immunol, 2022. **18**(3): p. 309-319.
128. Russell, S.E., et al., *IL-36alpha expression is elevated in ulcerative colitis and promotes colonic inflammation.* Mucosal Immunol, 2016. **9**(5): p. 1193-204.
129. Dinarello, C.A. and G. Fantuzzi, *Interleukin-18 and host defense against infection.* J Infect Dis, 2003. **187 Suppl 2**: p. S370-84.
130. Lyakh, L., et al., *Regulation of interleukin-12/interleukin-23 production and the T-helper 17 response in humans.* Immunol Rev, 2008. **226**: p. 112-31.
131. Tauber, M., et al., *IL36RN Mutations Affect Protein Expression and Function: A Basis for Genotype-Phenotype Correlation in Pustular Diseases.* J Invest Dermatol, 2016. **136**(9): p. 1811-1819.
132. Pace, C.N., et al., *Contribution of hydrogen bonds to protein stability.* Protein Sci, 2014. **23**(5): p. 652-61.
133. Schwarz, H., et al., *Residual endotoxin contaminations in recombinant proteins are sufficient to activate human CD1c+ dendritic cells.* PLoS One, 2014. **9**(12): p. e113840.
134. Sazonovs, A., et al., *Large-scale sequencing identifies multiple genes and rare variants associated with Crohn's disease susceptibility.* Nat Genet, 2022. **54**(9): p. 1275-1283.
135. Veitia, R.A., S. Caburet, and J.A. Birchler, *Mechanisms of Mendelian dominance.* Clin Genet, 2018. **93**(3): p. 419-428.
136. Hadjadj, J., et al., *Early-onset autoimmunity associated with SOCS1 haploinsufficiency.* Nat Commun, 2020. **11**(1): p. 5341.
137. Blair, H.A., *Spesolimab: First Approval.* Drugs, 2022. **82**(17): p. 1681-1686.
138. Ferrante, M., et al., *Safety and tolerability of spesolimab in patients with ulcerative colitis.* Expert Opin Drug Saf, 2023. **22**(2): p. 141-152.
139. Ahlmann, M. and G. Hempel, *The effect of cyclophosphamide on the immune system: implications for clinical cancer therapy.* Cancer Chemother Pharmacol, 2016. **78**(4): p. 661-71.
140. Scurr, M., et al., *Low-Dose Cyclophosphamide Induces Antitumor T-Cell Responses, which Associate with Survival in Metastatic Colorectal Cancer.* Clin Cancer Res, 2017. **23**(22): p. 6771-6780.

141. Monteiro, L.B., et al., *Leptin Signaling Suppression in Macrophages Improves Immunometabolic Outcomes in Obesity.* Diabetes, 2022. **71**(7): p. 1546-1561.
142. Santos-Alvarez, J., R. Goberna, and V. Sanchez-Margalet, *Human leptin stimulates proliferation and activation of human circulating monocytes.* Cell Immunol, 1999. **194**(1): p. 6-11.
143. Gainsford, T., et al., *Leptin can induce proliferation, differentiation, and functional activation of hemopoietic cells.* Proc Natl Acad Sci U S A, 1996. **93**(25): p. 14564-8.
144. Lord, G.M., et al., *Leptin modulates the T-cell immune response and reverses starvation-induced immunosuppression.* Nature, 1998. **394**(6696): p. 897-901.
145. Drabkin, M., O.S. Birk, and R. Birk, *Heterozygous versus homozygous phenotype caused by the same MC4R mutation: novel mutation affecting a large consanguineous kindred.* BMC Med Genet, 2018. **19**(1): p. 135.
146. Wang, L., et al., *PC1/3 Deficiency Impacts Pro-opiomelanocortin Processing in Human Embryonic Stem Cell-Derived Hypothalamic Neurons.* Stem Cell Reports, 2017. **8**(2): p. 264-277.
147. Harno, E., et al., *POMC: The Physiological Power of Hormone Processing.* Physiol Rev, 2018. **98**(4): p. 2381-2430.
148. Markham, A., *Setmelanotide: First Approval.* Drugs, 2021. **81**(3): p. 397-403.
149. Schee Genannt Halfmann, S., et al., *Personalized Medicine: What's in it for Rare Diseases?* Adv Exp Med Biol, 2017. **1031**: p. 387-404.
150. Bolton, C., et al., *An Integrated Taxonomy for Monogenic Inflammatory Bowel Disease.* Gastroenterology, 2022. **162**(3): p. 859-876.
151. Pijuan, J., et al., *Translational Diagnostics: An In-House Pipeline to Validate Genetic Variants in Children with Undiagnosed and Rare Diseases.* J Mol Diagn, 2021. **23**(1): p. 71-90.

7 Appendix

7.1 Publications

Publications that are part of this thesis:

Hecker J, Letizia M, Loescher BS, Siegmund B, Weidinger C. Early Onset of TNFα-Driven Arthritis, Auto-inflammation, and Progressive Loss of Vision in a Patient with ALPK1 Mutation. J Clin Immunol. 2022;42(4):880-884. doi:10.1007/s10875-022-01214-8

Other publications during the period of this thesis:

Richter FC, Friedrich M, Kampschulte N, Piletic K, Alsaleh G, Zummach R, **Hecker J**, Pohin M, Ilott N, Guschina I, Wideman SK, Johnson E, Borsa M, Hahn P, Morriseau C, Hammock BD, Schipper HS, Edwards CM, Zechner R, Siegmund B, Weidinger C, Schebb NH, Powrie F, Simon AK. Adipocyte autophagy limits gut inflammation by controlling oxylipin and IL-10. EMBO J. 2023 Mar 15;42(6):e112202. doi: 10.15252/embj.2022112202.

7.2 List of abbreviations

ACTH ..... Adrenocorticotropic hormone

ADP-heptose..... ADP-L-glycero-β-D-manno-heptose

AgRP ..... Agouti-related peptide

ALPK..... Alpha-kinase

AP-1 ..... Activator protein 1

APCs..... Antigen presenting cells

APS..... Ammonium persulfate

ARC ..... Arcuate nucleus

BCR ..... B cell receptor

BMI ..... Body mass index

BSA..... Bovine serum albumin

CBA ..... Cytometric bead array

CCL..... CC chemokine ligand

CCR7 ..... C-C chemokine receptor type 7

CD ..... Cluster of differentiation

CD ..... Crohn's disease

CV ..... Column volumes

CLIP ..... Corticotropin-like intermediate [lobe] peptide

CyTOF..... Cytometry by time of flight

DA ..... Dalton

DAPI ..... 4',6-diamidino-2-phenylindole, dilactate

DCs..... Dendritic cells

DITRA ..... Deficiency of interleukin thirty-six–receptor antagonist

DMEM..... Dulbecco's Modified Eagle's Medium

DMSO..... Dimethyl sulfoxide

DNA..... Deoxyribonucleic acid

DSS..... Dextran sulfate sodium

DTT..... Dithiothreitol

E. coli ..... *Escherichia coli*

EDTA ..... Ethylenediaminetetraacetic acid

eEF2K..... Eukaryotic elongation factor 2 kinase

ELISA ..... Enzyme-linked immunosorbent assay

ERK..... Extracellular signal-regulated kinase

FCS ..... Fetal calf serum

FMO ..... Fluorescence minus one

gnomAD ..... Genome Aggregation Database

GWAS..... Genome-wide association studies

h..... Hours

H. hepaticus ..... *Helicobacter hepaticus*

HBP ..... D-glycero-β-D-manno-heptose 1,7-bisphosphate

HD ..... Healthy donor

HLA-DR ..... Human leukocyte antigen – DR isotype

IBD ..... Inflammatory bowel disease

IC_{50} ..... Half maximal inhibitory concentration

ICAM-1..... Intercellular adhesion molecule 1

IFNγ..... Interferon γ

Ig ..... Immunglobulin

IL ..... Interleukin

IL-1RAcP..... IL-1 receptor accessory protein

IL-1RL2 ..... IL-1 receptor-like 2

IL-36R..... IL-36 receptor

IL-36RA ..... IL-36 receptor antagonist

ILCs..... Innate lymphoid cells

Iono..... Ionomycin

IPEX..... Immune dysregulation, polyendocrinopathy, enteropathy, X-linked

IRAK ..... IL-1R-associated kinase

JAK ..... Janus kinase

JNK ..... C-Jun N-terminal kinase

LB ..... Lysogeny broth

LEP ..... Leptin

LEPR ..... Leptin receptor

LPS ..... Lipopolysaccharide

MACS ..... Magnetic-activated cell sorting

MAPK ..... Mitogen-activated protein kinases

MC1R ..... Melanocortin 1 receptor

MC4R ..... Melanocortin 4 receptor

MFI..... Mean fluorescence intensity

MHC..... Major histocompatibility complex

min..... Minutes

MMP ..... Matrix metalloproteinase

MSH ..... Melanocyte-stimulating hormone

MyD88 ..... Myeloid differentiation primary response 88

NFκB ..... Nuclear factor kappa-light-chain-enhancer of activated B cells

NK ..... Natural killer

NPY ..... Neuropeptide Y

OD..... Optical density

PAMP ..... Pathogen-associated molecular pattern

PBMCs..... Peripheral blood mononuclear cells

PBS..... Phosphate-buffered saline

PC1/3 ..... Proprotein-convertase 1/3

PCR..... Polymerase chain reaction

PCSK1..... Proprotein convertase subtilisin/kexin type 1

PDVF ..... Polyvinylidene difluoride

PMA ..... Phorbol 12-myristate 13-acetate

PolyPhen-2..... Polymorphism Phenotyping v2

POMC..... Proopiomelanocortin

PPR..... Pattern recognition receptor

RAG..... Recombination-activating gene

Ripa..... Radioimmunoprecipitation assay

ROSAH ..... Retinol dystrophy, optic nerve edema, splenomegaly, anhidrosis, and migraine headache

RPMI ..... Roswell Park Memorial Institute Medium

RT..... Room temperature

SD..... Standard deviation

SDS..... Sodium dodecyl sulfate

SEAP..... Secreted alkaline phosphatase

SES-CD ..... Simple endoscopic score for Crohn's disease

SNPs..... Single nucleotide polymorphisms

STAT..... Signal transducer and activator of transcription protein

TBS..... Tris-buffered saline

TCR..... T cell receptor

TEMED ..... Tetramethlyethylenediamine

TfH ..... T follicular helper

Th..... T helper

TIFA..... TRAF-interacting protein with forkhead-associated domain

TIR..... Intracellular Toll/IL-1 receptor

TLR4 ..... Toll-like receptor 4

TNBS ..... 2,4,6-trinitrobenzenesulfonic acid

TNFα ..... Tumor necrosis factor α

TRAF6..... Tumor necrosis factor receptor-associated factor 6

Treg..... Regulatory T cell

TRPM ..... Transient receptor potential melastatin

TSB..... Tryptone soya broth

t-SNE..... t-Distributed Stochastic Neighbor Embedding

UC ..... Ulcerative colitis

UMAP..... Uniform manifold approximation and projection

Unstim. ..... Unstimulated

Untrans. ..... Untransfected

VCAM-1..... Vascular cell adhesion molecule 1

WES..... Whole exome sequencing

WT ..... Wild type

γc ..... Common gamma chain

7.2 List of figures

7.3 List of tables